The Skin-Deep Beauty of Dairy Cows

Investigation of Metabolic Disorders by using Morphological Traits Quantified with 3-Dimensional Vision

Xiangyu Song

Propositions

1. The real challenge in feeding management is to limit a farmer's gut feeling, not a cow's gut filling.
   (this thesis)

2. A 3D camera is the only sensor required for precision dairy farming.
   (this thesis)

3. 'Deep learning' is an anthropomorphic expression that insults artificial intelligence.

4. Cognitive biases in scientists inevitably lead to inadequacies in science.

5. True egalitarianism is not about striving for identical outcomes, but about accepting differences.

6. Strict planning kills creativity.

Propositions belonging to the thesis, entitled

The skin-deep beauty of dairy cows --- Investigation of metabolic disorders by using morphological traits quantified with 3-dimensional vision

Xiangyu Song

Wageningen, 18th November 2019

The Skin-Deep Beauty of Dairy Cows

Investigation of Metabolic Disorders by using Morphological Traits Quantified with 3-Dimensional Vision

Xiangyu Song

Thesis committee

Promotor
Prof. Dr P.W.G. Groot Koerkamp
Professor of Farm Technology
Wageningen University & Research

Co-promotors
Dr E.A.M. Bokkers
Associate professor, Animal Productions Systems Group
Wageningen University & Research

Dr P.P.J. van der Tol
Researcher, Farm Technology Group
Wageningen University & Research

Other members
Prof. Dr H. Hogeveen, Wageningen University & Research
Dr M. Pastell, Natural Resources Institute Finland (Luke), Helsinki, Finland
Dr R. Jorritsma, Utrecht University
Dr C.G. van Reenen, Wageningen University & Research

This research was conducted under the auspices of the Graduate School of Wageningen Institute of Animal Sciences (WIAS)

The Skin-Deep Beauty of Dairy Cows

Investigation of Metabolic Disorders by using Morphological Traits Quantified with 3-Dimensional Vision

Thesis
submitted in fulfilment of the requirements
for the degree of doctor

at Wageningen University
by the authority of the Rector Magnificus,
Prof. Dr A.P.J. Mol,

in the presence of the
Thesis Committee appointed by the Academic Board

to be defended in public
on Monday 18 November 2019
at 1:30 p.m. in the Aula.

Xiangyu Song

Xiangyu Song
The Skin-Deep Beauty of Dairy Cows. Investigation of Metabolic Disorders by using Morphological Traits Quantified with 3-Dimensional Vision

122 pages.

PhD thesis, Wageningen University, Wageningen, the Netherlands (2019)
With references, with summary in English

ISBN 978-94-6395-079-4
DOI https://doi.org/10.18174/497924

Table of Contents

Chapter 1

General Introduction

X. Song

1.1 Sustainable Development in the Dairy Sector

By 2050, the world population is expected to reach 9.8 billion (UN, 2019), and global food demand is expected to double (FAO, 2009). Feeding the growing population is a great challenge and requires increases in food production from limited natural resources (FAO, 2018a). Due to globalization and the rapidly growing economies in many countries, the dairy sector has become one of the fastest-growing segments among all food production sectors (FAO, 2011). The global production of dairy cow milk, for example, increased by 16 % over 10 years from 697 million tons in 2007 (Gerosa and Skoet, 2012) to 811 million tons in 2017 (FAO, 2018b). Meanwhile, the number of dairy cows has increased by 9 % and reached 274 million head (FAO, 2018b). Along with the increase in production and number of animals, the dairy sector has been significantly intensified (Bava et al., 2014), especially in some upper-middle-income countries and nearly all high-income countries throughout the world (Lowder et al., 2016). Intensified dairy farming challenges farmers to rear dairy cows with limited space, resources, and time and is a subject of growing concern among the general public with regard to food quality and animal health and welfare (Wolf et al., 2016; Busch and Spiller, 2018). Additionally, intensification can result in a large amount of nitrogen deposition and greenhouse gas emission and occurs at the expense of the environment, causing effects such as deforestation, and biodiversity loss (FAO, 2016, 2018c). To date, the dairy sector has been subject to enormous societal pressure to fulfill global food demand and meanwhile to ensure sustainable development for high-quality, animal-, and environment-friendly dairy products.

1.2 Precision Livestock Farming

With the significant development of technologies, precision agriculture has become a general approach to contribute to sustainable food production in farming. Precision agriculture is defined as “a management strategy that gathers, processes and analyzes temporal, spatial and individual data and combines it with other information to support management decisions according to estimated variability for improved resource use efficiency, productivity, quality, profitability and sustainability of agricultural production” (ISPA, 2019). The adoption of precision agriculture in livestock (e.g., dairy) farming is called precision livestock farming **(PLF)** (Berckmans, 2008). PLF has emerged as a result of the fast-growing sensor technologies available in the market and the requests of farmers to regularly obtain detailed farm and animal information to facilitate management decisions (Norton and Berckmans, 2018). It aims to make livestock farming more environmentally, economically, and socially sustainable (Berckmans, 2008). For a decade, PLF has received considerable attention and has been explored in many scientific studies across most livestock sectors (Tullo et al., 2019). A significant number of scientific studies have explored how to apply PLF to measure and monitor dairy cow bio-response with a specific focus on health management

(Neethirajan et al., 2017; Norton and Berckmans, 2018). PLF applications aim to help farmers optimize the health of cows through (early) disease detection and are implemented in 3 stages: measure, model, and manage (Tullo et al., 2019). Stage 1, measure. PLF implements a variety of sensors that can be deployed on farms for automatically measuring specific dairy cow bio-response and detecting anomalies. These responses can indicate diseases and are related to the physical, physiological, or behavioral traits of individual cows. Stage 2, model. PLF builds mathematical models with sensor measurements as inputs to predict or classify the severity of sickness associated with a specific disease. The models are validated by using a gold standard, which is often a manual assessment of cows provided by experts (e.g., clinical diagnoses provided by veterinarians). Stage 3, manage. PLF manages the models by applying controllers to the model inputs to reach specific goals for farmers (e.g., to maintain healthy production).

1.3 Limitations of PLF Applications for Dairy Cow Health Management

Currently, PLF applications have focused on detecting 3 main problems in dairy cows: mastitis, lameness, and metabolic disorders (Rutten et al., 2013). These diseases and disorders are the ones occurring most frequently on farms and cause discomfort, increased in mortality rate, and decreased in productivity and fertility in cows (Fischer et al., 2019). Treating these 3 diseases and disorders is costly to farmers and can increase the risk of drug residues in food (Baynes et al., 2016). Furthermore, these diseases and disorders can decrease feed conversion and production efficiency in cows, leading to detrimental environmental impacts (Mostert et al., 2018). Hence, PLF applications have intensively deployed different types of sensors to measure potential disease-related bio-response and built disease detection models aiming to detect these 3 problems as early as possible (Table 1-1).

The current PLF applications for dairy cow health management represent reactive management that detects diseases and alerts farmers to treat the diseased cows. Such applications aim to identify diseased cows as early as possible to prevent further loss in production, fertility, and farm profits. The problem-oriented PLF applications, however, have limitations with respect to their employment on farms.

Limitation 1

The problem-oriented attribute limits the PLF applications by focusing only on disease detection and improving the health management within the existing scope on farms. Thus, PLF applications lack a systematic reflection on current structures, improvement or design of new structures, and anticipation of reduced disease prevalence due to structural change (Bos et al., 2009).

Table 1-1. Precision livestock farming applications for mastitis, lameness, and metabolic disorder detection in dairy cows.

Disease/ Disorder	Disease-Related Bio-Response	Sensor Type	Diagnose Model	Gold Standard
Mastitis	Milk electrical conductivity (Khatun et al., 2018) Milk color (Kamphuis et al., 2010) Milk somatic cell count (Burmańczuk et al., 2018)	In-line spectroscopy milk sensors	The real-time mastitis detection model	The lab test result, California Mastitis Test, clinical examination
	Teat temperature (Colak et al., 2008)	Thermal camera	NA[1]	NA
Lameness	Leg weight distribution (Tasch and Rajkondawar, 2004) Daily walking and lying time (Chapinal et al., 2011) Walking distance (Barker et al., 2018) Hoof force distribution (Maertens et al., 2011) Gait features (Song et al., 2008)	Weighing scale Pedometer & 3D[2] accelerometer Indoor GPS Force and pressure plates Vision camera	Lameness classification model	Locomotion score, clinical examination
Metabolic disorders	Milk fat and protein content (de Roos et al., 2007)	In-line spectroscopy milk sensors	Ketosis detection model	β-hydroxybutyrate (blood test)
	Walking activity (Martiskainen et al., 2009) Rumination Time (Stangaferro et al., 2016)	3D accelerometer	NA	NA
	Rumen pH (AlZahal et al., 2007) Rumen temperature (AlZahal et al., 2011)	Radio-telemetric bolus	NA	NA

[1] NA: information is not available in the reference study; [2] 3D: 3-dimensional.

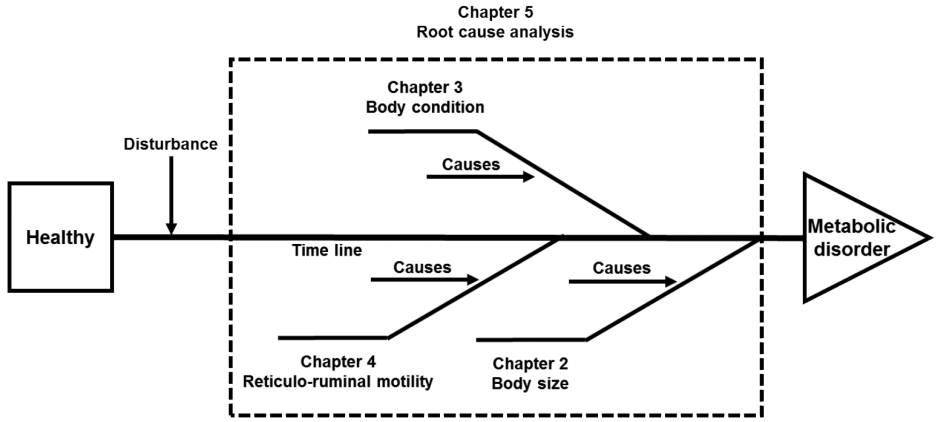

Figure 1-1. Overview of the thesis structure according to the root cause analysis deployed in precision livestock farming.

Limitation 2

Most PLF applications independently deploy single types of sensors to measure bioresponse related to specific health problems. These applications have limited the implementation of sensor integration into a complete package for farmers. Especially with the rapid development of sensor technology on dairy farms, farmers often receive only sensor measurement outputs from independently working sensors, which is difficult for them to extract useful information from overwhelming independent and uncorrelated data to identify the real health problems of cows (Van Hertem et al., 2017).

Limitation 3

The origin of a disease or disorder is significantly associated with the chronological relations of multiple clinical symptoms, each of which is represented by an anomaly in the bioresponse measurement using 1 type of sensor. Deploying single types of sensors without considering their chronological relations to other types of sensors could limit the understanding of the pathogenesis of a disease or disorder (Fournel et al., 2017).

1.4 Root Cause Analysis Incorporated in PLF

PLF applications in dairy cow health management should be more proactive and focus on finding the causes of diseases and preventing disease reoccurrence on farms. To improve PLF applications from reactive to proactive health management, we suggest incorporating root cause analysis **(RCA)** into PLF. RCA is defined as a method of problem-solving used for identifying the root (main) causes of problems (Kiruthika, 2015). RCA application to dairy cow health management can be generally divided into 3 steps: **(i)** establish a sequence of anomalies in a timeline from the time the cow was healthy to the time the metabolic disorder was detected, **(ii)** investigate the cause of each anomaly (e.g., anomalies caused by biology, physiology, pathology, farm management, or the environment), and **(iii)** determine the root cause of the disease. RCA application to dairy cow health management has the potential to reveal the main causes of diseases to farmers as a systematic reflection on current farm management strategies and to improve or redesign farm management to prevent disease reoccurrence. On the other hand, PLF deploys a variety of sensors on farms to automatically and regularly measure and monitor the disease-related bio-response of individual cows, which could offer sufficient inputs at Step 2 of RCA to collect data with a variety of clinical symptoms. PLF deployed sensor technology can thus contribute to better identification of the root cause of disease via RCA.

1.5 Dairy Cow Metabolic Disorders as a Case Study

Among the 3 PLF focused diseases or disorders, metabolic disorders have received the least focus with the fewest scientific studies, as shown in Table 1-1. Hence, this thesis chose

dairy cow metabolic disorders as a case study to incorporate PLF and RCA to investigate the root cause of metabolic disorders. Metabolic disorders are caused by the disturbance of 1 or more metabolic processes in dairy cows (McGuffey, 2017; Overton et al., 2017). These disturbances can be introduced by pathogens, feeding practice changes, or transition period, such as from gestation to lactation (Zebeli et al., 2015), which can change the delicate nutrition and energy balances and cause metabolic disorders, such as ketosis (Duffield, 2006), ruminal acidosis (Oetzel, 2017), fatty liver (Bobe et al., 2010), and milk fever (Saborío-Montero et al., 2017). Metabolic disorders have high impacts on a cow's health, production, and reproduction (Gross and Bruckmaier, 2019) and require proper management on farms (Overton et al., 2017).

The incorporation of RCA in PLF applications for dairy cow metabolic health management requires monitoring bio-response that indicate a cow's metabolism and are defined as metabolic indicators. The currently available metabolic indicators in PLF applications (Table 1-1) for monitoring dairy cow metabolism are still inadequate. **(i)** Milk composition (i.e., milk fat content and fat to protein ratio) can be measured by in-line spectroscopy milk sensors and used to detect clinical ketosis (de Roos et al., 2007). Although anomalies in milk composition are indicative of metabolic disorders, it is often affected by feed quality making milk composition less specific for indicating metabolism. **(ii)** Rumen pH and temperature can be measured by placing a radiotelemetric bolus in a cow's rumen (AlZahal et al., 2007, 2011). Although these 2 variables reflect the physiological function of the rumen and indicate the metabolism of a cow, the technique is invasive and costly to implement for all cows on farms. **(iii)** Daily activity and rumination time can be measured by using 3-dimensional **(3D)** accelerometer attached to a cow's neck to indicate a cow's metabolism (Martiskainen et al., 2009; Stangaferro et al., 2016). The identified cows with anomalies in daily activity and rumination time, however, were often severely ill and were accompanied by permanent health damage and production losses. Currently, additional metabolic indicators to quantify dairy cow metabolism are needed to deploy RCA on PLF applications with the requirements of automatic and noninvasive measurement on farms using low-cost sensors and having physiological or pathological meanings underlying their anomalies.

1.6 Dairy Cow Morphological Traits as Metabolic Indicators

When a cow is unable to maintain its energy or nutrition balances because of experiencing a disturbance to its metabolism, its lack of physiological adaptation can result in changes to the cow's morphology (Schröder and Staufenbiel, 2006; Bobe et al., 2010). Morphology is defined as the external appearance of the body and includes traits such as shape, structure, color, pattern, and size of the whole body or body regions (Pilat, 1988). The morphological traits of body size, body condition, hair coat, and paralumbar shape have been used for the manual clinical diagnosis of metabolic disorders (Mäntysaari et al., 2019).

Dairy cow morphological traits can be quantified automatically by using machine vision

cameras, including 2-dimensional **(2D)** vision, thermal vision (Stajnko et al., 2008), stereo vision using multiple calibrated 2D cameras (Tasdemir et al., 2011), and 3D vision using 1 or multiple 3D cameras (Salau et al., 2016). Images taken in 3D vision, in contrast to 2D vision, show a clear depth difference between a cow and the background. This difference can significantly simplify the background segmentation process (Rosell-Polo et al., 2015). Moreover, images taken in 3D vision include depth information on the body surface, whereas 2D and thermal images include only body contour and cross-sectional area information. Additionally, certain morphological traits quantified using 3D vision are more strongly correlated with manually measured reference values than stereo vision (Marinello et al., 2015). Last, along with the development of vision technology, the cost of 3D vision cameras has been substantially reduced (Kuzuhara et al., 2015). Hence, 3D vision cameras have the most advantages for remotely, inexpensively, and noninvasively quantifying dairy cow morphological traits.

1.7 Objectives and Thesis Outline

The objectives of this Ph.D. thesis are to develop and validate methods and models to automatically quantify dairy cow morphological traits as metabolic indicators using 3D vision and to acquire knowledge about the pathogenesis of metabolic disorders in dairy cows by incorporating RCA into PLF applications.

This thesis selects 3 types of morphological traits in dairy cows: body size, body condition, and body surface concavity on the left paralumbar fossa, which represents reticulo-ruminal motility. These morphological traits are chronologically organized by the speed of the bio-response time, from slow to fast, in **Chapters 2**, **3**, and **4**, respectively (Figure 1-1).

In **Chapter 2**, the body-size-related morphological traits of hip height, hip width, and rump length were automatically quantified by using a 3D vision camera to view the rump areas of dairy cows. The automated morphology quantification was validated with manual body measurements as a gold standard. As an example, the propagation of the automated measurement error to a mathematical model was quantified by using a body-weight prediction model.

In **Chapter 3**, body-condition-related morphological traits in 8 body regions (i.e., spinous processes, spinous to transverse processes, overhanging shelf, hook bone, pin bone, thurl area, spinous processes to hook bone, and cavity between tail head and pin bone) were quantified automatically by using 3 3D cameras viewing the top, rear, and right sides of a cow. A nearestneighbor classification model was built to classify the body condition scores **(BCSs)** of individual cows with automatically quantified morphological traits as inputs and manual BCSs as a gold standard.

In **Chapter 4**, body surface concavity on the left paralumbar fossa of a dairy cow in an automatic milking system **(AMS)** was quantified automatically by using a 3D camera. The

concavity from all 3D images of 1 cow during 1 recording was chronologically assembled to form an undulation signal. This undulation signal consisted of cyclic oscillations that represented reticulo-ruminal contractions. The cyclic oscillation frequency was calculated by using fast Fourier transformation and represented as the reticulo-ruminal motility.

In **Chapter 5**, all 3 vision systems were integrated to regularly monitor all 3 types of morphological traits of dairy cows over 66 days. All the anomalies in the morphological traits were identified and chronologically assembled to investigate the root cause of metabolic disorders by applying RCA.

In **Chapter 6**, a general conclusion was drawn based on the findings in the previous chapters, and the integration of PLF and RCA for dairy cow metabolic health management from a broader perspective was discussed.

Chapter 2

Automated Body Weight Prediction of Dairy Cows using 3-Dimensional Vision

X. Song
E.A.M. Bokkers
P.P.J. van der Tol
P.W.G. Groot Koerkamp
S. van Mourik

Published in Journal of Dairy Science, Volume 101, Issue 5, Pages 4448-445,

Abstract

The objectives of this study were to quantify the error of body weight prediction using automatically measured morphological traits in a 3-dimensional (3D) vision system and to assess the influence of various sources of uncertainty on body weight prediction. In this case study, an image acquisition setup was created in a cow selection box equipped with a top-view 3D camera. Morphological traits of hip height, hip width, and rump length were automatically extracted from the raw 3D images taken of the rump area of dairy cows (n = 30). These traits combined with DIM, age, and parity were used in multiple linear regression models to predict body weight. To find the best prediction model, an exhaustive feature selection algorithm was used to build intermediate models (n = 63). Each model was validated by leave-one-out crossvalidation, giving the root mean square error (RMSE) and mean absolute percentage error (MAPE). The model consisting of hip width (measurement variability of 0.006 m), DIM, and parity was the best model, with the lowest errors of 41.2 kg RMSE and 5.2% MAPE. Our integrated system, including the image acquisition setup, image analysis, and the best prediction model, predicted the body weights with a performance similar to that achieved using semi-automated or manual methods. Moreover, the variability of our simplified morphological trait measurement showed a negligible contribution to the uncertainty of body weight prediction. We suggest that dairy cow body weight prediction can be improved by incorporating more predictive morphological traits and by improving the prediction model structure.

Key words: dairy cattle, morphological trait, 3-dimensional vision, automation, uncertainty

2.1 Introduction

Since 1960, the average farm size has increased in some upper-middle-income countries and nearly all high-income countries throughout the world (Lowder et al., 2016). In the Netherlands, for example, the total number of dairy cows kept by farmers increased by 13%, while the number of dairy farms decreased by 29%, from 2005 to 2015 (Statistics Netherlands, 2016). Moreover, Dutch dairy farmers increased the average annual milk yield per cow to 8373 kg in 2015 (CRV, 2016). However, concerns about the welfare of production animals are growing among the general public (Wolf et al., 2016). Consumers significantly influence the dairy industry by choosing premium welfare products (de Graaf et al., 2016). With increasing production per cow and pressure from consumers, dairy farmers must provide intensive and high-standard care to individual cows to maintain high-quality and animal-friendly milk production. Due to farm upscaling, however, it becomes increasingly difficult to manage individual care because of the high number of cows per full-time equivalent and the high labor demand (Barkema et al., 2015). To ease the burden, farmers can choose to purchase available commercial products to automate certain routine labor-intensive procedures, such as milking and feeding (Jacobs and Siegford, 2012). For other procedures, such as health monitoring, available equipment to automate the procedures is less developed. Recent developments in sensor technology offer promising solutions to automate health monitoring by collecting daily information on the physical status of individual cows (Rutten et al., 2013). Continuous monitoring can help farmers gain insight into a cow's changes over time, identify anomalies in their health status, and take necessary actions. Automation of continuous health monitoring will contribute to maintaining highquality care for individual cows under increasing farm size and production.

An example of health monitoring includes monitoring of the body weight of dairy cows. Body weight changes during lactation. This change reflects the energy balance in the cow (Mäntysaari and Mäntysaari, 2015). A long-term negative energy balance could cause problems in health and reproduction (de Vries et al., 1999; Collard et al., 2000). To estimate the effect of a negative energy balance, frequently measured body weights can be used in farm management (Thorup et al., 2012). Thus, monitoring body weight can help farmers to make management decisions with respect to a cow's health status (van der Tol and van der Kamp, 2010). More importantly, the body weights of individual cows must be measured and monitored automatically to prevent additional labor input and to ensure farmers have time to maintain high quality and individual care (Maltz, 1997). Often, dairy cows are weighed routinely with automated weighing scales (Alawneh et al., 2011). Such scales, however, are relatively expensive and their electronics are prone to damage in the harsh environment covered with manure and urine and in direct contact with cows (Dickinson et al., 2013). Hence, there is a need for a low-cost and robust automated weighing system.

As an alternative to the use of scales, body weight can be predicted based on morphological traits that are significantly correlated with weight, such as heart girth

(Heinrichs et al., 1992), withers height (Tasdemir et al., 2011), and hip width (Enevoldsen and Kristensen, 1997). These morphological traits are typically measured manually. In addition to being labor-intensive, the measurement process can be stressful to cows (Dickinson et al., 2013). To automate the morphological trait measurement, new techniques, such as computer vision, have been explored (Tasdemir et al., 2011; Marinello et al., 2015). With computer vision, morphological traits are defined and measured as distances or areas among pre-identified anatomical landmarks on the surface of a cow's body (Kuzuhara et al., 2015). These anatomical landmarks are typically clearly visible, such as some bone structures (e.g., hip bones and spine) that clearly protrude from their surrounding region (Kawasue et al., 2013). Identifying anatomical landmarks with computer vision is the basis for automatically measuring morphological traits and their derivatives.

Currently used computer vision techniques to measure dairy cow morphological traits include 2-dimensional **(2D)** vision, thermal vision (Stajnko et al., 2008), stereo vision using multiple calibrated 2D cameras (Tasdemir et al., 2011), and 3-dimensional **(3D)** vision using 1 or multiple 3D cameras (Marinello et al., 2015; Salau et al., 2016)., Images taken in 3D vision, in contrast to 2D vision, show a clear depth difference between a cow and the background. This difference can significantly simplify the background segmentation (Rosell-Polo et al., 2015). Moreover, images taken in 3D vision include depth information on the body surface, whereas 2D and thermal images include only body contour and cross-sectional area information. Additionally, certain morphological traits quantified using 3D vision are more strongly correlated with manually measured reference values compared with stereo vision (Tasdemir et al., 2011; Marinello et al., 2015). Lastly, compared with a single 3D camera, the costs for multiple 2D or 3D cameras and a subsequent recording synchronization system are substantially higher (Kuzuhara et al., 2015).

In this case study, we chose to quantify dairy cow body morphological traits by automatically processing images taken in a 3D single-camera vision system. The error produced in the automated image processing will produce an error in the quantification of morphological traits, which in turn might have considerable consequences for body weight prediction. The objectives of this study were to quantify the error of body weight prediction using automatically measured morphological traits in a 3-dimensional vision system and to assess the influence of various sources of uncertainty in body weight prediction.

2.2 Materials and Methods

Image Acquisition

In December 2015, 3D images of 30 lactating Holstein cows (i.e., 1 image per cow) were acquired at a commercial dairy farm in the Netherlands. The farm had a freestall barn equipped with automatic milking systems (**AMS**, Astronaut A4, Lely Industries N.V., Maassluis, the Netherlands). Near 1 of the AMS, an image acquisition setup was constructed (Figure 2-1). The setup was placed next to the exit of the AMS so that cows could enter

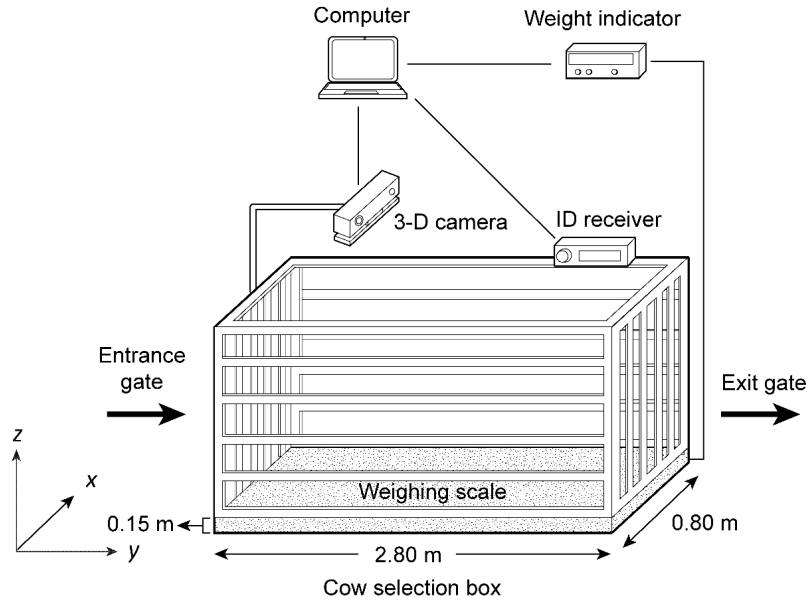

Figure 2-1. The layout of the image acquisition setup at the test farm with arrows indicating the walking route of a cow. The computer controls the acquisition and is connected with the 3-dimensional (3D) camera, identification (ID) receiver, and weight indicator.

it immediately after milking. The setup consisted of a cow selection box, an electronic weighing scale, a 3D camera, and a computer that connected and controlled the setup.

A cow selection box (Grazeway, Lely Industries N.V) was built with automatic entrance and exit gates. Near the exit gate, a cow identification **(ID)** receiver (longrange wireless base unit, SCR, Netanya, Israel) was mounted on the side of the box. The receiver automatically identified the cow in the setup through an ID tag (HR-LD, SCR) around its neck. The floor of the box was an iron plate (2.8 × 0.8 × 0.15 m) attached to an electronic weighing scale (AllScales, Hank Maas B.V., Veen, the Netherlands). One load cell was attached to each corner under the iron plate, and all 4 could weigh up to 1500 kg with a measurement precision of 0.5 kg. These load cells were connected to a digital weight indicator that showed a stable weight every second when the difference between the currently measured weight and the previous weight was no more than 1 kg.

A 3D camera (Kinect Sensor for Windows version 2, Microsoft, Redmond, Washington, United States) was mounted on the metal frame of the selection box to capture a top-view image of a cow's rump. The 3D camera was a depth-sensing timeof-flight camera with a resolution of 512 × 424 pixels and a field of view of 70 (horizontal) × 60 (vertical) degrees. Its range was between 0.5 m and 4.5 m, with a pixel size of 0.003 × 0.003 m and depth precision of 0.001 m at a viewing distance of 1 m. The camera was attached to the box at an angle of 3 degrees to the xy plane to capture the greatest possible amount of information on a cow's body. The angles to the other 2 planes were 0 degrees. Moreover, the center of the camera

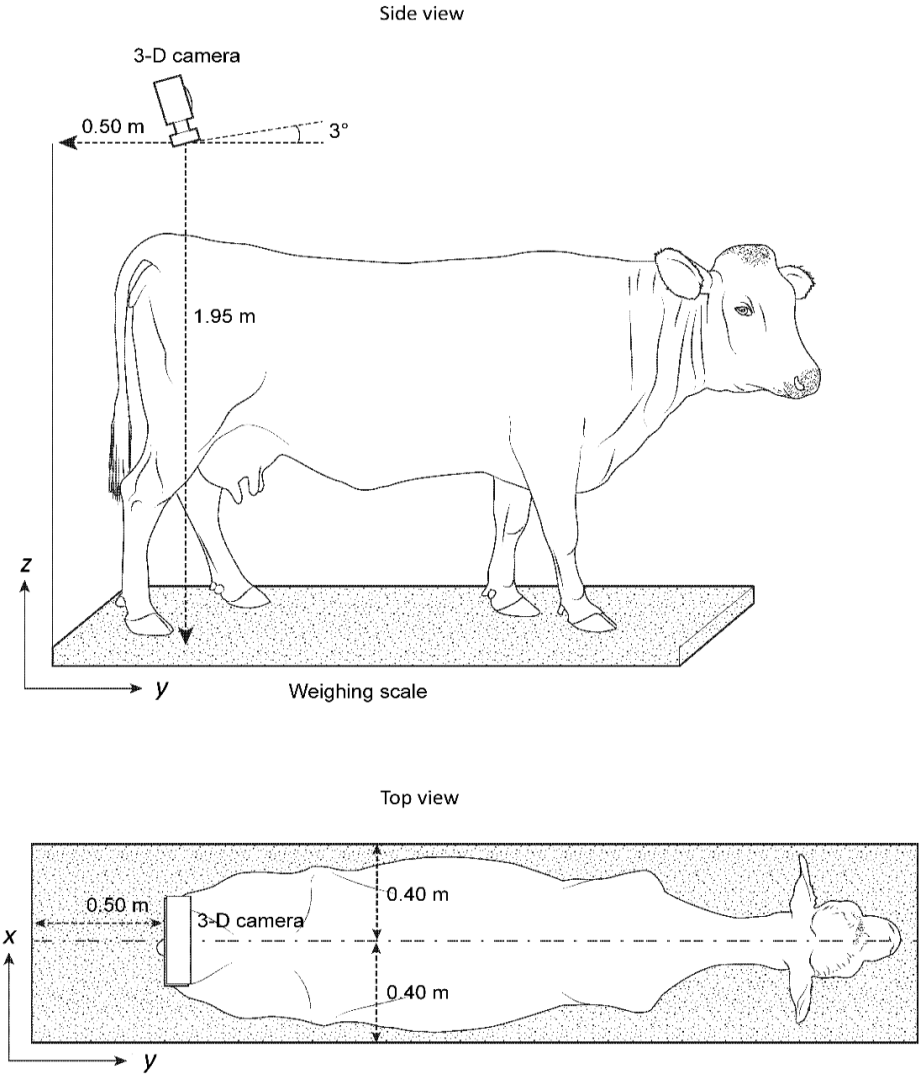

Figure 2-2. Image acquisition setup with a cow, a 3-dimensional (3D) camera, and a weighing scale from the side and top view.

lens was on the centerline of the box in the x direction, 0.50 m from the entrance gate in the y direction, and 1.95 m above the iron plate of the weighing scale in the z direction (Figure 2-2).

Image acquisition was triggered by a cow entering the setup after a successful milking. Both the entrance and exit gates of the selection box were closed to keep the cow in the box. After closing both gates, a raw 3D image of the cow's rump was taken and saved by an image recording algorithm in C-language. The recording algorithm also saved the cow's

ID, the recording time, and the weight measured at the recording time from the electronic weighing scale. Additionally, days in milk **(DIM)**, age, and parity were collected from a dairy farm management software (T4C, Lely Industries N.V.). After image acquisition, the exit gate was opened to release the cow.

Image Analysis

All raw images were processed in 6 steps (Figure 2-3) and using the Computer Vision System and Image Processing toolboxes in MATLAB (2016a, MathWorks, Natick, Massachusetts, United States). Each raw 3D image (e.g., Figure 2-4) was a point cloud consisting of a set of data points with xyz coordinates. The coordinates represented the relative position of each point on the object to the center of the camera lens in the x, y, and z directions. The raw 3D image included the surface of a cow's body, the frames of the selection box, the weighing scale, and image noise.

Step 1 Cow Body Segmentation. The body surface of each cow (Figure 2-5-a) was segmented from the raw image by determining the boundaries of a region of interest **(ROI)** in the *x*, *y*, and *z* directions and selecting points within the ROI as the cow body. The ROI boundaries in the *x* and *y* directions were assumed to be the positions of the metal frames of the selection box. These boundaries were determined by measuring the metal frames in an empty image without cows. The boundary in the *z* direction was set to 1 m to separate the body of each cow from the ground. After cow body segmentation, all points within the ROI boundaries were saved as the cow's body surface.

Step 2 Image Noise Removal. The remaining small groups of points or single points, which were isolated from the cow's body in the segmented image, were considered image noise and removed using a noise removal algorithm. The algorithm calculated the mean of the distances between every point in the ROI and its neighbors. Any point with a mean distance greater than the threshold (i.e., mean plus 1 standard deviation **(SD)** of the mean distances of all points) was identified as image noise and discarded from the image (Figure 2-5-b).

Step 3 Transformation. To correct for the fact that the camera was mounted at a 3-degree angle to the *xy* plane, the 3D image was rotated back by 3 degrees. Moreover, the starting point of the *z* axis was converted from the center of the camera lens to the surface of the iron plate of the weighing scale. The *z* axis conversion made each point's *z* coordinate the height above the plate (Figure 2-5-c).

Step 4 Interpolation. The 3D image was interpolated into a mesh grid with a grid spacing of 0.005 m in the *x* and *y* directions. For each grid point, we assigned its value as the *z* value of its nearest neighbor in the point cloud (Figure 2-5-d). The mesh grid image was considered a matrix. The columns and rows of the matrix were represented by the mesh grid points in the *x* and *y* directions, and the elements of the matrix were the heights of the grid points in the *z* direction.

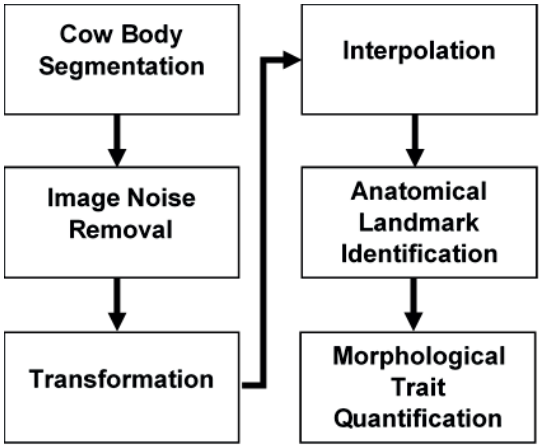

Figure 2-3. A flow chart of the 6 steps in image analysis using Computer Vision System and Image Processing toolboxes in Matlab.

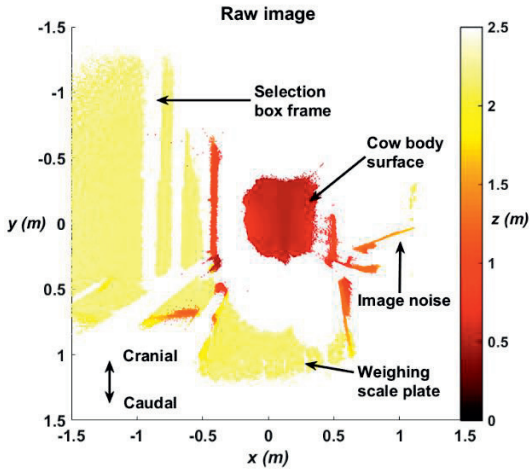

Figure 2-4. raw 3-dimensional (3D) point cloud image with different colors representing different distances to the camera lens. The image consisted of a cow's body surface, selection box frames, weighing scale, and image noise.

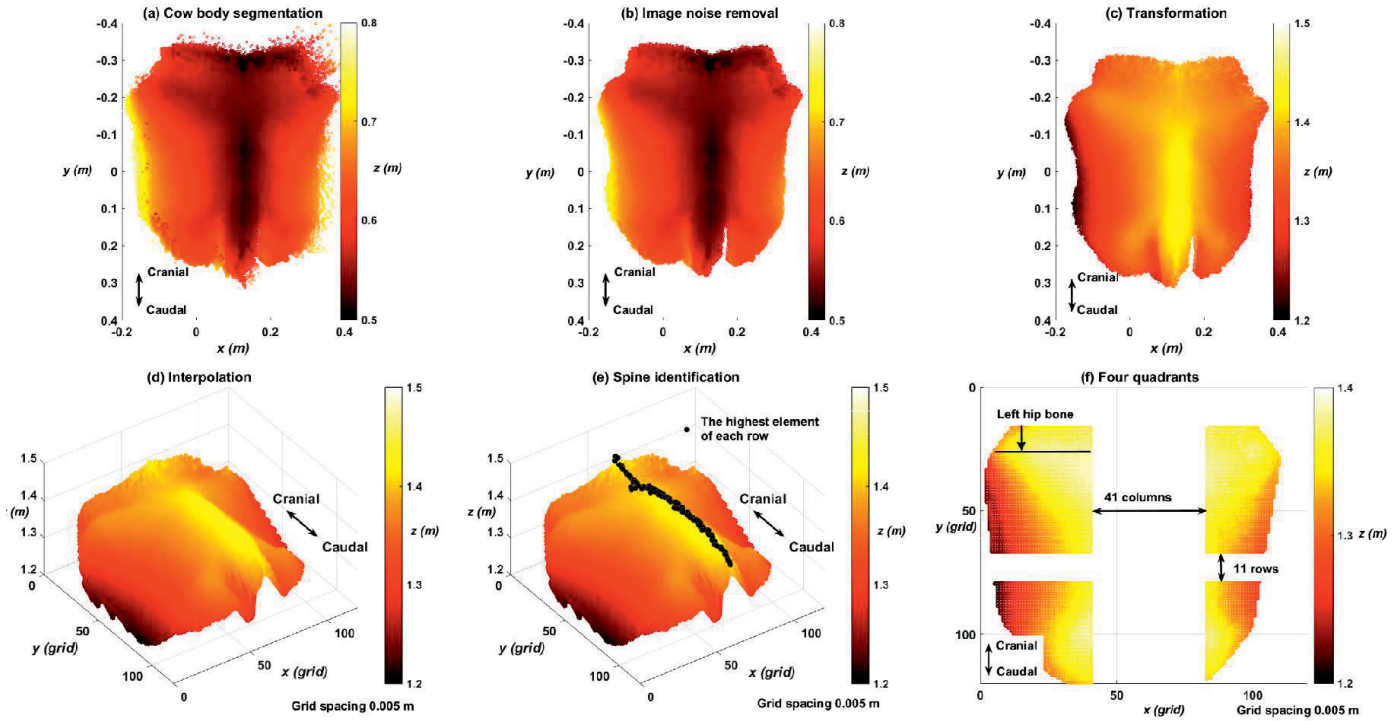

Figure 2-5. (a) The 3-dimensional (3D) image after cow body segmentation. Points remaining in the region of interest (ROI) were the cow's rump surface and image noise. (b) The 3-dimensional (3D) image after noise removal. Points with an average neighborhood distance greater than the threshold were discarded. (c) The 3-dimensional (3D) image after transformation. The image was rotated 3 degrees and the z coordinate was converted to the height above the iron plate of the weighing scale. (d) A mesh grid image of a cow's rump surface after interpolation. The grid spacing in the x and y directions was 0.005 m × 0.005 m. The value of each grid point was the height in the z direction. (e) The highest element of each row (shown as a dot) was identified and assumed to be located on the protruding ridge of a cow's rump. (f) The image (matrix) with 4 separated quadrants. The center of the hip bone from the left front quadrant was identified as being in the row with the highest mean height, being higher than the mean height of the quadrant, and being the furthest from the spine.

Step 5 Anatomical Landmark Identification. Vertebrae in the *lumbar*, *sacrum*, and *coccyx* of the spine form a clearly protruding ridge; therefore, they are seen as the highest part of the surface of a cow's rump. To find this ridge in the matrix, we first identified the highest element of each row (Figure 2-5-e). Then, these elements were connected in a line, which represented the spine in the *craniocaudal* direction. To standardize the mesh grid image (i.e., matrix), we rotated the image in the *xy* plane to align the spine line perpendicular to the *x* axis and parallel to the *y* axis. After rotation, the spine was represented as a single column in the matrix.

In addition to spine identification, we located the anatomical landmarks of hip bones and pin bones, which clearly protrude on the lateral sides of a cow's rump. To locate these bones, we first separated the matrix into left and right (in the x direction) by discarding the spine and its adjacent columns (n = 20) on both sides from the matrix. Second, both the left and right parts of the matrix were separated into the front and rear in the y direction by discarding the middle rows (n = 11) from the matrix. Excluding the middle columns and rows will separate the matrix into 4 quadrants (Figure 2-5-f), which ensured that only 1 protruding anatomical landmark (either a hip or pin bone) could be located in each quadrant. For each quadrant, the row with the greatest mean height was considered to cross the protruding bone. In this row, the farthest element from the spine, which was higher than the mean height of the quadrant, was identified as the center of the protruding bone (Figure 2-5-f).

Step 6 Morphological Trait Quantification. Three morphological traits were quantified in the matrix based on the pre-located centers of the anatomical landmarks (Figure 2-6). Hip height was defined as the mean height of the 2 hip bone centers. Rump length was defined as the mean distance in the *y* direction between the centers of the hip and pin bones from both sides of the body. Hip width was defined as the distance in the x direction between the 2 hip bone centers.

Body Weight Prediction Model

A multiple linear regression model was built with the dataset of 30 cows to predict dairy cow body weight (Equation 2-1). This dataset included automatically quantified morphological traits (i.e., hip height, rump length, and hip width), DIM, parity, age, and referential body weight (i.e., the weight measured using the electronic weighing scale). The model with all 6 traits as input variables was defined as the full model:

$$BodyWeight_i = \beta_0 + \beta_1 \times HipHeight_i + \beta_2 \times RumpLength_i + \beta_3 \times HipWidth_i + \beta_4 \times DIM_i + \beta_5 \times Age_i + \beta_6 \times Parity_i + \varepsilon, \qquad \varepsilon \sim \mathrm{N}(0, \sigma_\varepsilon^{\,2}) i.i.d. \qquad \textbf{(Equation 2-1)}$$

where β is a parameter vector, ε is an error term, $\sigma_\varepsilon^{\,2}$ is the error variance, and *i* denotes the i^{th} cow.

To improve the full model with respect to predictive power, an exhaustive feature selection algorithm was used to build and test intermediate models with all 63 possible input variable combinations. Each intermediate model was trained and validated by leave-one-out cross-validation using the Statistics and Machine Learning Toolbox in MATLAB. The predictive performances of the full and intermediate models were quantified by the root mean square error **(RMSE)** (Equation 2-2) and mean absolute percentage error **(MAPE)** (Equation 2-3):

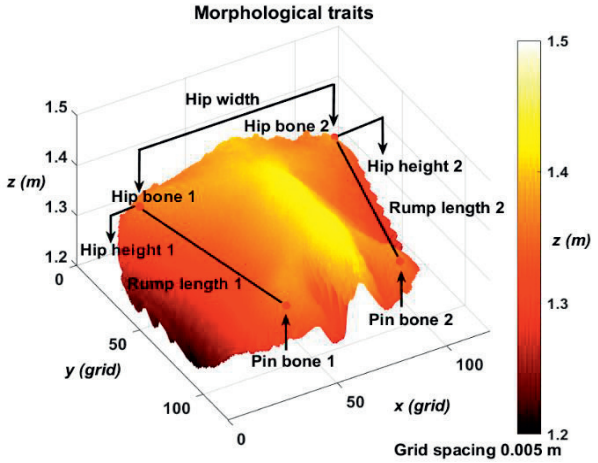

Figure 2-6. Hip bones, pin bones, and 3 types of morphological traits (i.e., hip height, rump length, and hip width) were projected on a 3-dimensional (3D) mesh grid image of the cow's rump surface (the complete surface without excluding the middle rows and columns).

$$RMSE = \sqrt{\frac{\sum_{i=1}^{n}(y_i - \hat{y}_i)^2}{n}}$$ ***(Equation 2-2)***

$$MAPE = \frac{1}{n}\sum_{i=1}^{n}\left|\frac{y_i - \hat{y}_i}{y_i}\right| \times 100\%$$ ***(Equation 2-3)***

where y_i is the referential body weight, $\hat{y}_i$ is the estimated body weight from the prediction model, n is the total number of cows (i.e., n = 30), and i denotes the ith cow. Of all 64 models, the one with the smallest RMSE was selected as our final (best) model to predict body weight.

Quantification of Variability in Morphological Trait Measurement

For each morphological trait, the variability of the automated measurement was estimated by the SD of the repeated measurements (n = 9) on a life-size model cow. These measurements were conducted by placing the model cow at 9 locations with a position difference of 0.05 m in either the *x*, *y*, or both directions in the image acquisition setup.

To compare with the automated measurement, the morphological traits of the same model cow were independently measured by 10 human assessors using a ruler attached to a spirit level and a stadiometer with a measurement precision of 0.005 m for both tools. The 10 assessors were engineers with no experience in quantifying cow morphological traits and were individually introduced to a predefined protocol (Appendix 2-1). They independently identified anatomical landmarks (e.g., hip and pin bones) and measured the morphological traits (i.e., distances and heights) of the model cow. The SD of each morphological trait measured by the 10 assessors was calculated as an estimate of the variability of the manual measurement.

Propagation of Morphological Trait Measurement Error into Body Weight Prediction

To compute the influence of the morphological trait measurement error (estimated by the variability of the measurement) on the body weight prediction error, we created 3 artificial datasets (A, B, and C) and referential body weights based on the final model (Equation 2-4):

$$BodyWeight = \beta_0 + \beta_1 \times X_1 + \beta_2 \times X_2 + ... + \beta_k \times X_k + \varepsilon, \qquad \varepsilon \sim \mathrm{N}(0, \sigma_\varepsilon{}^2) i.i.d. \qquad \textit{(Equation 2-4)}$$

where β is a parameter vector, X is the input variable in the final model (including morphological traits and age-related information), k is the number of input variables in the final model, ε is an error term with a normal distribution, and $\sigma_\varepsilon{}^2$ is the error variance. All 3 datasets were used to compute and compare body weight predictive performances. Dataset A represented a set of morphological traits in the final model without the influence of the measurement error; dataset B represented the same set of morphological traits under the influence of automated measurement error; dataset C represented the same set of morphological traits under the influence of manual measurement error.

Dataset A was created as follows: for each morphological trait, a collection of 1,000 samples was drawn from $\{X_A\}_{1000} \sim \mathrm{N}(\bar{X}, \sigma_X{}^2)$, where $\bar{X}$ is the mean of the trait in our 30-cow dataset and $\sigma_X{}^2$ is the variance of the trait calculated based on

$$\sigma_X{}^2 = \frac{1}{n-1}\sum_{i=1}^{n}(X_i - \bar{X}) \qquad \textit{(Equation 2-5)}$$

where X_i is the input variable (not including age-related information) of the i^{th} cow, n is the total number of cows (i.e., n = 30), and i denotes the i^{th} cow.

Dataset B was created in a similar way as dataset A, with only 1 difference: after creating a collection of 1,000 samples of each of the morphological traits, the samples were artificially disturbed by an error ε_{AM} stemming from the automated morphological trait measurement. This error was modeled as $\varepsilon_{AM} \sim N(0, \sigma_{AM}^2)$, where σ_{AM}^2 is the squared value of the automated measurement variability calculated in Section 2.4. Effectively, the 1,000-sample collection of dataset B was drawn from

$$\{X_B\}_{1000} \sim N\left(\overline{X}, {\sigma_X}^2 + {\sigma_{AM}}^2\right).$$

Dataset C was created in a similar way as dataset B. The samples, however, were artificially disturbed by a manual measurement error $\varepsilon_{MM} \sim N(0, \sigma_{MM}^2)$, where σ_{MM}^2 is the squared value of the manual measurement variability calculated in Section 2.4. Effectively, the 1,000-sample collection of dataset C was drawn from

$$\{X_C\}_{1000} \sim N\left(\overline{X}, {\sigma_X}^2 + {\sigma_{MM}}^2\right).$$

Referential body weight was a collection of 1,000 samples calculated based on Equation 2-4 with the morphological traits in dataset A, the means of the age-related information of the 30-cow dataset, and error term ε was drawn from $\varepsilon \sim N(0, \sigma_\varepsilon^2)$ *i.i.d.,* where σ_ε^2 is the error variance of our 30-cow dataset testing on the final model based on

$$\sigma_\varepsilon^2 = \frac{SSE}{n-(k+1)} \qquad \textit{(Equation 2- 6)}$$

where SSE is the sum of squared error, n is the number of samples (i.e., n = 30), and k is the number of the input variables in the final model.

For each dataset, a multiple linear regression was tested against the referential body weights. The body weight predictive performance of the dataset was quantified with the RMSE and MAPE in the same way as in Section 2.3. The prediction error differences among the dataset were the estimates of the influences of different measurement errors on body weight prediction.

2.3 Results

Descriptive statistics of the model input variables, referential body weights, and their respective Pearson correlation coefficients for the 30 dairy cows are shown in Table 2-1. Among the variables, hip width, age, and parity showed significant linear relationships with

Table 2-1. Descriptive statistics of model variables, referential body weights, and their respective Pearson correlation coefficients of 30 dairy cows.

Item	Minimum	Mean	Maximum	SD	PCC[2]
Body weight (kg)	485.5	597.4	767.5	81.0	-
Hip height (m)	1.302	1.359	1.414	0.029	-0.05‡
Rump length (m)	0.368	0.432	0.475	0.027	0.33†
Hip width (m)	0.385	0.442	0.510	0.035	0.76***
DIM[1] (day)	1	136	363	100	0.18‡
Age (year)	2.02	3.66	8.03	1.92	0.81***
Parity (number)	1	3	7	2	0.81***

‡$P < 1$, †$P < 0.10$, *$P < 0.05$, **$P < 0.01$, ***$P < 0.001$. Null Hypothesis: the population correlation coefficient is not significantly different from 0; alternate Hypothesis: the population correlation coefficient is significantly different from 0.
[1]DIM: days in milk; [2]PCC: Pearson correlation coefficient.

Table 2-2. The variabilities of the automated (n = 9) and manual (n = 10) morphological trait quantifications of a life-size model cow.

Morphological traits	Automated measurement variability	Manual measurement variability
Hip height (m)	0.003	0.001
Rump length (m)	0.012	0.011
Hip width (m)	0.006	0.009

Table 2-3. Predictive performances of the final body weight prediction model compared those of the full model and 2 intermediate models.

Multiple linear regression models	RMSE[1] (kg)	MAPE[2] (%)
Full model		
$BodyWeight = \beta_0 + \beta_1 \times HipHeight + \beta_2 \times RumpLength + \beta_3 \times HipWidth + \beta_4 \times DIM + \beta_5 \times Age + \beta_6 \times Parity + \varepsilon$	45.2	5.5
Two examples of intermediate models		
$BodyWeight = \beta_0 + \beta_1 \times HipWidth + \varepsilon$	55.4	7.4
$BodyWeight = \beta_0 + \beta_1 \times DIM + \beta_2 \times Age + \varepsilon$	49.5	6.1
Final model		
$BodyWeight = \beta_0 + \beta_1 \times HipWidth + \beta_2 \times DIM + \beta_3 \times Parity + \varepsilon$	41.2	5.2

[1]RMSE: root mean square error; [2]MAPE: mean absolute percentage error.
β: parameter; ε: error term; DIM: days in milk.

Table 2-4. Body weight prediction errors resulting from the tests on 3 artificial datasets with and without the error of the hip width measurement.

Dataset	RMSE[1] (kg)	MAPE[2] (%)
Dataset A (without measurement error)	38.6	5.1
Dataset B (with automated measurement error)	39.1	5.2
Dataset C (with manual measurement error)	39.5	5.3

[1]RMSE: root mean square error; [2]MAPE: mean absolute percentage error.

the referential body weight. Additionally, age and parity were highly correlated, with a Pearson correlation coefficient of 0.97 ($P < 0.001$).

The variabilities of the automated (n = 9) and manual (n = 10) morphological trait measurements of a life-size model cow are listed in Table 2-2. In both automated and manual measurements, hip height showed the smallest variability and rump length the largest.

The performances of the full, intermediate, and final prediction models with leave-one-out cross-validation are shown in Table 2-3. The final model consisted of the input variables hip width, DIM, and parity and included prediction errors that were 4.0 kg (RMSE) and 0.3% (MAPE) less than the full model. Moreover, the residuals of the final model were visually inspected and considered to be normally distributed.

The predictive performances of the final model test on all 3 artificial datasets are shown in Table 2-4. The automated measurement error increased 0.5 kg RMSE and 0.1% MAPE in the body weight prediction, while the manual measurement error increased 0.9 kg RMSE and 0.2% MAPE.

2.4 Discussion

This study predicted dairy cow body weight with automatically measured morphological traits using 3D vision and age-related information. The final multiple linear regression model with input variables of hip width, DIM, and parity predicted body weight with an RMSE of 41.2 kg. This predictive performance is similar to studies using manually measured morphological traits in combination with similar models: 36.7 kg from Banos and Coffey (2012), 47.0 kg from Haile-Mariam et al. (2014), and 35.9 kg from Vanrobays et al. (2015). It is also similar to results of the study of Kuzuhara et al. (2015), who found an RMSE of 42.6 kg using 3D vision combined with the manual identification of the anatomical landmarks in the 3D images.

Although the prediction error is similar to those of other studies, we are aware that an error of 41.2 kg is much larger than the cow's average daily weight change caused by net energy intake, which is less than 1 kg (Jensen et al., 2015). This is likely because our prediction model mainly contained variables (hip width, DIM, and parity) that do not fluctuate on a daily basis. This model is not yet suitable for monitoring shortterm body weight variation or detecting anomalies in a cow's health status. Practical application of automated monitoring,

therefore, requires addressing the error sources that significantly influence the prediction performance. We categorize those sources as stemming from the (1) quality of automated morphological trait measurement, (2) choice of model input variables, and (3) type of prediction model.

Source 1

The integrated system was validated on a life-size cow model with respect to the variance associated with morphological trait measurements. For both automated and manual measurements, the variabilities were no greater 0.012 m (Table 2-2). The low variability in the automated measurement could be attributed to the image resolution of 0.003 m (x) × 0.003 m (y) × 0.001 m (z) at a viewing distance of 1 m. This resolution enables consistent identification of anatomical landmarks on the surface of a cow's rump and precise quantification of the morphological traits. Moreover, the low variability in the manual measurement could be attributed to the predefined protocol (Appendix 2-1) followed by all the assessors. Although both types of measurement variabilities were low, the influence of measurement quality on body weight prediction requires further investigation. First, the variability tests in our study were done on a life-size cow model in an experiment hall using automatic and manual approaches. Thus, we simplified the measuring conditions and ignored the influences (e.g., illumination and fur color difference) of measurements on real cows on a farm. Second, the measurements were repeated on the cow model, whereas measurements on the real cows were not repeated at the farm. Third, when identifying the anatomical landmarks of different cows, the precision of the identification may depend on the shape of a cow. Bones from fat cows protrude less than the ones from thin cows. Lastly, the manual measurement variability of the cow model was low. However, performing manual measurements on real cows at farms will lead to a larger variability. Thus, further study is required to test the variability and reliability of the measurements on real cows at different farms and to quantify the error propagation from these sources.

Source 2

The input variables used in our body weight prediction model included morphological traits and age-related information. Among all the input variables, hip width had the largest and most significant linear correlation with referential body weight. It was also the only morphological trait remaining in the final model. The significance of hip width in body weight prediction was also found by Enevoldsen and Kristensen (1997) and Banos and Coffey (2012). Enevoldsen and Kristensen (1997) argued that body width development is the final step in dairy cow body development. In our study, 19 of the 30 cows were in their first or second lactation and therefore were still growing. This factor can likely explain the positive correlation found between hip width and referential body weight.

Hip height showed a weak linear correlation with referential body weight, which is consistent with the results of Tasdemir et al. (2011) and Enevoldsen and Kristensen (1997).

However, Heinrichs et al. (1992) found a strong correlation between body height and weight of dairy calves and heifers. The contradiction between the studies can be explained by the different ages of the studied animals. For young animals (Heinrichs et al., 1992), height-related traits are also indicators of early life growth and body weight gain. When cows are reaching maturity (e.g., in our study), height-related traits become stable, and this information is less useful for predicting body weight and changes.

Rump length also showed a weak correlation with referential body weight. This finding is inconsistent with Tasdemir et al. (2011) and Yan et al. (2009), who found a high correlation. A possible explanation is that in our image acquisition setup, the 3D camera focused only on a small part of the length of a cow, the rump, while Tasdemir et al. (2011) and Yan et al. (2009) used multiple cameras to guarantee a full body scan. Compared with full body length, rump length includes too little information on cow length variation. Therefore, incorporating additional morphological traits that correlate with full body length might improve models for body weight prediction.

Input variables DIM and parity remained in the final model. This is consistent with Enevoldsen and Kristensen (1997) and Kuzuhara et al., (2015). Although DIM was insignificantly correlated with the referential body weight, it might be a predictor for body weight changes during lactation. Moreover, DIM may also provide additional information related to the pregnancy status of a cow, especially in the later stage of lactation (Bereskin and Touchberry, 1967). Parity was strongly correlated to the referential body weights in the present study and was used as a linear input variable in the prediction model. This is inconsistent with the study of Kertz et al. (1997), who constructed different body weight prediction models for different parities. Parity was used as a linear input variable because the parities of the cows in our data were unevenly distributed (i.e., 19 cows had a parity of 1 or 2 and 1 cow had a parity of 4). In future studies, parity could be used as a random effect variable for predicting body weight. Age was highly correlated with parity in the present study and, hence, not included in the final model. Age being a linear variable in the prediction model of adult cows is consistent with Banos and Coffey (2012). However, to predict body weight of young cows (e.g., calf and heifer), the quadratic form of age may be more suitable.

Due to the limitation of the camera view, we could not measure all potential relevant input variables. Such variables can include morphological traits not tested in this study but that have shown significant contributions to the body weight prediction in previous studies, such as heart girth (Heinrichs et al., 2007), chest width (Banos and Coffey, 2012), paunch girth (Sieber et al., 1988), udder size (Haile-Mariam et al., 2014), full body length (Banos and Coffey, 2012), body surface area (Brandl and Jørgensen, 1996), and body condition (Haile-Mariam et al., 2014). These variables can also be those containing information about body weight changes in the short or mid-term, such as milk yield (Haile-Mariam et al., 2014), energy balance (Jensen et al., 2015; Mäntysaari and Mäntysaari, 2015), and days in pregnancy (Bereskin and Touchberry, 1967). These types of variables can be combined

with or replace the current input variables to potentially better predict body weight and its variations. Thus, to find other and preferably better body weight predictors that can be measured automatically is one possible means to improve the current body weight prediction.

Source 3

The prediction model was based on multiple linear regression as commonly applied in prior research (Tasdemir et al., 2011; Haile-Mariam et al., 2014; Kuzuhara et al., 2015). Alternatively, Banos and Coffey (2012) and Vanrobays et al. (2015) suggested using a mixed-effects model with random effects (e.g., cows, breeds, herds, etc.). In these studies, large datasets were collected from multiple herds and morphological traits were measured over time. As a case study, we limited the image acquisition to 30 cows from 1 herd with no repeated measurements from the same cow. For future studies, we suggest to include data from different breeds and herds, to do time-series measurements of morphological traits (e.g., subcutaneous fat deposit) that vary over time, and to investigate different types of models to provide short-term or daily weight changes that are indicative of the physiological status of interest.

Overall, the body weight prediction of the final model reached our expectation. We also observed that more input variables were used to predict body weight in existing studies. As a case study, we chose 3 commonly used morphological traits to be measured automatically using 3D vision, which was demonstrated as a technology with great potential in automation. Moreover, our study sets guidelines for follow-up research. We believe that this methodology is relevant for automated monitoring systems in general.

2.5 Conclusions

Our automated dairy cow body weight prediction achieved performance similar to those of manual and semi-automated methods. The bottleneck in the prediction lies not in the quality of automated morphological trait measurement but in the prediction model. Follow-up research should focus on selecting predictive traits, improving the model structure, or a combination thereof.

2.6 Acknowledgements

This research was funded by Lely Industries N.V.. The authors would like to thank Mr. Tomáš Šabata from the Faculty of Information Technology, Czech Technical University in Prague, for his contribution in designing the test and programming for Section 2.5; Mr. Emo van Halsema from Lely Innovation for his contribution in testing a variety of statistical models; and Mr. Wouter Beukeboom from Hazerswoude-Dorp, the Netherlands for the cooperation in collecting data at his farm.

Appendix 2-1. Protocol for a morphological trait measurement in a life-size model cow

a. Stand behind the cow, in line with the top of the spine.
b. Visually find the contour of the left hip bone and estimate the highest point on the contour.
c. Point out the highest point with a finger and adjust the location on closer inspection.
d. Label the point with a small sticker.
e. Repeat steps **a** to **d** for the right hip bone.
f. Stand to the left of the cow and face toward the left pin bone, in line with the tailhead.
g. Visually find the contour of the left pin bone and estimate the highest point on the contour.
h. Point out the highest point with a finger and adjust the location on closer inspection.
i. Label the point with a small sticker.
j. Repeat steps **f** to **i** for the right pin bone.

Use a spirit level with a length measuring function (measurement precision of 0.005 m) for the following distance measurements.

k. Place the level horizontally to measure the distance between the left and right hip bone markers as the hip width.
l. Place the level horizontally to measure the distance between the left hip-bone and pin-bone markers as the left rump length.
m. Place the level horizontally to measure the distance between the right hip-bone and pin-bone markers as the right rump length.
n. Calculate the mean of the left and right rump lengths.

Use a stadiometer with a ruler (accuracy of 0.005 m) and a sliding horizontal headpiece (including a level indicator) for the following height measurements.

o. Place the ruler of the stadiometer vertically and next to the left hip bone; place the sliding headpiece horizontally on the marker to measure the left hip height.
p. Place the ruler of the stadiometer vertically and next to the right hip bone; place the sliding headpiece horizontally on the marker to measure the right hip height.
q. Calculate the mean of the left and right hip heights.

Chapter 3

Automated Body Condition Scoring of Dairy Cows using 3-Dimensional Feature Extraction from Multiple Body Regions

X. Song
E.A.M. Bokkers
S. van Mourik
P.W.G. Groot Koerkamp
P.P.J. van der Tol

Published in Journal of Dairy Science, Volume 102, Issue 5, Pages 4294-4308,

Abstract

Machine vision technology has been used in automated body condition score (BCS) classification of dairy cows. The current vision-based classifications used information acquired only from a limited number of body regions of a cow. Our study aimed to improve the automated BCS classification by including multiple body-condition-related features extracted in 8 body regions from 3 viewpoints. The dataset of this study included 44 lactating cows with their BCSs evenly distributed over the scale of BCSs from 1.5 to 4.5 units. The body images of these cows were recorded over 2 consecutive days using 3-dimensional cameras positioned to view the cow from the top, right side, and rear. Each image was automatically processed to identify anatomical landmarks on the body surface. Around these anatomical landmarks, the bony prominences and body surface depressions were quantified to describe 8 body-conditionrelated features. Moreover, the manual BCS of each cow was independently assigned by 2 trained assessors using the same predefined protocol. With the extracted features as inputs and manual BCSs as the reference, we built a nearest neighbor classification model to classify BCSs and obtained an overall classification sensitivity of 0.72 using 10-fold cross-validation. We conclude that the sensitivity of automated BCS classification has been improved by expanding the selection of body-condition-related features extracted from multiple body regions.

Key words: dairy cattle, 3D camera, automatic, BCS

3.1 Introduction

The body condition of a dairy cow is a reflection of its fat reserves (Roche et al., 2009) and is influenced by the feed efficiency (Rathbun et al., 2017), diet type (McCarthy et al., 2007), and stocking rate (Coffey et al., 2017) on farms. As an indicator in farm management, body condition is associated with dairy cow energy balance (Thorup et al., 2012). It varies throughout lactation and is a net result of fat storage and depletion. Abnormal and sudden variation in the body condition can be a sign of metabolic failure caused by a disorder, disease, or improper management (Rathbun et al., 2017; Chebel et al., 2018). Therefore, dairy farmers are advised to regularly assess their cows' body condition to prevent metabolic failure and to maintain individual cow welfare.

Body condition is usually quantified by a body condition score (**BCS**). This BCS is assigned by trained assessors using a predefined scoring protocol containing, e.g., a five-point scoring system with 9 levels of fatness from lean to obese (Edmonson et al., 1989). The assessors use visual inspection and sometimes palpation of a cow's lumbar and sacral regions to classify body condition (Roche et al., 2004). The quality of manual scoring depends on the experience of the assessor and the quality of the scoring protocol (Kristensen et al., 2006). To incorporate high-quality manual scoring in farm management, farmers must regularly hire experienced assessors or to receive training to score their own cows, but both approaches are labor-intensive and costly (Roche et al., 2009). Consequently, regular high-quality manual body condition scoring of individual cows is difficult to incorporate as a routine procedure in farm management.

Two sensor technologies have been applied to replace the costly manual scoring method: ultrasonography and machine vision. Ultrasonography has been used to directly measure the subcutaneous fat thickness of dairy cows (Domecq et al., 1995). Although technology has improved the accuracy of fat measurements (Schröder and Staufenbiel, 2006), the procedure remains labor-intensive because it is conducted with a handheld device. In contrast, machine vision can automate body condition scoring and this automation can be inexpensive. Vision cameras, including two-dimensional **(2D)** (Bewley et al., 2008; Azzaro et al., 2011; Bercovich et al., 2013), thermal (Halachmi et al., 2008), and 3-dimensional **(3D)** (Fischer et al., 2015; Spoliansky et al., 2016) cameras, have been used to automatically extract body-conditionrelated features. These features include bony prominences and body surface depressions both of which are related to subcutaneous fat reserves and are quantified as variables of the automated body condition scoring.

In current machine vision-based studies, BCS is often assumed a continuous variable and is predicted with regression models. BCS, however, is an ordinal variable as it classifies cows into different categories of body condition. Moreover, all machine vision-based studies are conducted using a single camera. The single-camera views fewer body regions than those are assessed by manual scoring. Recent studies have demonstrated the feasibility of using multiple 3D cameras to record the entire body surface of the cow (Guo et al., 2017;

Salau et al., 2017). We hypothesized that features can be extracted from all the body regions assessed in manual body condition scoring using multiple 3D cameras and that machine vision-based scoring will be improved if all these features are included. Therefore, we aim to improve the 3D vision-based BCS classification by expanding the selection of the automatically extracted body features from multiple viewpoints.

3.2 Materials and Methods

Cow Selection

We aimed to build a balanced dataset with 5 cows in each half-point BCS class. Two Dutch (farms A and B) and 2 German (farms C and D) farms were selected based on the expected body condition of the cows, which were suggested by local farm management advisors. Farm A was selected for its high proportion of lean cows, farms B and C were selected for their average cows, and farm D was selected for its obese cows. All farms were commercial free-stall barns equipped with automatic milking systems (Astronaut A4, Lely, Maassluis, The Netherlands). On each farm, half of the herd was randomly selected and independently assigned a BCS by 2 trained assessors following a manual body condition scoring protocol. When a cow received the same BCS from both assessors and its BCS contributed to the balanced dataset, it was selected for this study.

Data Collection

Data from 44 cows were collected twice on 2 consecutive days in October 2017. These cows were Holstein Friesian (n = 33) and Simmental (n = 11), ranging from 34 to 451 days in milk and with parities ranging from 1 to 11. On the days of data collection, all the selected cows were gathered at the feed fences in a separate area for manual body condition scoring and image recording.

Manual Body Condition Scoring. On the days of data collection, 2 assessors independently assessed all 44 cows. Before cow selection and data collection, the 2 assessors were trained by an expert regarding how to use the manual body condition scoring protocol. This method is based on the work of Edmondson et al. (1989) and is used by advisors of the GD Animal Health (Deventer, The Netherlands). The protocol is a guidance to assess the fatness of 8 body regions on a 5-point scale from lean to obese with half-point increments (i.e., 9 levels). The protocol focuses on the right side of the body to help the assessor visually assess (1) the bony prominences of the spinous and transverse processes and hook and pin bones, and (2) the body surface depressions above the transverse processes, the thurl area, the area between the spinous processes and hook bone, and the cavity between the tail head and pin bone (Figure 3-1). In addition, this protocol guides the assessor in assigning an overall BCS based on the conditions of all the assessed body regions.

Image Recording. A moveable setup for image recording was built to be placed behind a cow to capture its 3D body surface from different views with 3D cameras. The setup

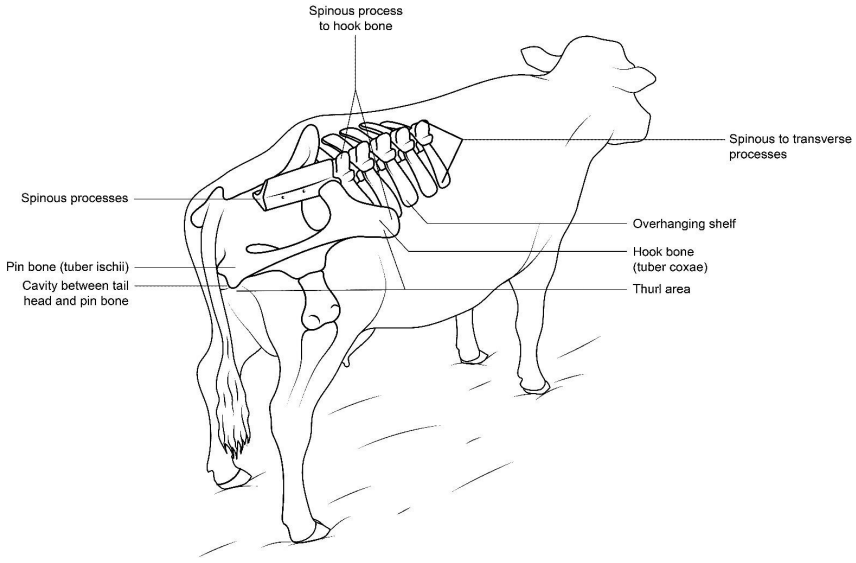

Figure 3-1. Body regions assessed in the manual body condition scoring protocol.

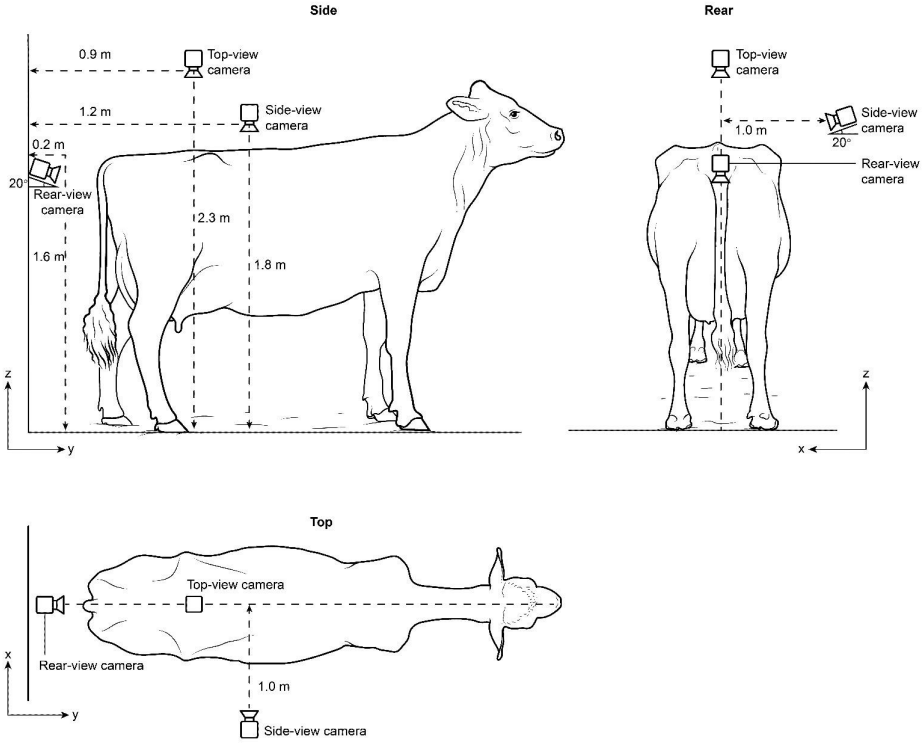

Figure 3-2. Image recording setup with the mounting positions and angles of the 3 cameras.

consisted of an aluminum frame supporting 3 identical 3D cameras (Realsense SR300, Intel, Santa Clara, California, USA) to record images from the top, right, and rear sides of the cow. The mounting positions and angles of each camera on the frame were selected to cover all the body regions assessed in the manual scoring protocol (Figure 3-2). The cameras and the corresponding body regions that they covered are listed in Table 3-1.

The 3D cameras are coded light cameras with a resolution of 640 × 480 pixels and field-of-view angles of 71.5° (horizontal) and 55.0° (vertical). The camera viewing distance ranged from 0.2 to 1.5 m, with a pixel size of 0.002 (horizontal) × 0.002 (vertical) × 0.001 m (depth) at a viewing distance of 1.0 m. Each camera was connected to a USB 3.0 port of a recording computer (NUC-6i3SYK, Intel).

After a cow underwent manual BCS assessment, the setup was manually moved behind the cow. When the cow was standing still, image recording was manually initiated. Five images were consecutively recorded at 2 Hz from the top-view camera, from the side-view camera, and finally from the rear-view camera. After recording, the cow was returned to the herd, and data collection continued for the next cow.

Table 3-1. Body-condition-related feature extractions in their corresponding body regions, anatomy in vivo, camera view, anatomical landmarks, and the rectangular regions of interest.

Body region	Anatomy in vivo	Camera view	Anatomical landmark	A rectangular region of interest
Spinous processes	Bony projection of the posterior of each vertebra in the sacral region	Top	Vertebral column	11 columns with the spine trend line in the center and from the centerline of the sacral ligament to the end of the body
Spinous to transverse processes	An area between the tips of the spinous and transverse processes of each vertebra in the lumbar region	Top	Vertebral column, hook bone, sacral ligament	From the vertebral column to the center of the hook bone and 20 rows starting from the top edge of the sacral ligament in the cranial direction
Overhanging shelf	An area near the tips of the transverse processes	Side	Hook bone	25 columns starting from the edge of the hook bone in the cranial direction and 10 rows starting from the edge of the hook bone in the ventral direction
Hook bone	Tuber coxae	Side	Hook bone	21 rows and columns with the hook bone as the square center
Pin bone	Tuber ischii	Rear	Pin bone	21 rows and columns with the pin bone as the square center
Thurl area	An area where the pelvis connects to the femur bone through the hip joint	Top	Vertebral column, sacral ligament	From the vertebral column to the center of the hook bone and from the lower edge of the sacral ligament to the end of the body
Spinous processes to hook bone	Ligament connecting the spinous process and the tuber coxae ossis ilium	Top	Vertebral column, hook bone, sacral ligament	From the vertebral column to the center of the hook bone and 11 rows with the centerline of the sacral ligament in the center
Cavity between the tail head and pin bone	An area between the coccyx and tuber ischii in the caudal region	Rear	Tail region, pin bone	From the tail head to the pin bone center and from the top of the tail to the pin bone center

Image Processing.

Raw images were processed by using the Image Processing Toolbox in MATLAB (2017b, MathWorks, Natick, Massachusetts, USA).

Image Rotation and Orthogonal Decomposition. Each raw image provided a depth map with each image pixel containing a distance measurement from the center of the camera lens to the projection of the pixel on an object. The specific pixels projected the body surface of a cow, the floor, other cows in the camera view, or the frame of the image recording setup.

Because the 3 cameras were mounted at different locations in the image recording setup, all the images from different cameras were first transformed from their corresponding camera coordinate systems to that of the image recording setup. The transformation included rotation and orthogonal decomposition. First, the image was rotated by multiplying the rotation matrices (Equation 3-1) with the camera-mounting angle about each axis. The top-view image was rotated 180° about the y-axis and 90° about the z-axis, the side-view image was rotated 160° about the y-axis and 90° about the z-axis, and the rear-view image was rotated 160° about the x-axis. Then, the image was orthogonally decomposed into X, Y, and Z matrices in the image recording setup coordinate system.

$$R_x(\theta_x)=\begin{bmatrix}1 & 0 & 0\\ 0 & \cos\theta_x & -\sin\theta_x\\ 0 & \sin\theta_x & \cos\theta_x\end{bmatrix},\quad R_y(\theta_y)=\begin{bmatrix}\cos\theta_y & 0 & \sin\theta_y\\ 0 & 1 & 0\\ -\sin\theta_y & 0 & \cos\theta_y\end{bmatrix},\quad R_z(\theta_z)=\begin{bmatrix}\cos\theta_z & -\sin\theta_z & 0\\ \sin\theta_z & \cos\theta_z & 0\\ 0 & 0 & 1\end{bmatrix}$$

(Equation 3-1)

where θ_x , θ_y , and θ_z are the clockwise rotation angles and R_x (θ_x), R_y (θ_y), and R_z (θ_z)are the rotation matrices for rotating images about the x-, y-, and z-axes respectively, in 3 dimensions.

Background Subtraction. The background in an image was defined as the pixels that were not projected onto the body surface of the selected cow. The background included the floor, the bodies of other cows, and the recording setup frame. Based on the distance between the camera lens and the pixel projection, these background pixels were removed from all decomposed matrices to retain only the selected cow body surface. For a top-view image, the background pixels were identified from the Z matrix with the selection criteria shown in Equation 3-2. The criteria were determined by estimating the range of body surface heights of all the cows in top-view images. For side- and rear-view images, the background pixels were identified from the X and Y matrices, respectively, with the selection criteria shown in Equation 3-3. After all the background pixels in a matrix were identified, these pixels were discarded by assigning them a value of zero in the X, Y, and Z matrices.

$$Z_{i,j} = \begin{cases} Cow\ body\ surface & 1.8m \geq Z_{i,j} \geq 1.0m \\ Background & 1.8m < Z_{i,j}\ or\ Z_{i,j} < 1.0m \end{cases} \quad \textbf{(Equation 3-2)}$$

$$X_{i,j} = \begin{cases} Cow\ body\ surface & X_{i,j} \geq \overline{X} + SD(X) \\ Background & X_{i,j} < \overline{X} + SD(X) \end{cases} \quad \textbf{(Equation 3-3)}$$

where , $Z_{i,j}$ is a pixel in the *Z* matrix, , $X_{i,j}$ is a pixel in the X matrix, i is the row number of the matrix, j is the column number of the matrix, $\bar{X}$ is the average of all the pixels in the X matrix, and SD (*X*) is the standard deviation of all the pixel values in the X matrix.

Noise Removal. After background subtraction, the matrix retained some pixels that did not belong to the cow body surface but had similar pixel values. These pixels were considered noise and were removed in the following steps. First, a binary matrix was converted from the Z matrix in the top-view image. The conversion assigned a value of 1 to the pixels of the cow body surface and a value of zero to the background pixels. Second, the binary image was processed using the morphological operations of erosion, filling holes, and dilation with a 7 × 7-pixel disk-shaped structuring element. The operations and the size of the structuring element were determined by testing different combinations of operations and sizes and visually inspecting the results for all images of all cows. Third, the binary image was divided into groups of pixels with a value of 1 that were connected to each other. The size of each group was determined as the number of connected pixels, and the group with the largest size was considered the body surface of the cow. The remaining groups were considered noise and were discarded by assigning a value of zero to each pixel in the groups. Fourth, the X, Y, and Z matrices were multiplied by the binary matrix to remove noise in all matrices of the top-view image. Finally, the same procedure was applied to the matrices of the side- and rear-view images.

Image Interpolation. The X, Y, and Z matrices of each image were combined by interpolating them into a 2D mesh grid image. For top-view image interpolation, the grid spacing was 0.005 m in the X and Y directions to guarantee at least 2 pixels in each grid and each direction for a proper interpolation. The boundaries in the X and Y directions of the mesh grid were the minimum and maximum values of the X and Y matrices, respectively. The value of each grid was calculated by triangulation-based linear interpolation of the Z matrix. This 2D mesh grid image could be viewed as a matrix where the rows and columns were represented in the X and Y directions of the recording setup coordinate system and where the size of the matrix element was the same as that of the grid. For side-view image interpolation, the Y and Z matrices were used to produce the mesh grid, and the X matrix was interpolated. For rearview image interpolation, the X and Z matrices were used to produce the mesh grid, and the Y matrix was interpolated.

Anatomical Landmark Identification

Vertebral Column. The vertebrae form a prominent ridge on the cow's body surface. In the lumbar and sacral regions, these vertebrae were viewed as the highest part of the body surface from the top-view Z matrix. To identify the vertebrae, we selected the highest element in each row of the matrix as part of the vertebral spinous processes and combined all these elements as the vertebral column.

Additionally, all the images were standardized because the cows could stand in different positions in the recording setup. We rotated the body surface of the cow in the x-y plane to align its vertebral column with the y-axis of the recording setup (Figure 3-3-A). This rotation procedure included fitting the vertebral column with a linear trend line, calculating the angle θ between the trend line and the y-axis, and multiplying the X, Y, and Z matrices by the rotation matrices with rotation angles 0, 0, and θ about the x-, y- and z-axes, respectively (Equation 3-1).

Sacral Ligament. The sacral ligament is a tendon plate that consists of connective tissues linking the spinous processes and the center of the hook bone. The visible part of the sacral ligament in the Z matrix was viewed as a group of rows, and the highest row was designated the centerline of the sacral ligament. To identify the highest row, we halved the topview Z matrix into left and right regions by the rotated vertebral column. On the right side of the body, the row with the highest mean was considered the centerline of the sacral ligament (the solid line in Figure 3-3-A).

Hook Bone. The palpable and visible part of the hook bone is the tuber coxae. When viewed from above the cow, the tuber coxae prominently extend from the body surface and are located at the iliac crest of the ilium (i.e., the craniodorsal part of the hook bone). The highest point on the tuber coxae projected onto the body surface was designated the center of the hook bone projection and was considered to be located on the centerline of the sacral ligament. To identify the center of this bone, we selected 20 elements on the centerline that were the furthest from the vertebral column in the lateral direction. Among these 20 elements, the one with the largest value was designated the highest point of the tuber coxae and the center of the hook bone (the dot in Figure 3-3-A).

When viewed from the right side of the cow, the tuber coxae prominently extend in the lateral direction. The most distal point of the tuber coxae was designated the center of the hook bone. This point, however, was not the same as the center of the bone from the top view (i.e., the highest point of the ilium). In the side-view X matrix, this point was designated the element with the largest value. We selected the row and column with the highest means and designated their cross element as the center of the hook bone (Figure 3-3-B).

Pin Bone. The palpable and visible part of the pin bone is the tuber ischii. When viewed from the rear of the cow, this structure prominently extends in the caudal direction. The most prominent point of the tuber ischii is the caudal point of the ischium, which we designated the center of the pin bone. In the rear-view Y matrix, this point was designated the element with the largest value other than the tail. Therefore, to identify the center of the pin bone,

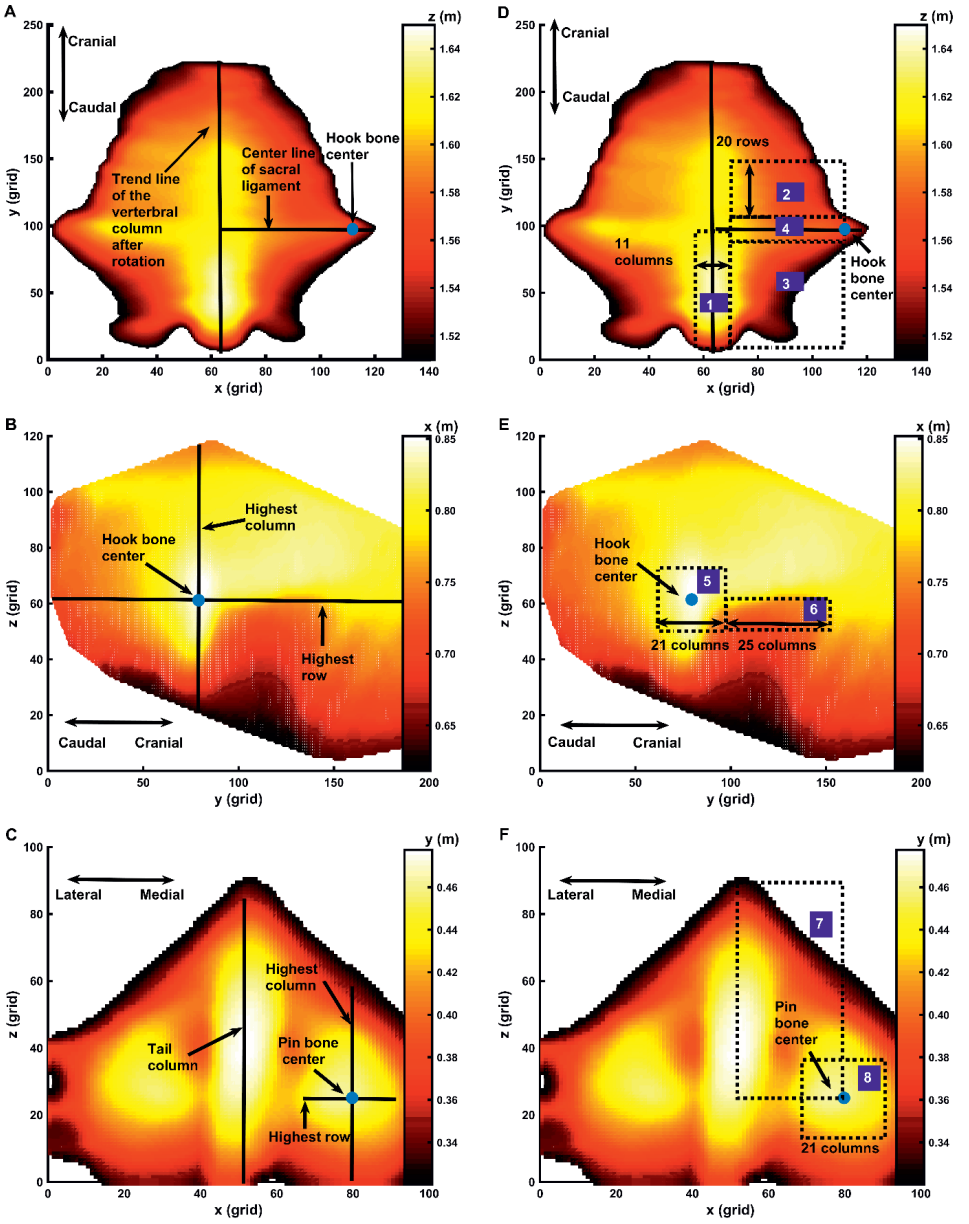

Figure 3-3. Figure 3. Anatomical landmarks on one side of a cow's body in different camera-view images: vertebral column, centerline of the sacral ligament, and hook bone center in a top-view image after image rotation (A), hook bone center in a side-view image (B), tail region and pin bone center in a rear-view image (C). The regions of interest (1. spinous processes, 2. spinous to transverse processes, 3. thurl area, and 4. spinous processes to hook bone) were selected from the top-view image (D). The regions of interest (5. hook bone and 6. overhanging shelf) were selected from the side-view image (E). The regions of interest (7. cavity between tail head and pin bone and 8. pin bone) were selected from the rear-view images (F).

we first identified the tail region by selecting the column with the highest mean and its 5 adjacent columns on both the left and right sides and excluded them from the matrix. Then, the row and column with the highest means were selected on the right half of the matrix, and their cross element was designated the center of the pin bone (Figure 3-3-C).

Feature Extraction

After identifying anatomical landmarks, we measured the bony prominence or the body surface depression around these landmarks and defined those morphological measures as the body-condition-related feature extraction. Within each body region, a rectangular area was selected and defined as a region of interest (**ROI**). The size of the ROI was determined as the distance between the anatomical landmarks located in this ROI. When only 1 anatomical landmark was presented, the size was determined by estimating the maximum size of the ROIs of all cows. The detailed ROI selections are shown in Figure 3-3-D, E, and F for 3 camera views and the selection criteria are listed in Table 3-1. The ROI was designated a matrix, and its averaged row was designated the average cross-sectional contour line of the ROI in the mediolateral direction for the top- and rear-view images and in the craniocaudal direction for the side-view images. The shape of the average contour line was then quantified as a bodycondition-related feature.

Spinous Processes. The bony prominences of the spinous processes were represented by the shape of the average contour line. This contour line was fitted with a second-degree polynomial regression line (Figure 3-4-A) based on Equation 3-4. The coefficient β_2 was always negative because the spinous process was in the middle and always higher than the rest of the parts on the contour line. Additionally, the absolute value of the coefficient β_2 determined the sharpness of the contour line. For an obese cow, the spinous processes were less prominent and the contour line was rounder than for a lean cow. Moreover, the absolute value of the coefficient β_2 was less than the 1 from a lean cow. Thus, β_2 was defined as the spinous process feature.

$$y = \beta_0 + \beta_1 \cdot x + \beta_2 \cdot x^2 \qquad \textbf{(Equation 3-4)}$$

where β_0 , β_1 , and β_2 are the coefficients of the second-degree polynomial regression line and x and y are the coordinates of the points on the average contour line.

Spinous to Transverse Processes. The amount of subcutaneous fat accumulated above the transverse processes was represented by the shape of the average contour line (the solid line in Figure 3-4-B). To quantify this shape, we first drew a straight line (the dashed line in Figure 3-4-B) to connect the 2 ends of the contour line. The height differences between pairs of corresponding points on the 2 lines were averaged and defined as the feature of the area between the spinous and transverse processes.

Thurl Area. The centerline of the thurl area in the medio-lateral direction was designated the average contour line of the ROI. The inclination of the contour line represented the

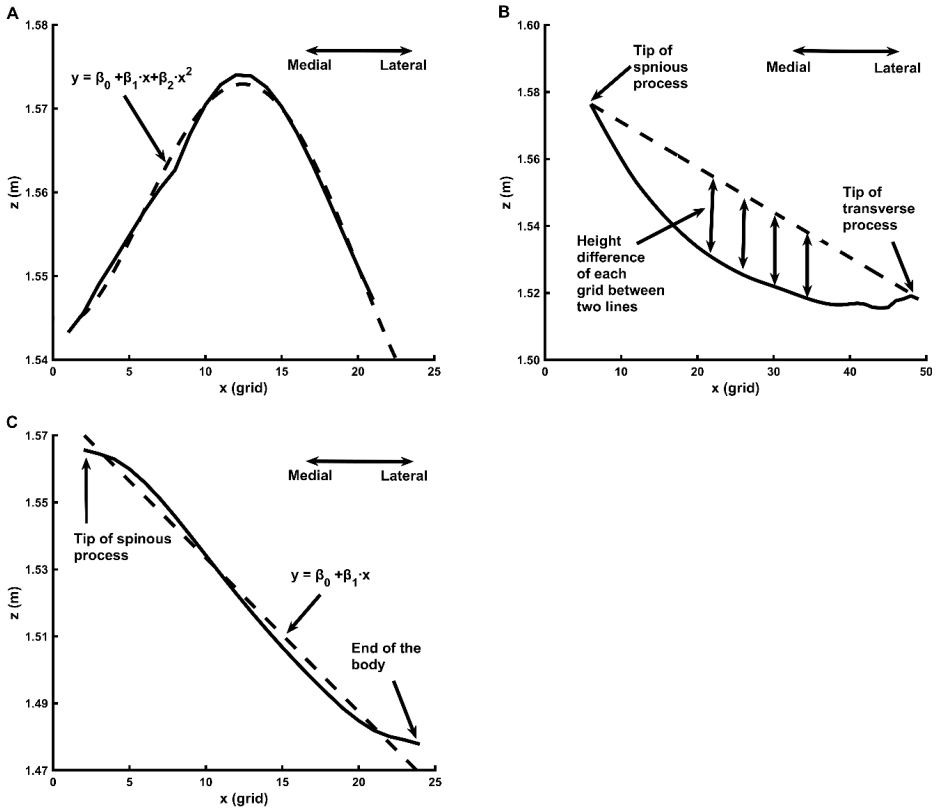

Figure 3-4. Three examples of automated feature extractions: second-degree polynomial fit of the average cross-sectional contour of the spinous processes (A), the average height difference between the spinous and transverse processes (B), and the slope of the centerline of the thurl area (C).

amount of subcutaneous fat accumulated in the area where the pelvis connects to the femur bone through the hip joint. This inclination was quantified by fitting the contour line to a linear regression line (Figure 3-4-C) based on Equation 3-5. For an obese cow, a great amount of subcutaneous fat was accumulated on the thurl area, which caused minor inclination of the contour line. For a lean cow, little or no subcutaneous fat was accumulated on the thurl area, which caused a great inclination of the contour line. The coefficient β_1 was the slope of the regression line and defined as the thurl area feature.

$$y = \beta_0 + \beta_1 \cdot x \qquad \textbf{(Equation 3-5)}$$

where β_0 and β_1 are the coefficients of the linear regression line and x and y are the coordinates of the points on the average contour line.

Spinous Processes to Hook Bone. The amount of subcutaneous fat accumulated in the sacral ligament area was represented by the shape of the average contour line. This shape was quantified as the height difference between the hook bone center and the mean of the contour line. This height difference was defined as the feature of the area between the spinous processes and the hook bone.

Hook Bone. The bony prominence of the tuber coxae was represented by the shape of the average contour line. This shape was quantified using the same procedure as that for the spinous processes by fitting the contour line with a second-degree polynomial regression line based on Equation 3-4. The absolute value of the coefficient β_2 was defined as the hook bone feature.

Pin Bone. The shape of the average contour line was quantified using the same procedure as that for the hook bone based on Equation 3-4, and the absolute value of the coefficient β_2 was defined as the pin bone feature.

Overhanging Shelf. Around the overhanging shelf, the bony prominence of the overhanging shelf was represented by the shape of the average contour line. Similar to the spinous to transverse processes, this shape was quantified by calculating the height difference between the hook bone center and the mean of the contour line from the side view. This height difference was defined as the overhanging shelf feature.

The cavity between Tail Head and Pin Bone. The amount of subcutaneous fat accumulated in the cavity between the tail head and pin bone was represented by the shape of the average contour line. This shape was quantified by calculating the largest height difference between the pin bone center and the mean of the contour line from the rear view. The height difference was defined as the feature of the cavity between the tail head and pin bone.

Statistical Analysis

Intra- and Inter-Assessor Agreement and Correlation for Manual Body Condition Scoring. The quality of manual body condition scoring of the 2 assessors was quantified by the scoring agreement Cohen's kappa (κ) and the scoring correlation coefficient Spearman's rho (ρ). The agreement of a scoring is defined as the identical half-point BCS that is assigned in a pair of scorings. Cohen's κ measures the pairwise agreement of 2 assessors or 1 assessor across 2 days, including the possibility of agreement occurring by chance. The interpretation of the κ value was the one used in the study of Altman (1990). Spearman's ρ is a pairwise rank correlation coefficient and is defined as the statistical dependence between the rankings of 2 manual scores without interference from the systematic scoring difference. The ρ value ranges from 1 (i.e., a pair set of scores with identical ranks) to -1 (i.e., a pair set of scores with completely opposite ranks). Both κ and ρ values were calculated for intra-assessor comparison of each assessor's scores between days 1 and 2, and for inter-assessor comparison of the twoday average scores between assessor 1 and assessor 2.

Test-Retest Reliability of Automated Feature Extraction. Test-retest reliability of feature extraction is used to quantify the closeness of the results of successive extractions over 2 days performed under the same conditions. For each feature, test-retest reliability was assessed by calculating Pearson's correlation coefficient (r) of this feature across all the cows quantified between days 1 and 2. On each day, this feature of each cow was the average of the extractions from the 5 images.

Correlation between Manual BCS and Features. For each body region, the correlation between the manual BCS and the automatically extracted feature on each day was quantified by the pairwise rank correlation coefficient Spearman's ρ. For each cow, a feature was the average of the extractions from the 5 images of 1 day, and the manual BCS was the average of the scores assigned by the 2 assessors on the same day.

Half-point Overall BCS classification. The overall BCS of a cow was classified with a k-nearest (k = 1) neighbor classification model. The inputs of the model were 8 automatically extracted features, and each feature of a cow was the average of the extractions from the 5 images. The reference of the model was the average of the manual BCSs assigned by both ssessors on that day. The model with 8 features as inputs was defined as the full model.

To test this model, we built a dataset of 88 samples including the data of all 44 cows from 2 days. The model was tested on this dataset using a 10-fold cross-validation. In each iteration of the cross-validation, 90% of the samples were used to train the model and 10% were used to test the model. For each testing sample, the model assigned a half-point BCS from the reference BCS of its closest neighbor sample in distance in the training dataset. The distance between these 2 samples was the normalized Euclidean distance calculated in a Euclidean 8-space with all 8 inputs of a sample as the Cartesian coordinates.

After cross-validation, all the samples had a model classified half-point BCS and a reference BCS from manual scoring. The samples were divided into 9 half-point BCS classes anging from 1.0 to 5.0, where all the samples with the same reference half-point BCSs were in 1 class. For each class, the samples with the model-classified BCS being identical to the reference BCS were defined as true positives (**TP**) and the samples with the model-classified BCS different from the reference BCS were defined as false negatives (**FN**). The quality of the model classification in this reference BCS class was tested by the sensitivity, which was defined as the fraction of the number of TPs over the number of all the cows with the same reference BCS in this class and calculated based on Equation 3-6:

$$Sensitivity_q = \frac{TP_q}{TP_q + FN_q} \qquad \textbf{(Equation 3-6)}$$

where *q* is a half-point reference BCS that all the samples have in 1 class, $Sensitivity_q$ is the sensitivity of the model classification in the class with reference BCS equal to q, TP_q is the number of samples with both model classified and reference BCS equal to q, and FN_q is the

Table 3-2. Intra- and inter-assessor agreements and correlation coefficients for manual body condition scoring and the test-retest reliability of automated feature extractions

Scoring agreement, scoring correlation coefficient, and testretest reliability***		Spinous processes	Spinous to transverse processes	Overhanging shelf	Hook bone[1]	Pin bone[1]	Thurl area	Spinous processes to hook bone	Cavity between tail head and pin bone	Overall body condition score
Intra-assessor 1	Cohen's kappa	0.54	0.52	0.46	0.43	0.43	0.52	0.35	0.52	0.52
	Spearman's rho	0.95	0.93	0.88	0.91	0.91	0.94	0.93	0.96	0.95
Intra-assessor 2	Cohen's kappa	0.49	0.43	0.51	0.67	0.67	0.54	0.37	0.44	0.72
	Spearman's rho	0.91	0.90	0.89	0.96	0.96	0.94	0.94	0.94	0.96
Intra-assessor	Cohen's kappa	0.36	0.38	0.40	0.33	0.33	0.36	0.41	0.31	0.48
	Spearman's rho	0.91	0.88	0.88	0.93	0.93	0.90	0.91	0.92	0.95
Feature extraction	Pearson's r	0.97	0.97	0.89	0.94	0.93	0.94	0.94	0.92	

[1] The hook bone and pin bone were assessed together and assigned 1 score in manual body condition scoring
***$P < 0.001$ for all calculations of scoring agreement, scoring correlation coefficient, and test-retest reliability.

Table 3-3. Absolute correlation coefficients (Spearman's rho) between automatically extracted features and manual body condition scores

Absolute correlation coefficients Spearman's rho (ρ)***	Spinous processes	Spinous to transverse processes	Overhanging shelf	Hook bone	Pin bone	Thurl area	Spinous processes to hook bone	Cavity between tail head and pin bone
Features and manual score of corresponding body regions	0.89	0.81	0.76	0.85	0.83	0.69	0.88	0.88
Features and overall manual body condition score	0.90	0.83	0.73	0.87	0.83	0.72	0.84	0.85

***$P < 0.001$ for all the of correlation coefficient calculations.

number of samples with the reference BCS equal to q and model classified BCS different from q. Moreover, the overall sensitivity of the nearest neighbor classification model was calculated by averaging the sensitivity of all the half-point BCS classes.

For comparison with the full model, we built another nearest neighbor classification model with inputs of features extracted from body regions of the spinous processes, hook bone, pin bone, and the cavity between the tail head and pin bone. These body regions have been used in other studies to automated body condition scoring using machine vision. This model with 4 features as inputs was defined as the partial model. This model was also validated by a 10-fold cross-validation and tested by calculating the sensitivity of each half-point BCS class.

3.3 Results

We compared the intra- and inter-assessor agreements and correlation coefficients of the manual body condition scoring of the 2 assessors (Table 3-2). Assessor 1 scored 8 of 9 body regions, including the overall BCS, with a moderate intra-assessor agreement (i.e., κ values between 0.40 and 0.59). Assessor 2 scored 3 body regions, including the overall BCS, with a good intra-assessor agreement (i.e., κ values between 0.60 and 0.79) and 5 body regions with a moderate intra-assessor agreement. Both assessors scored the body region of the spinous processes to the hook bone with the lowest κ value compared with the rest of the body regions. In comparing the 2 assessors, 2 of 9 body regions were scored with a moderate inter-assessor agreement, 6 of 9 body regions were scored with a fair inter-assessor agreement (i.e., κ values between 0.20 and 0.39), and the overall BCS was scored with a moderate inter-assessor agreement ($\kappa = 0.48$, $P < 0.001$). Additionally, both assessors scored 8 of 9 body regions, including the overall BCS, with high intra- and inter-assessor correlation coefficients (i.e., $\rho > 0.90$). The body region with the lowest intra- and inter-assessor ρ values was the overhanging shelf. In addition, the result of test-retest reliability of the automated feature extraction was the Pearson's correlation coefficient between days 1 and 2 for the indicated feature (Table 3-2). Among all features, 7 of 8 were extracted with a Pearson's r value greater than 0.90 ($P < 0.001$), and the overhanging shelf feature extraction had the lowest r value of 0.89 ($P < 0.001$).

The correlations between the body features and the manual BCSs were quantified with Spearman's ρ (Table 3-3). The ρ values calculated for the manual BCSs of the corresponding body regions were similar to the overall BCS. A comparison of the ρ values in all body regions revealed that the spinous processes had the highest absolute ρ values for both the manual BCSs of this body region (0.89, $P < 0.001$) and the overall BCS (0.90, $P < 0.001$). In contrast, the thurl area had the lowest absolute ρ values for both the manual BCS of this body region (0.69, $P < 0.001$) and the overall BCS (0.72, $P < 0.001$).

The correlations between the features and the manual BCSs of their corresponding body regions are presented in Figure 3-5. The spinous process feature had almost equal

Table 3-4. A confusion matrix1 with the numbers of samples classified in half-point BCS classes resulting from the k-nearest neighbor (k = 1) body condition score (BCS) classification model with all 8 features as inputs (i.e., the full model)

Manual BCS	Model classified BCS									Total	Sensitivity
	1.0	1.5	2.0	2.5	3.0	3.5	4.0	4.5	5.0		
1.0	2									2	1
1.5		7	4							11	0.64
2.0		3	8							11	0.73
2.5				12	4					16	0.75
3.0				2	9	2	1			14	0.64
3.5					3	6	2			11	0.55
4.0					1	1	8			10	0.85
4.5							2	11		13	0.85
5.0											

[1] An empty cell indicates no cows.

Table 3-5. A confusion matrix1 with the numbers of samples classified in half-point BCS classes resulting from the k-nearest neighbor (k = 1) body condition score (BCS) classification model with features of spinous processes, hook bone, pin bone, and the cavity between the tail head to pin (i.e., the partial model)

Manual BCS	Model classified BCS									Total	Sensitivity
	1.0	1.5	2.0	2.5	3.0	3.5	4.0	4.5	5.0		
1.0	2									2	1
1.5		8	2	1						11	0.73
2.0		2	9							11	0.82
2.5				12	4					16	0.75
3.0				4	6	4	0			14	0.43
3.5					4	6	1			11	0.55
4.0					2	1	6	1		10	0.60
4.5				1			1	11		13	0.85
5.0											

[1] An empty cell indicates no cows.

average values for the cows in the half-point BCS classes from 3.5 to 5.0. This feature varied less for the obese cows than for the lean cows. A similar trend was found for the pin bone feature. In contrast, the hook bone feature had almost equal average values for the cows in the half-point BCS classes from 1.0 to 2.0. This feature varied less for the lean cows than for the obese cows. A similar trend was also found for the feature of the spinous processes to the hook bone. For the feature of the spinous to transverse processes, cows could be classified into 3 main groups: those within the half-point BCS classes from 1.0 to 2.5, those with the half-point BCS class 3.0, and those within the half-point BCS classes from 3.5 to 5.0.

The results of half-point overall BCS classification using nearest neighbor classification models are the numbers of cows in the confusion matrix. The full model included all 8 features as inputs and the overall manual BCS as a reference. After the 10-fold cross-validation, this model yielded an overall sensitivity of 0.72 for all the samples in all the half-point BCS classes. In the confusion matrix (Table 3-4), the highest sensitivity was 1 for half-point BCS class 1.0, and the lowest sensitivity was 0.55 for half-point BCS class 3.5. The partial model included only the features of the spinous processes, hook bone, pin bone, and tail head to pin bone as inputs and the overall manual BCS as a reference. After the 10-fold cross-validation, the partial model yielded an overall sensitivity of 0.68 for all the samples in all the half-point BCS classes. In the confusion matrix (Table 3-5), the highest sensitivity was 1 for half-point BCS class 1.0, and the lowest sensitivity was 0.43 for half-point BCS class 3.0.

3.4 Discussion

Improvement of Automated BCS Classification

This study aimed to improve the automated BCS classification by expanding the inclusion of the body-condition-related features extracted from multiple body regions using 3D cameras. The validation results of the BCS classification model with 8 features (i.e., the full model) were compared to the results reported in previous 2D and 3D vision-based studies and the results of our partial model with 4 features.

First, our full model yielded a BCS classification sensitivity of 0.72. This classification sensitivity is greater than that reported by Bercovich et al. (2013), who used 2D vision to quantify the bony prominences on the body contour and obtained a sensitivity of 0.53. The differences between our results and those of Bercovich et al. (2013) demonstrate 2 limitations of classifying BCSs using 2D vision. The first limitation is related to the assessed body regions. Studies using 2D vision aimed to extract the 2D body contour and to quantify the bony prominences of the hook bones, pin bones, and tail head. The surfaces of many body regions that are related to the BCS, however, cannot be quantified or included in BCS classification. The reason is that these surfaces are not located on the body contour, and thus the surface depression cannot be recorded in the 2D images. The lack of sufficient BCS-related information caused the low sensitivity of the BCS classification using 2D vision. The second limitation is related to the bony prominences quantification from the body contours

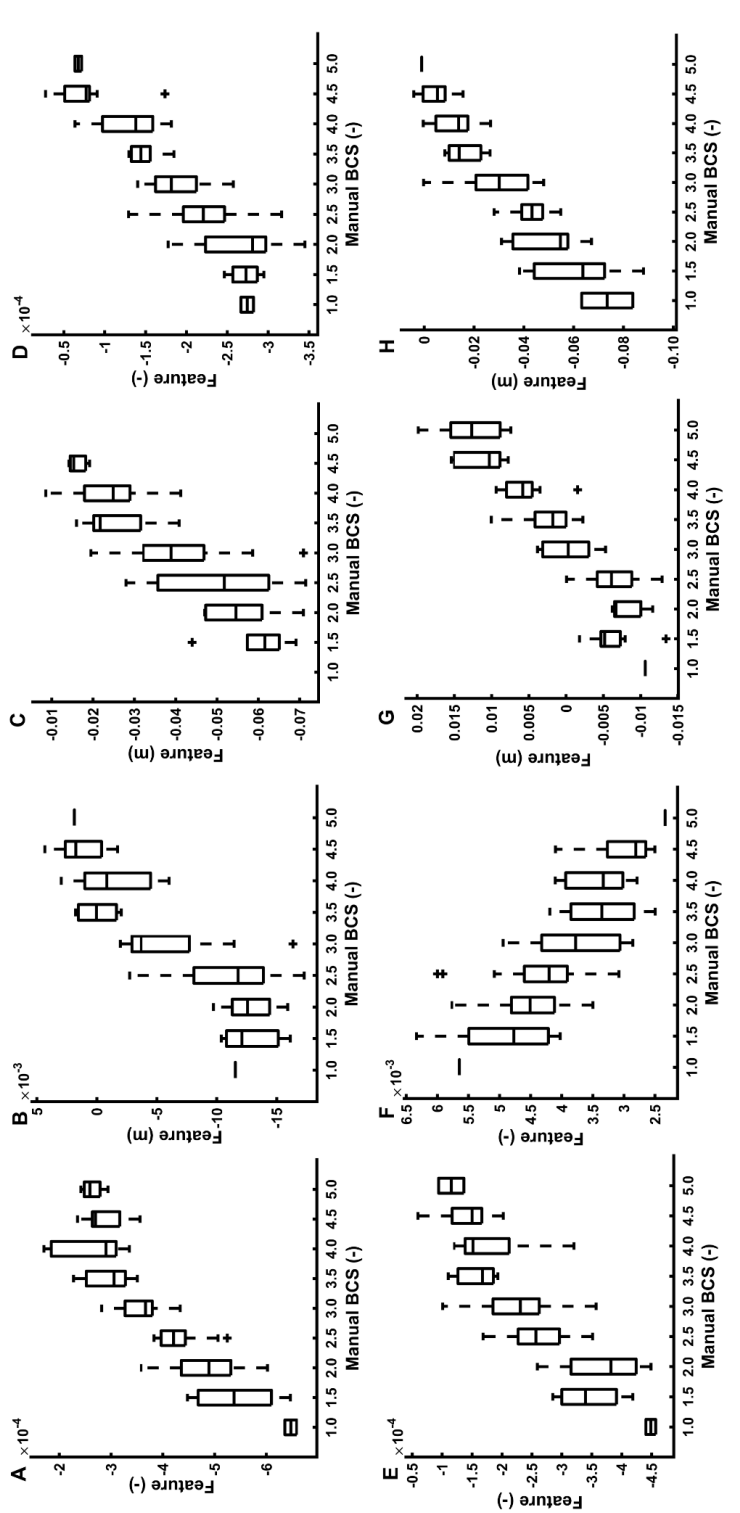

Figure 3-5. IBox plots of manual BCS in the 8 body regions versus the corresponding automatically extracted features: spinous processes (A), spinous to transverse processes (B), overhanging shelf (C), hook bone (D), pin bone (E), thurl area (F), spinous processes to hook bone (G), and tail head to pin bone (H). On each box, the central mark in each box indicates the median of all the feature values with certain manual BCS. The bottom and top edges of the box indicate the 25th and 75th percentiles of the feature values, respectively. The whiskers extend to the most extreme data points that are not considered outliers. The outliers in the feature values are plotted individually using the '+' symbol

projected onto a 2D plane. The body contour varies in the 2D plane when a cow's posture varies, which can introduce extra measurement variation in the features extracted from fixed-position cameras and reduce the sensitivity of the BCS classification. To address these limitations of 2D vision, we recommend using 3D vision to extract body-condition-related features for BCS classification.

Second, we evaluated the BCS classification model by calculating the sensitivity of the classification. Different from our statistical analysis, previous 3D vision-based studies chose regression models to predict BCS and calculated the mean absolute error (**MAE**) between the model outputs and reference of all their samples. Considering BCS as an ordinal variable, the classification sensitivity should be the valid statistical measure instead of the MAE. However, to be able to compare our BCS classification performance to those of other studies, we have to calculate the MAE of our full model as well. Our full model yielded an MAE of 0.15 BCS units, which is less than the MAE of 0.28 BCS units reported by Fischer et al. (2015), 0.26 BCS unit reported by Spoliansky et al. (2016), and 0.21 BCS unit reported by Hansen et al. (2018). These error differences may be due to the differences in the body regions used to extract features. Previous 3D vision-based studies recorded and analyzed cow body surfaces from the top view with only 1 3D camera. In top-view images, however, some important body regions are not completely visible, such as the overhanging shelf, hook bone, pin bone, and the cavity between the tail head and pin bone. Hence, features representing these body regions were neither extracted from these body regions nor included in the BCS classification. In contrast to the top-view recording, the body prominences and surface depressions in these regions are more visible from either the side or rear of a cow's body. Therefore, to improve the current 3D vision-based BCS classification, features should be retrieved from more than 1 camera placed
at different viewpoints.

Finally, the discrepancy in the results between our study (i.e., the full model) and previous studies may also be due to the different models selected. We selected a classification model because BCS is defined as an ordinal variable. The appropriateness of defining BCS as an ordinal variable can be observed in the boxplots (Figure 3-5), which show a variety of correlations between different features and manual BCSs. Previous studies, however, considered BCS a continuous variable and selected linear regression models to predict BCS. The model selections cause the results to incorrectly represent the BCS-predictive abilities of the extracted features. Therefore, it is not accurate to directly compare the BCS classification results among studies. For a valid comparison, we used the partial model to simulate the BCS classification by limiting the selection of the assessed body regions in the current machine vision-based studies. The partial BCS classification model yielded lower sensitivity than what was achieved with our full model including features in 8 body regions. The difference in BCS classification sensitivity between the full and partial models demonstrates the improvement in BCS classification when features are extracted in multiple body regions.

Multiple 3D Camera System

To capture the BCS-related information that cannot be captured by using a single 3D camera, we chose to use multiple 3D cameras in this study. The use of multiple cameras can improve the BCS classification because they mimic human assessors evaluating different body regions of a cow from different views. This multi-camera approach to cow morphological measurements and feature extraction is consistent with studies by Guo et al. (2017) and Salau et al. (2017). Moreover, during our data collection, images from different cameras were recorded 1 at a time to prevent inter-camera interference. We also minimized the time that the cows were required to stand in the recording setup by recording only 5 images per camera per cow. The total recording time for 1 cow was approximately 1 minute, including the time spent for initializing the cameras and saving the recorded images. During the one-minute image recording, the cow could still move in the setup, which can influence the quality of the image and feature extraction. In future studies, new types of 3D cameras without inter-camera interference should be used for simultaneous image recording by multiple cameras, which will significantly reduce the recording time and improve the quality of feature extraction.

Cow Selection Influencing the Sensitivity of the BCS Classification

The design of this study included the selection of cows that could contribute to a heterogeneous dataset with evenly distributed BCSs in the samples. Our cow selection plan differed from those of previous studies, which collected homogeneous datasets of all the cows in a herd. Depending on the herd, the number of cows in different BCS classes can vary substantially. For the underrepresented BCS classes (i.e., less than 2.0 units or greater than 4.0 units), the sensitivities of the BCS classification can be biased. To prevent inducing a sensitivity bias, we built the dataset with the numbers of cows evenly distributed in the BCS classes ranging from 1.5 to 4.5. Hence, the sensitivities of the classification for BCS classes 1.5 and 4.5 were more reliable than the ones calculated from the homogeneous datasets. Nevertheless, our study had fewer cows with extreme BCS values. There was only 1 cow with a BCS of 1.0 unit and no cow with a BCS of 5.0 units in the dataset. Although lacking cows with extreme BCS values is common on commercial farms, we must employ sufficient samples with extreme BCS values in future studies because cows in those less-represented BCS classes are also the ones that need extra attention in farm management.

Additionally, most of the selected cows in this study were Holstein Friesian cows (n = 33) with BCSs ranging from 1.0 to 3.5. It was difficult to find many obese Holstein Friesian cows to contribute to an evenly distributed BCS dataset. Therefore, we chose a farm with Simmental cows and selected 11 cows with BCSs ranging from 3.5 to 4.5. By including 2 breeds in the dataset, we created a breed variance in the BCS class of 3.5 units. We assumed the breed variance caused the lowest classification sensitivity (i.e., 0.55) on the BCS class of 3.5. Hence, we recommended including breed variance in future BCS classification models or building a breed-specific body condition scoring system.

Quality of Manual Body Condition Scoring

The 2 assessors in this study were trained together by an expert using a detailed protocol for manual body condition scoring. We found that the inter-assessor agreement for the overall BCS was moderate, and the correlation coefficient reached 0.95, which is greater than the value found in a study by Halachmi (2013). Additionally, we found the same trend of a moderate agreement with a high-rank correlation coefficient for the intra-assessor scoring of both assessors. Therefore, the quality of the overall BCSs assigned by our 2 assessors was acceptable. However, their scoring agreement and rank correlation coefficient indicated the presence of systematic differences in their scoring, which were reduced by averaging the BCSs of the 2 assessors in our study. The use of 2 assessors for reference BCSs was consistent with the recommendation of Morin et al. (2017), who stated that more than 1 assessor should be used to obtain accurate BCSs.

Future Work

This cross-sectional study is an intermediate step towards a fully automated system that can continuously measure dynamic variations in body fat reserves of cows. In this step, we aimed to find body features, which were highly correlated with body condition. The manual BCS was used as the reference of this study because alternative solutions (e.g. ultrasonography) were not feasible to offer a comprehensive fat measurement on all the body regions we needed. The manual BCS, however, is an ordinal variable and its smallest increment is 0.25 BCS units (Edmonson et al., 1989). Furthermore, we had an increment of 0.5 BCS units based on the scoring abilities of our assessors. When an automated BCS classification uses manual BCS as a reference, the automated method is limited and cannot detect any BCS variation less than the increment of its reference. The automatically extracted features used in the automated classification, however, are continuous variables and can continuously represent body condition variations in different body regions without the limitation of the manual scoring increment. Therefore, in future work, we suggest conducting longitudinal studies focusing on detecting the variations of the body features found in this study. These variations are continuous variable and can be an important health indicator of dairy cows.

3.5 Conclusions

This study used BCS as an ordinal variable and included all the extracted features from multiple 3D cameras in a BCS classification model. We increased the sensitivity of BCS classification compared to that reported for current machine vision-based body condition scoring methods.

3.6 Acknowledgements

This research was funded by Lely Industries N.V. (Maassluis, the Netherlands). The authors would like to thank Daniel Herd and Janine Niehaus from Lely Deutschland GmbH in Waldstetten, Germany, for their contributions in arranging farm visits for data collection; A.C.M. Meeuwesen, Beatrice Cortesi, E.J.P.M. Leijdekkers, Friso van Ooststroom Brummel, and Pierre Natur from Lely Innovation in Maassluis, The Netherlands, for their contributions in data collection on the farms; F.A. Steenstra from the Animal Production Systems Department of Wageningen University and Research, The Netherlands, for her contribution in training the 2 assessors in body condition scoring; Jose Gomez Lopez from Madrid, Spain, for his contribution in developing the image recording algorithm; and 4 anonymous dairy farmers from Germany and The Netherlands, for cooperating with data collection on their farms.

Chapter 4

Automated Assessment of Reticulo-Ruminal Motility in Dairy Cows using 3-Dimensional Vision

X. Song
P.P.J. van der Tol
P.W.G. Groot Koerkamp
E.A.M. Bokkers

Published as Hot Topic in Journal of Dairy Science, Volume 102, Issue 10, Pages 9076–9081,

Abstract

Reticulo-ruminal motility is a well-established indicator of gastrointestinal health in dairy cows. The currently available methods to assess this motility are labor-intensive, costly, and impractical to use regularly on all cows on a farm. We hypothesized that the reticulo-ruminal motility of dairy cows can be assessed automatically and remotely by using a low cost 3-dimensional (3D) camera. In this study, a 3D vision system was constructed and mounted on the frame of an automatic milking robot to capture the left paralumbar fossa of 20 primiparous cows individually. For each cow, the system recorded 3D images at 30 frames per second during the milking process. Each image was automatically processed to locate the region of the left paralumbar fossa and to quantify the average concavity in the region. The average concavity values from all images of 1 cow during 1 milking process were chronologically assembled to form an undulation signal. By applying a fast Fourier transformation to the signal, we identified cyclic oscillations in the signal that occurred in the same frequency range as the reticulo-ruminal contractions. To validate the oscillation identification, 2 trained assessors visually identified the reticulo-ruminal contractions from the same 3D image recordings on screen. The matching sensitivity between the automatically identified oscillations and manually identified reticuloruminal contractions was 0.97. In conclusion, the 3D vision system can automate the assessment of the reticulo-ruminal motility of dairy cows. It is non-invasive and can be implemented on farms without distressing cows. This automated system is a promising tool for farmers to obtain regular information about the gastrointestinal health status of individual cows and can help them in their daily farm management.

Key words: dairy cattle, automatic, ruminal motility, 3D camera

4.1 Introduction

The reticulo-rumen is the first chamber in a dairy cow's gastrointestinal tract. It provides an anaerobic environment for the microbial fermentation of ingesta and ensures a consistent flow of ingesta in the gastrointestinal tract through its cyclic contractions (Hungate, 1966). The reticuloruminal contractions comprise 2 parts: a primary contraction starting from the reticulum and passing across the rumen to mix and circulate ingesta for rumination and digestion and a secondary contraction occurring only in the rumen for eructation (Ruckebusch and Thivend, 1980). The strength and duration of reticulo-ruminal contractions are positively correlated with the amount of ingesta in the reticulo-rumen, whereas the frequency of the contractions indicates the digestive ability and health of the reticulo-rumen (Ruckebusch and Thivend, 1980). In a healthy cow, the contractions occur approximately 1 to 3 times per minute, with a high frequency during feeding and a low frequency during rest (Ruckebusch and Thivend, 1980). When a cow suffers certain diseases, such as ruminal acidosis, tympany, or endotoxemia, its reticulo-ruminal motility can be inhibited or even ceased because of the rumen distension or the increased ruminal volatile fatty acid (Meyer and Bryant, 2017). Hence, reticulo-ruminal motility is a well-established indicator of gastrointestinal health in dairy cows.

Reticulo-ruminal motility is often examined by veterinarians via simultaneous auscultation and palpation on the left paralumbar fossa (Ruckebusch and Thivend, 1980). This examination is only performed when a cow shows certain clinical symptoms and is not applied for routine health assessment. The examination of all cows on a farm by veterinarians is time-consuming and hence costly to perform. Braun et al. (2018) combined ultrasonographic and radiographic rumen scanning to shorten the physical examination time. However, similar to the manual examination, this technique is impractical and costly for regular application on cows.

A recent study used a low-cost 3-dimensional **(3D)** camera to automatically quantify the concavity of certain body surfaces of a dairy cow from a single image (Song et al., 2019a). Such a non-invasive technique has the potential to quantify the changes in concavity over time from a sequence of images in a video. An example of changes in concavity is the undulation of the left paralumbar fossa, which represents the reticulo-ruminal contractions. We hypothesized that the reticulo-ruminal motility of dairy cows can be assessed automatically and remotely by quantifying the undulation of the left paralumbar fossa using a low-cost 3D camera.

4.2 3D Vision System

A 3D vision system was designed to capture the morphology of a cow's left paralumbar fossa. The system comprised a 3D depth camera (Realsense D415, Intel, Santa Clara, California, USA) connected to and controlled by a recording computer through a USB 3.0 port. The

camera had a depth detection, an output resolution of 1280 × 720 pixels, and field-of-view angles of 69° × 43° × 77° (horizontal × vertical × diagonal). The camera was mounted on the left fence of an automatic milking robot (**AMS**, Astronaut A5, Lely Industries N.V., Maassluis, The Netherlands), the arm of which approached the cow from the right side of its body. The camera captured the view of the left paralumbar fossa of a cow in the AMS from above at a 30° angle to the horizontal plane (Figure 4-1). This 3D vision system was installed 1 month prior to data collection to habituate cows to the hardware changes in the AMS.

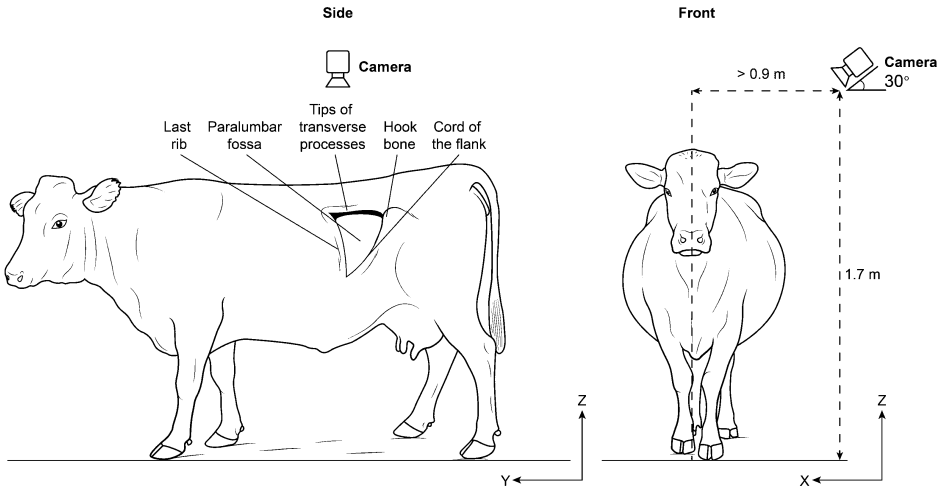

Figure 4-1. The mounting positions and angles of the 3-dimensional camera used to view the cow's left paralumbar fossa. The camera was mounted at least 0.9 meters away from the center of the cow in the X direction to guarantee a complete view of the left paralumbar fossa. In addition, the camera was mounted 1.7 m above the floor at a 30° angle to the horizontal plane.

4.3 Data Collection

Twenty primiparous cows (Holstein × Swiss-Brown) at 1 to 200 days in milk from 1 herd were recorded once with the vision system on a Dutch commercial farm on 28th June 2018 from 1100 to 1600 h. On that day, each cow was fed approximately 40 kg of fresh feed consisting of grass, maize, hay, and barley with a feed ration of 5:3:1:1 on a wet basis. The feed was supplied 4 times at 0400, 1000, 1600, and 2200 h by an automatic feeding robot (Vector, Lely Industries N.V.). The cows were also fed concentrate in the AMS. The amount of concentrate provided to each cow was determined based on its lactation stage and milk yield of the previous day. Among the 20 cows, the average amount of concentrate provided

during image recording was 2.4 kg, with a minimum of 0.7 kg, a maximum of 3.0 kg, and an SD of 0.5 kg.

When a cow entered the AMS and the milking process started, the AMS sent a digital signal to the recording computer to activate the 3D camera to take depth images at 30 frames per second. When the first teat cup detached from the cow, the AMS sent another signal to stop the recording. Among the 20 cows, the average image recording time was 4.3 minutes, with a minimum of 1.8 minutes, a maximum of 7.0 minutes, and an SD of 1.4 minutes. After the cow leaving from the robot, the recorded data, including all captured 3D depth images, cow identification number, and time of the recording, was saved on the computer.

4.4 Image Processing

The 3D camera captured a cow's body surface in raw depth images. Each image was a point cloud with a resolution of 1280 × 720 pixels. The depth value of each point was a 3D distance measured from the center of the camera lens to the projection of the point on the cow's body surface. Each image was processed by using an image processing script that we developed in MATLAB (2018b, MathWorks, Natick, Massachusetts, USA).

1. We downsized each point cloud to a resolution of 128 × 72 pixels to increase the image processing speed. The downsizing method was a bi-cubic interpolation in which each output point was the weighted average of all the points in the nearest 4-by-4 neighborhood surface area from the original point cloud.

2. The downsized point cloud, containing 3D depth values, was orthogonally decomposed to X, Y and Z coordinates. Thereafter, the X, Y, and Z coordinates were converted to a same-size matrix containing the estimated surface curvatures to represent the geometry of the point cloud (Figure 4-2). This conversion was based on the procedure of 'estimating surface normal and curvature in a point cloud' described by Rusu (2009). In the conversion, each point (p) of the downsized point cloud was selected as a center point of a plane. This plane was fitted by p and its 9 nearest neighbors with the shortest 3D Euclidean distance calculated based on the X, Y, and Z coordinates. On each 10-point fitted plane, a normal vector that was perpendicular to the plane was determined for each of the 10 points. Thereafter, the absolute length variance of these 10 normal vectors was calculated as the approximation of the surface curvature around the selected point p. A matrix containing the estimated surface curvatures of all the points in the downsized point cloud was constructed and defined as the curvature matrix.

3. From the curvature matrix of the first recorded image of the first recorded cow in the AMS, we manually selected a template that included the cow's last rib, transverse processes, and part of the left paralumbar fossa between these 2 bones. This template was a square, with the top of the cow's last rib as its upper left vertex (Figure 4-2). The square side length was set at half the distance between the top of the last rib and the hook bone

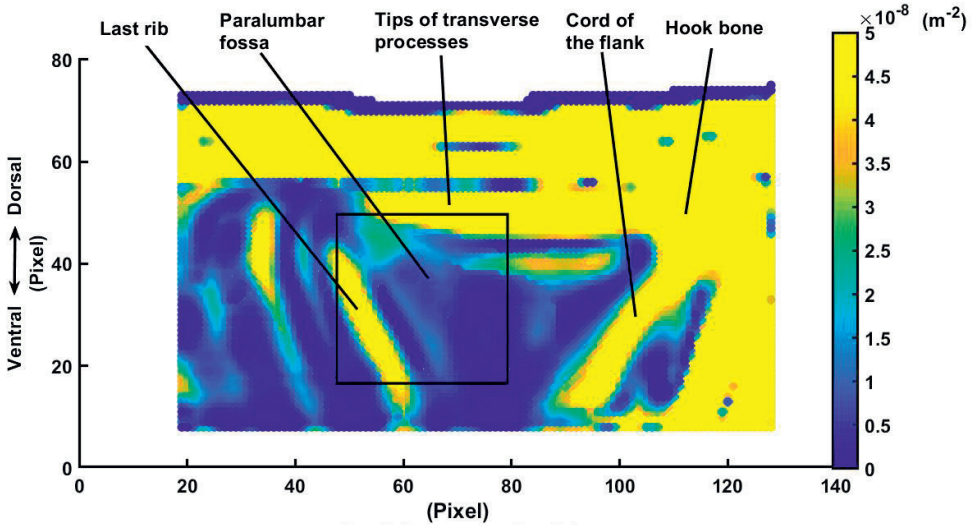

Figure 4-2. An example of the downsized point cloud containing the estimated surface curvatures of all the points used to represent the geometry of a cow's left paralumbar fossa. The point cloud recorded the left paralumbar fossa and surrounding outstanding bone landmarks. A square template was manually fitted with its upper left vertex at the top of the cow's last rib. The square side length was set as half the distance between the top of the last rib and the hook bone center.

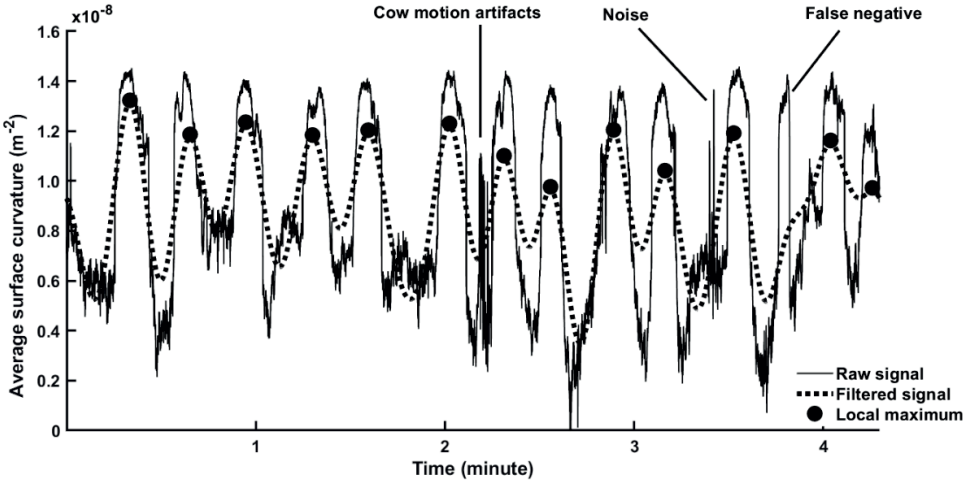

Figure 4-3. Signal processing using fast Fourier transformation to extract the reticulo-ruminal contractions of a cow. The solid line is a raw signal that was formed by chronologically assembling the average surface curvatures of the left paralumbar fossa over time. The dotted line is the filtered signal resulting from fast Fourier transformation filtering of only the information within the frequency range (0.017 to 0.050 Hz) of the reticulo-ruminal contractions. The dots on the dotted line are the local maxima identified using the 'findpeaks' function in MATLAB (2018b, MathWorks, Natick, Massachusetts, USA). Examples of cow motion artifacts, image noise, and a false negative are labeled on the raw signal.

center. The template overlaid a body region with unique morphological features and was used to consistently locate the same region on all cows.

4. The template was matched to each subsequent curvature matrix. This matching was quantified by a normalized two-dimensional cross-correlation between the template and any region of the same size as the template (Taylor et al., 2015). The region showing the highest crosscorrelation with the template was then labeled as the matched region of interest (**ROI**). This ROI had the greatest morphological similarity to the template among all the regions and contained the morphological feature of the left paralumbar fossa. Hence, we considered the ROI in the curvature matrix overlying the left paralumbar fossa, and the concavity of the ROI was quantified by averaging the estimated surface curvatures of all the points in the ROI.

4.5 Signal Processing

We chronologically assembled the surface concavity of the ROI from all the images of 1 recording to form a raw signal (solid line in Figure 4-3). The raw signal had a sampling frequency (i.e. image recording speed) of 30 Hz and contained oscillations that potentially denoted reticuloruminal contractions. This raw signal also contained noise caused by cow motion artifacts and the unstable illumination around the 3D camera. Examples are shown in Figure 4-3. We assumed that different components in the raw signal varied in their frequency of occurrences. Hence, frequency analysis was applied to remove the noise from the potential signal of interest. We applied the discrete fast Fourier transformation to convert the raw signal from its time domain to a representation in the frequency domain. Based on the study of Ruckebusch and Thivend (1980), we assumed the reticulo-ruminal contractions occurred 1 to 3 times per minute and the contractions ranged in frequency from 0.017 to 0.050 Hz. Hence, we filtered the frequency-domain representation to only retain the information within the frequency range of the reticulo-ruminal contractions. Within this range, the frequency with the greatest amplitude was considered to denote the reticulo-ruminal contraction frequency.

Thereafter, the filtered signal was inversed to the time domain (dotted line in Figure 4-3). From the filtered signal, local maxima (dots on the dotted line in Figure 4-3) were identified using the 'findpeaks' function in MATLAB (2018b). These local maxima were defined as any point with a value higher than the values of its 2 neighboring points in the signal. We considered each local maximum as the moment when the reticulo-rumen inflated to its maximum in a contraction. Then, the filtered signal between 2 local maxima was identified and considered a complete cycle of reticulo-ruminal contraction.

4.6 Validation of the Automated Reticulo-Ruminal Contraction Identification

Ideally, the automated identification of the reticulo-ruminal contractions would be validated by simultaneous palpation on the left paralumbar fossa of a cow while the contractions were being recorded. However, because such palpation would block the view of the camera, this real-time validation was not feasible. Hence, we used the visual identification of reticulo-ruminal contractions from the recorded 3D images for post-recording validation. Two assessors with experience in machine vision were trained by a veterinarian regarding the morphological changes of the left paralumbar fossa during the reticulo-ruminal contraction. Thereafter, the assessors independently observed the undulation on the left paralumbar fossa from a video, which was constructed from the chronological sequence of 3D images of 1 cow during 1 milking process. When an assessor identified an upward wave pattern from the left paralumbar fossa, he recorded the time in the video as the occurrence time. A reticulo-ruminal contraction was only confirmed when both assessors independently identified the contraction and the time difference between their recorded times of occurrence was less than 4 seconds. In total, the 2 assessors agreed on 261 and disagreed on 11 contraction identifications.

For each visually identified reticulo-ruminal contraction, we defined a time frame of 3 seconds before and after the averaged occurrence time from the 2 assessors. This time frame was used to compare the time of the automatically identified local maxima to the visually identified time of occurrence. When a local maximum was automatically identified within the time frame of a visually identified contraction, the case was identified as a true positive. When no local maximum was automatically identified within the time frame, the case was identified as a false negative. Moreover, any automatically identified local maximum without a matched visually identified contraction was identified as a false positive. The matching sensitivity (i.e. the number of true positives divided by the number of visually identified reticulo-ruminal contractions) and positive predictive value (i.e. the number of true positives divided by the number of automatically identified local maxima) were then calculated as the validation results of the automated identification.

Among the videos of the 20 cows, 261 reticulo-ruminal contractions were visually identified by both assessors, whereas 259 local maxima were automatically identified by image and signal processing. With the visual identifications used as the reference, the automated identification produced 253 true positives, 8 false negatives, and 6 false positives. All 8 false negatives were produced due to technical complications of the signal processing. In half of the false negatives, the image recording started at approximately the time when the rumen inflated to its maximum. The assessors identified the contraction in retrospect; however, the signal processing failed to identify the contraction because the signal did not completely oscillate. In the remaining half of the false negatives, the signal processing missed those contractions that were short in time and that was immediately followed by a new contraction. An example is shown in Figure 4-3. These visually identified

contractions were considered as incomplete contractions. Additionally, we found that all the false positives involved cases in which the assessors were unable to detect the reticulo-ruminal contractions from the video. In 4 cases, the reticulo-rumen was fully filled and the video showed only small variations in the concavity of the left paralumbar fossa. Hence, the assessors had difficulty observing changes in the cow's body surface from the video and failed to identify the reticulo-ruminal contractions. The other 2 false positives were caused by motion artifacts due to the rapid movement of the cows during image recording. The motion artifacts did not allow the assessors to clearly locate the left paralumbar fossa or to identify the reticulo-ruminal contractions. Among the 261 visually identified reticulo-ruminal contractions, 253 contractions were identified within the time frame by the automated system, yielding a matching sensitivity of 0.97 and a positive predictive value of 0.98. The results indicated that the 3D vision-based automated identification of the reticulo-ruminal contractions performed similarly to the reference manual identification.

4.7 Reticulo-Ruminal Motility in the AMS

Across the 20 cows, the average frequency of the automatically identified reticulo-ruminal contractions was 3.1 times per minute (SD = 0.28 times per minute), with a minimum of 2.4 times per minute and a maximum of 3.4 times per minute. This contraction frequency is in the upperfrequency range for normal cows. This relatively high level of reticulo-ruminal motility in the AMS likely reflects the cows' consumption of the concentrate because feeding increases cow reticulo-ruminal motility as described by Ruckebusch and Thivend (1980).

The 20 studied cows were also examined via rumen palpation by a trained assessor immediately after the 3D recording. This palpation was conducted in a passage that connected to the exit of the AMS and where a cow remained for 2 minutes with concentrate offered. The assessor placed a hand on the left paralumbar fossa of the cow and counted the number of contractions for 2 minutes. Across the 20 cows, the average frequency of the contractions identified by palpation was 2.4 times per minute (SD = 0.61 times per minute), which was 0.7 times per minute less than the average frequency automatically identified in the AMS. It is possible that the human handling in this examination, including the manual palpation and the close proximity of a non-familiar human, not being a normal procedure on the farm, caused additional distress to the cows. According to Ruckebusch and Thivend (1980), distress can inhibit the reticulo-ruminal motility of cows and consequently reduce the contraction frequency.

4.8 Future Work

This study demonstrated a low-cost 3D vision system that can automatically and remotely assess the reticulo-ruminal motility of dairy cows. The automated assessment performed similarly to referential manual assessment. In contrast to the other available methods of

reticulo-ruminal assessment, this automated system is non-invasive and distress-free to cows. As proof of concept, this automated system has the potential to operate as a standalone system not only on farms with AMSs but also on conventional farms with individual feeding stations. Upcoming studies should focus on validating this system on cows of different breeds, and with different parities, lactation stages, feed intakes, and morphological characteristics. Additionally, longitudinal studies should be performed to automatically and regularly monitor the changes in the reticulo-ruminal motility of individual cows on the farm. The automated monitoring system can allow farmers and veterinarians to frequently collect information about individual cows' gastrointestinal conditions and assist them in the disease diagnosis. Moreover, automated reticulo-ruminal assessment can be combined with the outputs of other sensors implemented on farms to further improve the health care and daily management of dairy cows.

4.9 Acknowledgements

This research was funded by Lely Industries N.V.. The authors thank Yu Yang Quek from Delft University of Technology in Delft, The Netherlands, for his contributions in image preprocessing; Adrie Meeuwesen, Augustin Toueille, Koen van Dinther, Laurine Hetterscheid, and Zhaolin Li from Lely Innovation in Maassluis, The Netherlands, for their contributions to data collection on the farm; and an anonymous dairy farmer in The Netherlands for cooperating with data collection on his farm.


453

Chapter 5

Root Cause Analysis of Metabolic Disorders in Dairy Cows Based on Morphological Traits Quantified with 3-Dimensional Vision

X. Song
P.P.J. van der Tol
E.A.M. Bokkers
S. van Mourik
P.W.G. Groot Koerkamp

Submitted for publication.

Abstract

High milk production and insufficient feeding often challenge dairy cows' metabolism, cause shortages in energy and nutrients, and lead to metabolic disorders that have strong impacts on health, production, and reproduction. The objectives of this study were to deploy dairy cow morphological traits as metabolic indicators that can be correlated with dairy farmer feeding practices and to develop a qualitative method to apply root cause analysis (RCA) on metabolic indicator anomalies in order to investigate the pathogenesis and root causes of metabolic disorders. Images of 42 lactating cows were recorded approximately 3 times per day for 66 days using a multicamera 3-dimensional vision system. Customized image processing algorithms were developed to automatically extract morphological traits that included the body condition, reticulo-ruminal contraction frequency, and rumen fill. These morphological traits were associated with cows' metabolism and were observed at both the herd and individual levels to detect anomalies over time. At the herd level, rumen fill drastically decreased 1 day after the cows began grazing on premature grass and was thus considered the metabolic indicator that rapidly responded to feeding practice changes. At the individual level, when a cow was identified at the onset of developing metabolic disorders, reticulo-ruminal contraction frequency and rumen fill tended to change in opposite directions over time, indicating rumen hypomotility. The anomalies of the metabolic indicators were chronologically assembled and analyzed with RCA. The root cause of the metabolic disorder of a cow was revealed to be the farmer lacking sufficient information on the cow's metabolism when he adjusted the feeding practice multiple times. This study developed a promising method of applying RCA on farms to assist dairy farmers in understanding the pathogenesis of metabolic disorders and managing dairy cow metabolic health.

Key words: root cause analysis, precision livestock farming, 3D vision, dairy cow metabolic disorder

5.1 Introduction

In recent decades, the dairy sector has experienced growing demands to feed the increasing population worldwide (FAO, 2018a). These demands have led the sector to select highperformance dairy cows that are genetically predisposed to prioritize milk production (Gross and Bruckmaier, 2019). Such high production challenges cows' metabolism, which maintains the balance between nutrition supply and production demand (McGuffey, 2017). In addition to facing the challenges of high production demand, dairy cows often experience disturbances caused by a variety of factors, including pathogens, feeding practices, and transition periods, such as the period from gestation to lactation (Zebeli et al., 2015). These disturbances can interfere with the metabolism of converting feed to energy and nutrients (e.g., proteins, lipids, and carbohydrates) and cause energy and nutrient shortages in cows (McGuffey, 2017). When a cow cannot maintain a balanced metabolism, it may develop health disorders (Sundrum, 2015), such as ketosis, ruminal acidosis, fatty liver, and milk fever (Ametaj, 2010). These disorders have substantial impacts on cow health, production, and reproduction and on-farm profitability (Overton et al., 2017; Gross and Bruckmaier, 2019). Hence, it is essential for farmers to proactively manage and control metabolic disorders on farms.

Metabolic health management should involve not only detecting and treating cows with metabolic disorders but also aiming to understand the metabolic disturbances to the cows (Overton et al., 2017), which are considered the causes of metabolic disorders. Identifying the causes is vital for farmers to understand the pathogenesis of metabolic disorders. This understanding can provide them with the knowledge to start proactively managing the health of cows, adjusting farm management strategies accordingly, and preventing the reoccurrence of metabolic disorders. We propose to employ a root cause analysis (**RCA**) to identify the metabolic disturbances that cause metabolic disorders on farms. RCA is a problem-solving method used to identify the root cause of a problem (Kiruthika, 2015). For the metabolic health management of dairy cows, RCA can be divided into 3 steps: (i) establish a sequence of clinical symptoms in a timeline from the time that the cow was healthy up to the time that the metabolic disorder was detected, (ii) investigate the cause(s) of each symptom (e.g., biology, physiology, pathology, farm management, or the environment), and (iii) determine the root cause of the metabolic disorder. In RCA, a clinical symptom can be represented by an anomaly in a cow's metabolism, which deviates from the metabolism of other cows in a herd or the past metabolism of the same cow. This anomaly is quantified by metabolic indicators that are visible, palpable, or measurable on farms and are related to the physical, physiological, morphological, and behavioral traits of a cow.

The current available metabolic indicators measured on farms include metabolite contents in the blood, measured by blood tests (Overton et al., 2017); rumen temperature and pH, measured by radiotelemetric boluses in the rumen (AlZahal et al., 2011); milk composition, measured by inline spectroscopy milk sensors (de Roos et al., 2007); and cow

activity and rumination time, measured by 3-dimensional (**3D**) accelerometers (Stangaferro et al., 2016). When detecting clinical symptoms (i.e., anomalies) on farms, these indicators need to be measured regularly and individually in each cow. However, blood tests and boluses are invasive to cows and impractical and costly for farmers (McGuffey, 2017). Moreover, milk composition, daily activity, and rumination time are not necessarily indicative of metabolism or metabolic disorders and are often influenced by feed quality and other diseases. Additionally, farmers often use low milk yield as an alert of a metabolic disorder developing in a cow (Overton et al., 2017). This alert, however, occurs too late for farmers and cows because a cow with low milk-yield is often severely ill, resulting in permanent health declines and reproductive losses (Overton et al., 2017). To date, additional metabolic indicators for quantifying dairy cow metabolism are needed, with the requirements of being measured automatically and noninvasively on farms using low-cost sensors and having physiological or pathological mechanisms underlying their anomalies.

When a cow is unable to maintain its energy or nutrition balance because of a disturbance to its metabolism, its lack of physiological adaptation can result in altered morphology (Schröder and Staufenbiel, 2006; Bobe et al., 2010). Dairy cow morphology is the external appearance of the body and includes traits such as shape, structure, color, pattern, and size of the whole body or body parts (Pilat, 1988). The morphological traits of body size, body condition, hair coat, and paralumbar fossa have often been examined for manual clinical diagnoses performed by veterinarians (Mäntysaari et al., 2019) and denote metabolic indicators. Among all the morphological traits, body condition is a morphological reflection of a cow's fat reserves and is associated with energy balance (Thorup et al., 2012). A change in body condition can be the result of a metabolic disorder (Rathbun et al., 2017). Moreover, changes in the shape of the left paralumbar fossa have been used to assess reticulum-rumen motility of dairy cows (Burfeind et al., 2010). Inhibited reticulo-ruminal motility is indicative of digestion problems and is associated with metabolic disorders such as ruminal acidosis and tympany (Snyder and Credille, 2017). Quantification of body condition and the shape of the left paralumbar fossa has been automated using low-cost 3D vision cameras, enabling the regular monitoring of individual cows on farms (Song et al., 2019a, 2019b). The objectives of this study were to deploy dairy cow morphological traits as metabolic indicators that can be correlated with dairy farmer feeding practices and to develop a qualitative method to apply RCA metabolic indicator anomalies in order to investigate the pathogenesis and root causes of dairy cow metabolic disorders.

5.2 Materials and Methods

Cows and Milk Production

Forty-two lactating cows from a commercial farm in the Netherlands were selected for this study. All cows were Holstein Friesian and Brown Swiss crossbreeds and were milked with an automatic milking system (**AMS**, Astronaut A5, Lely Industries N.V., Maassluis, The

Netherlands). This study was carried out for 66 days, from March to May 2019. Data on the parity, days in milk (**DIM**), milk yield, milking time per day, and milk composition of the 42 cows over the 66 days were collected using farm management software (T4C, Lely Industries N.V.). The descriptive statistics of these data are listed in Table 5-1.

Table 5-1. Descriptive statistics of the parity, DIM1, and production of the 42 studied cows over the 66 days.

Item	Minimum	Mean	Maximum	SD
Parity (number)	1	1.2	3	0.5
DIM on Day 66 (day)	73	425	232	102
Milkings per day (number)	1	3	5	1
Daily milk yield (kg)	4.3	25.4	40.4	5.5
Fat content (%)	3.0	3.8	5.0	0.3
Protein content (%)	3.0	3.8	5.0	0.3
Lactose content (%)	4.1	4.5	4.7	0.1

[1]DIM: days in milk

Table 5-2. Indoor average feed composition changes over the 66 days for each cow.

		Day 1 to 10[2]		Day 10 to 24		Day 24 to 52		Day 52 to 66	
Feed composition	DM[1] digestibility	Fresh weight (kg)	DM weight (kg)	Fresh weight (kg)	DM weight (kg)	Fresh weight (kg)	DM weight (kg)	Fresh weight (kg)	DM weight (kg)
Grass silage	38%	20.0	7.6	19.0	7.2	19.0	7.2	19.0	7.2
Corn silage	39%	13.0	5.1	12.0	4.7	15.5	6.0	12.0	4.7
Barley	85%	4.0	3.4	3.5	3.0	3.5	3.0	3.5	3.0
Hay	80%	4.0	3.2	3.5	2.8	0	0	3.5	2.8
Total		41.0	19.3	38.0	17.7	38.0	16.2	38.0	17.7

[1]DM: dry matter; [2] all cows were let out freely for grazing on Day 10

Feeding Practice

This is an observational study without any experimental treatments or feeding adjustment on the farm; hence, the farmer practiced the feeding plan independently. The feed for indoor feeding was supplied to cows 4 times per day at 0400, 1000, 1600, and 2200 h by an automatic feeding robot (Vector, Lely Industries N.V.) with the feed composition listed in Table 5-2. Additionally, cows were fed a concentrate supplement during milking with the AMS. The amount of concentrate provided to each cow was dynamically determined based on the cow's DIM and milk yield from the previous day. Among the 42 cows, the average daily concentrate intake measured by the AMS was 5.1 kg, with a minimum of 0.2 kg, a maximum of 10.0 kg, and an SD of 0.1 kg. Furthermore, the farmer changed the feeding practices four times over the 66 days.

- From Days 10 to 66, all cows were freely allowed in a pasture to graze on grass (i.e., English ryegrass and Bermuda grass) from 0600 to 1400 h each day.
- On Day 10, the farmer reduced the average indoor feed for each cow from 41 kg of fresh weight to 38 kg with a similar feed composition ratio.
- From Days 24 to 52, the farmer replaced 3.5 kg of hay with 3.5 kg of corn silage for each cow.
- From Days 52 to 66, the farmer returned the 3.5 kg of hay to the indoor feeding of each cow and withdrew the concentrate supplement from the feed of sick cows he identified.

General Health Check

A noninvasive general health check was performed twice a week for all the cows during the study. The health check was noninvasive and aimed to detect general health abnormalities using only visual inspections and palpations. A trained assessor performed the health checks following a protocol based on 'Clinical Examination of Farm Animals' guidelines (Jackson and Cockcroft, 2002). The general health check included visual inspections of awareness (normal or dull), hair coat condition (normal or presenting bare spots, lesions, or an irregular hair coat), breathing (normal or difficult), and nose discharge (normal or discharge). Palpations were conducted to detect ear temperature (normal or cold ear) and udder condition (normal or presenting lesions and inflammation). Each cow was given an overall health score by summing the number of aspects that were normal. The maximum score was 6, denoting healthy, and the minimum score was 0, denoting severely sick. Additionally, clinical treatment records of the cows on the farm were included as a reference for this study. To prevent interference with the farmer's standard health management, however, we performed the general health checks independently, and the results were not shared with the farmer or the veterinarians of the farm.

3D Vision System

A 3D vision system was designed to capture the morphology of the cows. It integrated 2 vision systems: one for body condition scoring according to the study by Song et al. (2019a)

and the other for reticulum-rumen motility assessment according to the study by Song et al. (2019b). The integrated system comprised 4 cameras (Realsense D415, Intel, Santa Clara, California, USA) with a 3D depth-sensing function that were connected to and controlled by 2 recording PCs through separate USB 3.0 ports. Each camera had a depth-sensing resolution of 1280 × 720 pixels and field-of-view angles of 69° × 43° × 77° (horizontal × vertical × diagonal). The 3D vision system setups were identical to those from the 2 reference studies of Song et al. (2019a, 2019b).

During the 66-day observational period, images of all the cows were recorded during and after each successful milking in the AMS. **(i) Left paralumbar fossa.** When a cow was standing in the AMS and the milking process had started, the AMS sent a digital signal to the first recording computer to activate camera 1 for recording, which was mounted on the left fence of the AMS to capture the view of the left paralumbar fossa of the cow in the AMS. The recording was set at 4 frames per second (**fps**) for 4 minutes. If the milking was shorter than 4 minutes, then the recording stopped when the first teat cup detached from the cow. **(ii) Body condition in 8 body regions.** As the cow left the AMS through the exit gate after milking, its body triggered a photocell that was mounted above the gate and connected to the second recording PC. The photocell sent a digital signal to the recording PC to activate cameras 2, 3, and 4 to record 3D images simultaneously at 10 fps for 2 seconds. Cameras 2, 3, and 4 were mounted on a metal frame that was placed above the AMS exit gate to capture the views of the top, right, and rear body sides, respectively. After image recording, both PCs recorded the cow identification number and time of the recording and reset the cameras for the next cow to enter the AMS.

Morphological Trait Extraction using Image Processing

Body Condition. Morphological traits representing the body conditions of 8 body regions (i.e., the spinous processes, spinous to transverse processes, overhanging shelf, hook bone, pin bone, thurl area, spinous processes to hook bone, and cavity between the tail head and pin bone) were extracted using the same image processing algorithms as those in Song et al. (2019a). For each cow, the daily morphological trait for each body region was calculated by averaging the results of all the recordings from the same day.

Reticulo-Ruminal Contraction Frequency. The surface concavity of a cow's left paralumbar fossa was calculated using the image processing algorithms of Song et al. (2019b). For each milking, the surface concavities calculated from all the images were chronologically assembled to form a raw signal. The raw signal contained oscillations that potentially denoted dairy cow reticulo-ruminal contractions. Discrete fast Fourier transformation was first applied to convert the raw signal from its time domain to a representation in the frequency domain. Then, the frequency range of 0.017 to 0.050 Hz was selected to retain only the information related to the reticulo-ruminal contractions. Within this range, the frequency with the highest amplitude was considered to denote the reticulo-ruminal contraction frequency.

Rumen Fill. The median of all the values of the raw signal in the time domain was calculated as the average surface concavity over the 4 minutes and denoted a cow's rumen fill (i.e., the total amount of liquid and dry matter stored in the rumen). Finally, the daily reticulo-ruminal contraction frequency and rumen fill were calculated by averaging the results of all the recordings of a single cow on the same day.

Metabolic Indicator Selection. Eight variables were selected as dairy cow metabolic indicators, including milk yield (kg), milk fat content (%), milk protein content (%), the milk fat-to-protein ratio (-), milk electrical conductivity (-), the concavity of the spinous processes (-), reticulo-ruminal contraction frequency (contractions per minute), and rumen fill (m-2). The concavity of the spinous processes was chosen to represent all the body conditions in 8 body regions of a cow because it was previously shown to have the highest correlation coefficient (i.e., Spearman's rho = 0.90, $P < 0.001$) with the reference measurements among all the body regions (Song et al., 2019a).

Cross-Correlations among Metabolic Indicators at the Herd Level

At the herd level, the selected metabolic indicators can respond differently in time to specific feeding practice changes. We chose to calculate a cross-correlation between two indicators over the 66 days. A cross-correlation compares 2 time-series datasets to determine the time delay between the 2 sets having the best fit. Each time-series dataset consisted of the median value of a metabolic indicator of all the cows each day. Upon shifting the first dataset forward and backward from 0 to 65 days, the cross-correlations between the first and second datasets were calculated. The lag time (i.e., the number of days shifted from the first to the second datasets) with the highest absolute cross-correlation was calculated to represent the best data match of the 2 time-series metabolic indicators.

RCA of Metabolic Disorders at the Individual Level

For a cow with a metabolic disorder, the anomalies in all 8 metabolic indicators of this cow were first identified. These anomalies were assigned chronologically in a timeline from the time that the cow was healthy up to the time that the metabolic disorder was detected. Each anomaly was considered the symptom of a metabolic disorder, and the combined sequence of anomalies denoted the pathogenesis of the metabolic disorder. Thereafter, the causes of each anomaly (i.e., symptom) were investigated from the perspectives of biology, physiology, pathology, farm management, and the environment. Finally, the root cause(s) of this metabolic disorder was determined based on expert knowledge.

5.3 Results and Discussion

Herd-Level Metabolic Response to the Changes in Feeding Practice

The distribution of each metabolic indicator among all the cows in the herd on each day is presented in a boxplot (Figure 5-1). In each box, the central mark is the median of the indicators of all the cows on 1 day. The bottom and top edges of the box are the 25th (Q1) and 75th (Q3) percentiles of the indicators, respectively. The whiskers extend to the most extreme data points that are within the range of [Q1 – 1.5 × (Q3 – Q1), Q3 + 1.5 × (Q3 – Q1)] and thus are not considered outliers. The outliers are located outside of the range and plotted individually as dots.

Rumen Fill and Milk Fat Content. When all the cows were allowed to freely graze in the pasture on Day 10, a few metabolic indicators responded quickly. Rumen fill responded first among the indicators, responding on Day 11. The 25th and 75th percentiles and median rumen fill of the herd decreased significantly over a period of approximately 13 days (Figure 5-1-H). Similar to rumen fill, milk fat content significantly decreased from Day 11, with a median of 4.7%, to Day 13, with a median of 4.3%. Milk fat content subsequently increased to 4.7% on Day 24 and then decreased to 4.4% on Day 27 (Figure 5-1-B). Significant changes in other metabolic indicators at the herd level were not observable, as evident in the boxplots. The cause of the decrease in rumen fill might have been insufficient feed at the start of grazing. We believe that the start of grazing was too early in the year (i.e., Day 10 was on the 24th of March), as the grass in the pasture was premature and insufficient for the nutritional needs of the cows. The decrease in milk fat content was not expected. Generally, when cows are shifted from indoor feeding to outdoor grazing, milk fat content increases because of the increased proportion of roughage intake (Salfer et al., 2018). In this study, the milk fat content changed in the opposite direction than expected, which can be explained by insufficient feeding during grazing, resulting in the roughage intake being lower than that associated with indoor feeding. In addition, when the farmer replaced hay with corn silage in the feed on Day 24, the proportion of roughage decreased, causing the milk fat content to decrease from Day 24 to 27.

Milk Protein Content, Milk Fat-to-Protein Ratio, Milk Electrical Conductivity, and Reticulo-Ruminal Contraction Frequency. In contrast to milk fat content, protein content remained stable when the feeding practices were changed (Figure 5-1-C). This observation is in line with the finding by Leskinen et al. (2019), who reported that changes in nutrition, ration formulation, or feed intake affected milk fat content much more than protein content. The milk fatto-protein ratio followed the same pattern of decrease as milk fat content (Figure 5-1-D) because the milk protein content remained stable. Milk electrical conductivity (Figure 5-1-E) and reticuloruminal contraction frequency (Figure 5-1-G) remained stable over time, as deviations in these measurements are mainly associated with diseases (Leek, 1987; Khatun et al., 2018). This stability indicated that the herd was clinically healthy.

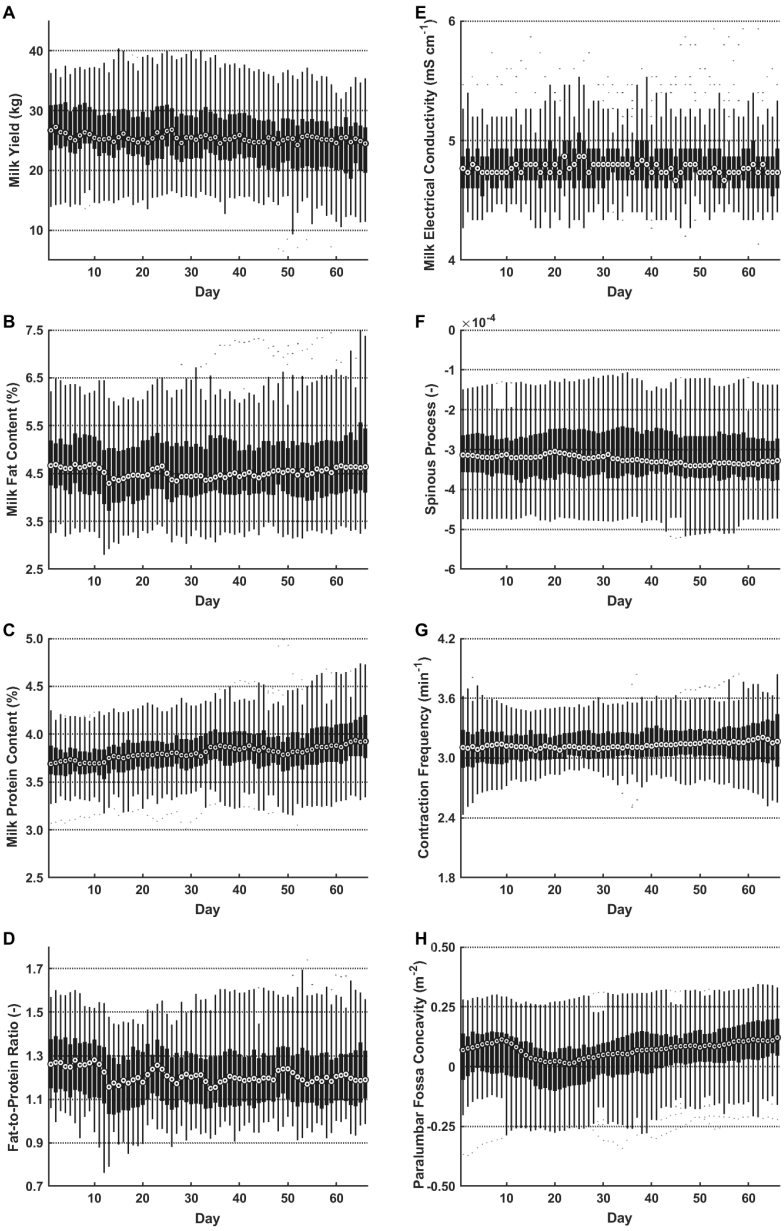

Figure 5-1. Boxplots of 8 dairy cow metabolic indicators at the herd level, including (A) milk yield (kg); (B) milk fat content (%); (C) milk protein content (%); (D) the milk fat-to-protein ratio (-); (E) milk electrical conductivity (-); (F) the concavity of spinous processes (-), representing body condition; (G) reticulo-ruminal contraction frequency (times per minute); and (H) rumen fill (m-2). In each box, the central mark is the median of the indicators of all the cows on 1 day. The bottom and top edges of each box are the 25th (Q1) and 75th (Q3) percentiles, respectively, of the indicator. The whiskers extend to the extreme data points that are within the range of [Q1 − 1.5 × (Q3 − Q1), Q3 + 1.5 × (Q3 − Q1)] and not considered outliers. The outliers are located outside of the range and plotted individually as dots.

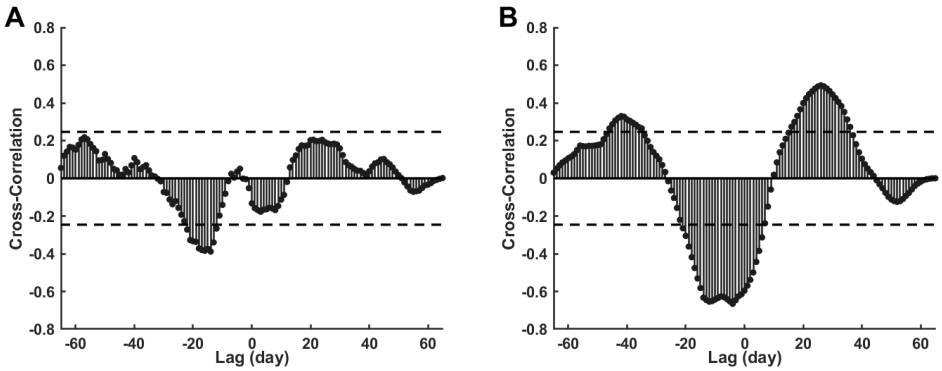

Figure 5-2. Plots of the cross-correlations between the herd median rumen fill (i.e., fastresponding metabolic indicator) and (A) herd median milk yield and (B) herd median body condition (i.e., slow-responding metabolic indicators). Each cross-correlation was calculated between rumen fill and the shifted slow-responding indicator. The positive and negative lags indicate that the slow-responding indicator series was shifted forward and backward in time, respectively. The confidence bounds (two dashed lines) of the cross-correlations were calculated as 2 times the standard error. The peak cross-correlation between rumen fill and milk yield was - 0.39 with a lag of -14 days, indicating that milk yield had a significant decrease 14 days later than the rumen fill decrease (i.e., the start of grazing). Moreover, the peak cross-correlation between rumen fill and body condition was -0.67 with a lag of -4 days, indicating that body condition had a significant decrease 4 days later than the rumen fill decrease.

Milk Yield and Body Condition. Over the entire 66 days, both milk yield and body condition decreased gradually. The herd median milk yield decreased from 26 kg on Day 1 to 24 kg on Day 66 (Figure 5-1-A). Moreover, the milk yield decrease in the 25th percentile was greater than the corresponding decreases in the 75th percentile and the median of the herd. This difference indicated that the herd-level milk yield decrease was mainly due to the cows in the herd with relatively low milk yields, which were impacted to a greater extent than the other cows by the insufficient feed during grazing. The herd median body condition also decreased over the 66 days, whereas the 25th and 75th percentiles remained approximately stable. The distribution curve on each day changed from equal on Day 1 to skewed towards a low body condition on Day 66 (Figure 5-1-F). This finding indicates that the body condition decrease was mainly due to the condition decreases in the cows of higher body condition in the herd.

Cross-Correlations among Metabolic Indicators at the Herd Level.

As shown in Figure 5-1-F, milk yield and body condition exhibited much weaker decreases than rumen fill and milk fat content. The influences of the insufficient feed supply during grazing on milk yield and body condition were represented by the cross-correlations between the fastresponding metabolic indicator,namely, rumen fill, and the 2 slow-responding metabolic indicators, namely, milk yield and body condition. The cross-correlation calculation and

lag determination revealed how many days elapsed until milk yield and body condition responded to rumen fill changes (indicating the effect of insufficient feeding during grazing).

Figures 5-2-A and 5-2-B show the cross-correlations between rumen fill and milk yield and between rumen fill and body condition, respectively. The confidence interval (i.e., the dashed line in Figure 5-2) of the cross-correlation was determined to be 2 standard errors, which was estimated as the standard error of the cross-correlation between the data of 2 series, assuming that the series were uncorrelated. The cross-correlation with the highest absolute value located outside of the confidence interval (i.e., approximate 95% confidence interval) was the peak crosscorrelation. The corresponding lag indicated the delay in days in the slow-responding data (i.e., milk yield and body condition). The peak cross-correlation between rumen fill and milk yield was -0.39 with a lag of -14 days, indicating that milk yield had a significant decrease 14 days later than the rumen fill decrease (i.e., the start of grazing). Moreover, the peak cross-correlation between rumen fill and body condition was -0.67 with a lag of -4 days, indicating that body condition had a significant decrease 4 days later than the rumen fill decrease. Although rumen fill started increasing on Day 24, both milk yield and body condition continued to decrease over the remaining days, resulting in both peak cross-correlations being negative.

Dairy Cows with Metabolic Disorders

Among all cows, 2 cows received health scores lower than 5. The first cow, denoted Cow A, received a health score of 4 for 2 consecutive checks on Days 52 and 53, with abnormalities in awareness and ear temperature on both days. The second cow, denoted Cow B, received a health score of 4 on Day 48, with abnormalities in awareness and ear temperature, and a health score of 5 on Days 33 and 52, with abnormalities in awareness and hair coat condition, respectively. According to the farmer's on-farm clinical treatment records, both had received oral sodium bicarbonate power from Days 52 to 54. Because the two cows showed similar trends in their metabolic indicators, we selected Cow A to a typical example (Figure 5-3). On Day 1, rumen fill and milk fat content were low and located in the lowest 25^{th} percentiles of the herd, whereas the remaining metabolic indicators were at approximately the median levels of the herd. At the start of grazing on Day 10, the rumen fill of Cow A was similar to that of the herd: a strong change from a flat paralumbar fossa on Day 11 to a concave surface indicating an empty rumen on Day 17 (Figure 5-3-H). On Day 24, when the farmer replaced hay with corn silage in the feed, the milk fat content of Cow A showed a slight decrease (Figure 5-3-B). From Days 41 to 47, the reticuloruminal contraction frequency decreased, whereas the rumen fill increased slightly (Figure 5-3-G and 5-3-H). The opposing trends of these 2 variables indicate subtle reticulo-ruminal motility inhibition; such inhibition can cause an increased amount of digestion but with insufficient contractions and, consequently, an increased level of acidity in the rumen. Starting on Day 47, the rumen fill of Cow A decreased markedly and was accompanied by an increase in reticulo-ruminal contraction frequency, indicating an extremely low rumen fill. On Day 48, the milk yield of the

cow started decreasing (Figure 5-3-A), and its milk fat content started increasing (Figure 5-3-B). On Day 52, rumen fill and milk yield reached their lowest levels, while reticulo-ruminal contraction frequency reached its peak. On the same day, the cow received a health score of 4 because the cow was dull and had cold ears. Additionally, the farmer identified this cow due to its milk yield decrease and inconsistent manure. The farmer adjusted the feeding plan from Day 52 for this cow by offering an additional kilogram of hay, removing the concentrate supply from the feed, and administering oral sodium bicarbonate to the cow for 3 days to increase its reticulorumen motility. Two days later, on Day 54, the rumen fill and milk yield of the cow started to recover, whereas its reticulo-ruminal contraction frequency remained stable. It seemed that the cow actively responded to the rumen stimulation treatment and feeding changes. In contrast, the milk fat content and fat-to-protein ratio of Cow A remained high from Days 52 to 57 (Figure 5-3-B and 5-3-D). Although the cow was recovering from disturbances due to the treatment and feeding practice changes, by the end of the study, its milk production had not reached the same level as that before Day 48. Starting on Day 57, its milk fat content and milk fat-to-protein ratio also remained high.

RCA of Cow A with Metabolic Disorders

RCA was applied to the morphological traits of Cow A for the 66 days and is presented in a fishbone diagram (Figure 5-4). This cow was suspected of having metabolic disorders (i.e., mainly ruminal acidosis and ketosis) based on its responses to the rumen stimulation treatment and it was not completely recovered from the metabolic disorders by the end of Day 66. Hence, we established a timeline of 66 days in the fishbone diagram. On the timeline, all the observed anomalies in metabolic indicators (i.e., anomalies described in the previous paragraph) were chronologically assigned. This timeline with anomalies in the metabolic indicators could represent the pathogenesis of the metabolic disorders in Cow A over the 66 days. The biological, physiological, pathological, farm management, or environmental causes of each anomaly are summarized in Table 5-3. Among all the causes, we believe that the changes in feeding practices and the insufficient ability to overcome metabolic disturbances resulted in the pathogenesis of ruminal acidosis and ketosis in Cow A. The root cause of the ruminal acidosis and ketosis in Cow A was determined to be the farmer lacking sufficient information about the cow's metabolism (i.e., metabolic indicators) when he adjusted the feeding practice multiple times.

Morphological Traits as Metabolic Indicators

Herd Level. The rumen fill of the herd decreased 1 day after the cows started grazing on premature grass; hence, rumen fill responded quickly to this change in feeding practice, as shown in the 3D images. Rumen fill is an estimate of the total amount of liquid and dry matter stored in the rumen and is associated with the dry matter intake, ration composition, and digestion function of a cow. Typically, rather than using rumen fill, farmers evaluate milk

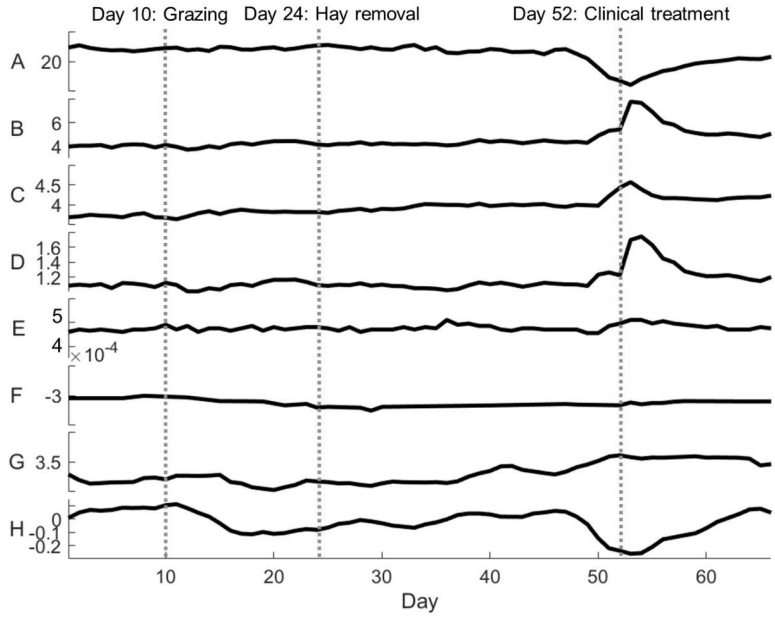

Figure 5-3. Plots of 8 metabolic indicators of cow A over 66 days, including (A) milk yield (kg); (B) milk fat content (%); (C) milk protein content (%); (D) the milk fat-to-protein ratio (-); (E) milk electrical conductivity (-); (F) the concavity of spinous processes (-), representing body condition; (G) reticulo-ruminal contraction frequency (times per minute); and (H) rumen fill (m-2). Additionally, the farmer's feeding practice changes are labeled with three vertical dashed lines. On Day 10, all cows, including Cow A, were left out for grazing on premature pasture. On Day 24, hay was replaced by corn silage from the indoor feeding. On Day 52, cow A was identified as having health issues by the farmer based on a milk yield decrease and inconsistent manure. The farmer adjusted the feeding plan for this cow from Day 52 by offering an additional 1 kilogram of hay, removing concentrate from the feed, and providing the cow with sodium bicarbonate to increase reticulo-rumen motility.

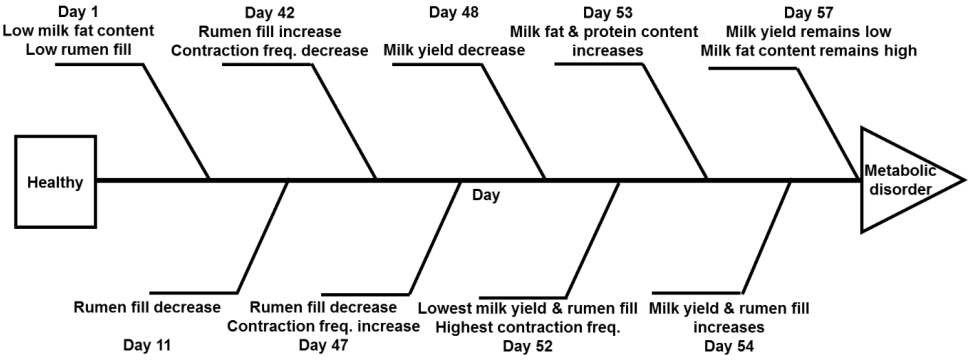

Figure 5-4. A fishbone diagram representing the root cause analysis applied to the metabolic disorders of a dairy cow.

yield to assess the effects of their on-farm feeding practice change (Schorr and Lips, 2018). In addition, some farms are equipped with automated body condition scoring systems. Farmers on such farms can also use body condition scores to help them perform feeding practice management (Bewley et al., 2008). Nevertheless, neither milk yield nor body condition responded rapidly to insufficient feeding during grazing in our study. Relative to rumen fill, milk yield and body condition had response delays of 12 and 4 days, respectively. Hence, the monitoring of rumen fill at the herd level via a 3D vision system can allow farmers to detect rapid responses of dairy cows to changes in feeding practices.

Individual Level. When the farmer replaced hay with corn silage in the feed, the rumen fill at the herd level remained stable. Anomalies in the metabolic indicators occurred in only a few cows that later developed metabolic disorders. Two cows were suspected of

Table 5-3. The observed anomalies in metabolic indicators and the causes of each anomaly chronologically assigned over the 66 days.

Day	Observed anomalies in metabolic indicators	Causes of the anomalies
1	1. Low mil k fat content 2. Low rumen fill	1. Insufficient feed intake 2. Low social rank in the herd 3. Low metabolic plasticity
11	1. Rumen fill decrease	1. The start of grazing 2. Premature grass in the pasture 3. Decreased amount of indoor feeding 4. Lower indoor feed intake
42	1. Rumen fill increase 2. Reticulo-ruminal contraction frequency decrease	1. Lower roughage intake 2. Not fully recovered from the influence of grazing 3. Hay removed too early after the start of grazing 4. The farmer lacked metabolism information as feedback for the feeding changes
47	1. Rumen fill decrease 2. Reticulo-ruminal contraction frequency increase	1. Development of ruminal acidosis 2. Drastic feed intake decrease 3. High acid level in the rumen
48	1. Milk yield decrease	1. Feed intake decrease 2. Ruminal acidosis
52	1. Lowest milk yield & rumen fill 2. Highest reticulo-ruminal contraction frequency	1. Empty rumen 2. No clinical sign could be detected before this day 3. Had not received any clinical treatment 4. Long time with a low feed intake
53	1. Milk fat and protein content increases	1. Extremely low milk yield 2. Low feed intake 3. Roughage intake increase 4. Concentrate intake decrease
54	1. Milk yield and rumen fill increases	1. Received clinical treatments 2. Roughage intake increase 3. The rumen acid level decreased to a normal level 4. Rumen motility recovered
57	1. Milk yield remained low 2. Milk fat content remained high	1. Long-term damage to production 2. Not fully recovered 3. Development of ketosis 4. Roughage intake increase

developing metabolic disorders after the farmer replaced hay with corn silage in the feed. The reticulo-ruminal contraction frequency and rumen fill of these cows started deviating from the herd-level median approximately 10 days before the farmer observed the more apparent signs in the cows. Hence, to obtain adequate information about the effects of the feeding practice and to detect metabolic disorders in the early stages, farmers also need to monitor metabolic indicators at the individual cow level.

The milk yield of Cow A decreased markedly on Day 48. This decrease, however, was not necessarily indicative of disease, as milk yield can be influenced by a variety of factors (e.g., feed quality and heat distress). Hence, after receiving the alert about the milk yield decrease, the farmer had to physically examine the cow for further investigation. The farmer claimed to be unable to detect any clinical signs in that cow on Day 48, which was in line with our general health check on the same day (i.e., the cow had a health score of 6 on Day 48). Without any detected health problems and treatment, further deterioration of the cow's rumen health consequently occurred. If the farmer had detected a milk yield alert in combination with a rumen health alert, then more targeted and effective disease detection and treatment could have occurred. Furthermore, the milk fat content and fat-to-protein ratio in Cow A strongly increased and remained high during and after disease detection and treatment by the farmer. A high milk fat content and fat-to-protein ratio accompanied by a low milk yield can indicate ketosis in a cow (de Roos et al., 2007). The finding of multiple metabolic disorders occurring in Cow A in this study is in line with the finding of Ametaj (2010), who stated that metabolic disorders are strongly associated with each other because the recovery of one unbalanced metabolic process requires compensation by others in the body. Hence, it is suggested that a variety of metabolic indicators in individual cows be chronologically incorporated in a timeline to adequately represent the pathogenesis of metabolic disorders.

5.4 Conclusions

This study demonstrated that 3D vision-quantified rumen fill was a metabolic indicator that rapidly responded to feeding practice changes at the herd level and that both reticulo-ruminal contraction frequency and rumen fill have great potential to identify metabolic disorders at an early stage. The root cause of the metabolic disorders in Cow A was revealed to be the farmer lacking sufficient information about the cow's metabolism when he adjusted the feeding practice multiple times. This study developed a promising method of applying RCA on farms to assist dairy farmers in managing dairy cow metabolic health.

5.5 Acknowledgements

This research was funded by Lely Industries N.V.. The authors thank Adrie Meeuwesen, Jannie van der Lelij, Jeroen de Bruin, and Piet Boes from Lely Innovation in Maassluis, The

Netherlands, for their contributions to the data collection on the farm, and the participating dairy farmer in The Netherlands for cooperating with the data collection on his farm.

Chapter 6

General Discussion

X. Song

6.1 General Conclusions

This Ph.D. thesis aimed to develop and validate methods and models to automatically quantify dairy cow morphological traits as metabolic indicators using 3-dimensional **(3D)** vision and to acquire knowledge about the root cause of metabolic disorders in dairy cows by incorporating precision livestock farming (**PLF**) and root cause analysis (**RCA**).

In **Chapter 2**, a 3D vision system was designed, built, and validated to automatically quantify dairy cow body size, including hip height, hip width, and rump length. With these morphological traits as inputs, we achieved body-weight-prediction performance similar to that of manual and semiautomated methods. Moreover, the propagation of measurement error into the prediction model was negligible, which indicated that the bottleneck in prediction is not in the quality of the 3D vision system. This chapter chose 3 commonly used morphological traits of dairy cows for automatic quantification and demonstrated that 3D vision technologies have great potential for automation on farms. Additionally, this chapter set guidelines for data collection, image processing, measuring error quantification, mathematical model selection, and referential assessment protocols for Chapters 3, 4, and 5.

The body condition score (**BCS**) of a dairy cow is a metabolic indicator and is influenced by feed efficiency, dietary composition, stocking rate on farms, and all other aspects related to the energy balance of a cow. The current vision-based BCS classification systems used information acquired from only a limited number of cow body regions. In **Chapter 3**, a multicamera 3D vision system was designed to extract the body-condition-related features of 8 body regions from 3 viewpoints. Moreover, all extracted morphological traits were used as inputs in a BCS classification model with the BCS as an ordinal output. The sensitivity of our 3D vision-based BCS classification was significantly higher than the sensitivities of currently available automated systems.

In **Chapter 4**, a low-cost 3D vision system was demonstrated to automatically and remotely assess dairy cow reticulo-ruminal motility, which is a well-established metabolic indicator. Our automated assessment performed similarly to the reference manual assessment. In contrast to the other available methods, this automated system is noninvasive and distress-free for cows. It is a promising tool for farmers and veterinarians to obtain information on a daily basis about the metabolic status of individual cows and can help them in farm management and clinical diagnoses.

Chapter 5 describes an on-farm longitudinal study that integrated all the 3D vision systems and mathematical models designed in Chapters 2, 3, and 4. As a case study, a cow with metabolic disorders was analyzed by applying RCA to all the available metabolic indicators of the cow over 66 days. The results revealed that the 3D vision-quantified rumen fill could serve as a metabolic indicator that responds rapidly to feeding practice changes. Moreover, the root cause of this case was that the farmer lacked information about the cow's metabolism when he adjusted the feeding practices several times. This study developed a

promising method of applying RCA to farms to assist dairy farmers in managing dairy cow metabolic health.

This thesis successfully proved the useful application of 3D vision technology for automating dairy cow morphology quantification on farms. The designs of the vision systems and mathematical models were validated on commercial farms with a harsh and uncontrolled environment, demonstrating the great potential of these tools for farmers to deploy in daily farm management. The automatically quantified morphological traits were shown to be significantly correlated with the metabolism of cows. The root cause of a metabolic disorder was revealed by chronologically combining all metabolic indicators and applying RCA. This thesis developed and validated a method to incorporate PLF and RCA to assist farmers in dairy cow metabolic health management.

In the following paragraphs, I will discuss the findings of this thesis in a more general and broader context: (6.2) the characterization of the selected morphological traits and added values for indicating cows' metabolism compared to current metabolic indicators, (6.3) comments in relation to metabolic plasticity, (6.4) moving towards disease prevention with PLF applications, (6.5) measuring the quality of the 3D vision systems, (6.6.) the acceptance of a 3D vision system, and (6.7) future work.

6.2 Morphological Traits Related to the Metabolism of Dairy Cows

This thesis describes the use of a 3D vision system to quantify 3 types of dairy cow morphological traits, including body size, body condition in 8 body regions, and concavity of the left paralumbar fossa, representing reticulo-ruminal motility. These automatically quantified dairy cow morphological traits are reliable indicators of cows' metabolism and can assist farmers in feeding management and the detection of metabolic disorders. **(i)** The median rumen fill of the herd decreased substantially after the start of grazing, which was interpreted as a **fast metabolic response** to a change in feeding practice. The reticulo-ruminal contraction frequency and rumen fill can together be used to assess rumen function and health condition and to classify ruminal diseases (e.g., ruminal acidosis and bloat). **(ii)** Body condition is a reflection of a cow's fat reserves and is associated with a dairy cow's energy balance (Roche et al., 2009). As it is a **slow metabolic response**, we considered body condition a long-term result of feeding practices and not a sufficient indicator to detect metabolic disorders at an early stage. **(iii)** Compared to adult cows, body size, as a metabolic indicator, is essential in the analysis of the metabolism of heifers and calves because metabolism significantly influences their growth (Kertz et al., 2017).

The currently available metabolic indicators are greatly varied in their applicability and practicality. The blood metabolites measured by blood tests and the rumen pH and temperature measured by using boluses are physiological variables and can directly represent the metabolism of cows. Their measurements, however, reply on blood drawing or implantation of a bolus in the rumen of a cow. Hence, the measurements are invasive

to cows and impractical for deployment on farms on a regular basis. On the other hand, daily activity, rumination time, milk composition, and milk yield are noninvasive metabolic indicators deployed in PLF applications on farms. Although they can be measured automatically and noninvasively, they are not necessarily indicative of metabolic disorders and can be influenced by a variety of factors, such as cow behaviors and different diseases. The automatically quantified morphological traits can fill the gap between these current types of metabolic indicators, providing the advantages of revealing rapid responses to feeding practice changes and of automatic and noninvasive measurement. In PLF applications for dairy cows' metabolic health management, these morphological traits can be chronologically incorporated with currently available metabolic indicators (e.g., milk composition and yield) to represent the pathogenesis of metabolic disorders and to help farmers improve their farm management.

6.3 Rumen Fill as an Indicator of Metabolic Plasticity

The 3D vision-quantified rumen fill has the potential to be an indicator of dairy cow metabolic plasticity, which is defined as the adaptation capacity of a cow to maintain energy and nutrition balances when it experiences metabolic disturbances (Gross and Bruckmaier, 2015). As described in Chapter 5, the herd-level rumen fill exhibited a marked decrease after the start of grazing and gradually recovered to the pre-grazing level by the end of the study. The changes in rumen fill were associated with insufficient feed intake during grazing and influenced by the premature grass on the pasture land. At the individual cow level, the changes in rumen fill varied: some cows took less time than the herd average to reach the same level of rumen fill as before grazing, whereas others never returned to the same rumen fill level as before grazing (e.g., Cow A in Chapter 5). The recovery time of rumen fill has the potential to indicate the capability of a cow to adapt to disturbances and changes. Cows that fail to recover to the pre-grazing level of rumen fill may experience shortages in nutrition and energy, possibly resulting in production decreases and metabolic diseases. In addition to grazing, the farmer changed the indoor feed composition by replacing hay with corn silage on Day 24, which was during the period of cow adaptation to feeding on pasture since Day 10. The metabolic indicators of most cows remained stable, indicating that they adjusted their metabolisms to this change; however, a few cows did not fully recover from the second disturbance, and 2 cows started developing metabolic disorders. I consider these cows metabolically vulnerable. Hence, automatically quantified rumen fill could be deployed as an indicator of dairy cow metabolic plasticity at both the herd and individual levels. Furthermore, when farmers make feeding plans, it would be beneficial for them to know the metabolic plasticity of each cow and attend to those cows with low metabolic plasticity after changing feeding practices to prevent production reduction or occurrence of metabolic disorders.

6.4 Towards Understanding the Anomalies of Bio-Response and Disease Prevention

Current PLF applications for dairy cow health management focus on **(i)** measuring dairy cows' bio-responses by using a variety of sensors, **(ii)** identifying anomalies in the measurements on the herd or individual level, and **(iii)** developing models to link anomalies to specific diseases (Norton and Berckmans, 2018). These applications assume that anomalies in bio-response are a sufficient condition for detecting the occurrence of clinical diseases. However, such anomalies in bio-responses can be the result of physiological adaptations of a cow to maintain metabolic balances when it experiences disturbances. A cow with higher plasticity that is able to sufficiently respond and adapt to disturbances may avoid becoming sick in the future. Hence, the occurrence of anomalies of bio-response in a cow does not necessarily indicate that the cow is developing a disease. Without considering cows' physiological adaptation and plasticity, such PLF applications can assess cows with successful adaptations as diseased cows, increase false alerts on farms, cause unnecessary treatment, and reduce the confidence of farmers in PLF applications on farms.

PLF could learn from dairy veterinary science, in which the paradigm has shifted in dairy cow health management from the detection and treatment of clinical disease to disease prevention. Along with the intensification of dairy farming over decades, the assumption in veterinary science has gradually changed from "if all the sick animals are treated properly, a healthy dairy herd will result" to "if the problems produced in a dairy production system are fixed, a healthy dairy herd will result" (LeBlanc et al., 2006). This fundamental change is economically beneficial to dairy farmers and contributes to the sustainability of farms, especially large farms. PLF emerged as a result of the demand to maintain sustainability in intensified dairy farming. Hence, to effectively apply PLF in dairy cow health management, the research focus should also shift from detecting diseased cows to preventing disease (re) occurrence; this goal can be achieved by investigating the causes of bio-response anomalies in dairy cows and identifying the root causes of disease.

6.5 3D Vision System for Dairy Cow Morphological Quantification

The 3D vision-based morphological quantifications were designed to mimic human assessments performed on dairy cows. Using the assessments provided by experts as references, the errors in the automated body size measurements were negligible; the highest correlation coefficient (Spearman's ρ) between automatic and manual body condition assessment was 0.90 ($P < 0.001$); and the matching sensitivity between the automatically identified reticulo-ruminal contraction and manual identification was 0.97. The above results show that the automated morphological quantifications attained almost the same performance as human experts. Furthermore, 3D vision systems can provide measurements with much more detailed information and more features than human assessment. The

body-condition-related morphological traits were measured as continuous variables, whereas the outputs of the manual assessment were ordinal BCSs consisting of only 9 levels of body fatness. The standard manual reticulo-ruminal rumen motility assessment consisted of quantifications of contraction frequency and rumen fill. In the automatically extracted reticulo-ruminal contraction signals, additional features can potentially be extracted, such as the amplitude and duration of each contraction. These additional features have the potential to improve the evaluation of a cow's digestion ability and rumen health condition, for which manual assessment is not feasible. Hence, compared with other sensors and manual assessments, the 3D vision systems offer farmers a precise and cow-distress-free solution for monitoring the metabolism of individual cows and applying PLF on farms.

6.6 Acceptance of 3D Vision Technology

This study deployed morphological traits measured with 3D vision as metabolic indicates. We did not include daily activity and rumination time as metabolic indicators because the measurements of these two indicators for individual cows were expensive. When considering only hardware cost, I estimated the cost of a 3D accelerator housed in a tag with an attached neck belt could be approximately 150 euros for each cow. Moreover, a signal receiver and recording PC are also required for on-farm measurements. Hence, the cost of measuring these two indicators for individual cows in a herd (e.g., 50 cows) is substantial for farmers. On the other hand, the commercial 3D camera we selected costs approximately 150 euros. Even when deploying a multicamera system (i.e., 4 sets of 3D cameras, 1 recording PC, and other electronic parts) for a herd of 50 cows, the total cost is still less than 10 % of the cost of deploying 3D accelerators.

For almost a decade, 3D vision technology has been commercialized and industrialized on dairy farms with implementations of measuring dairy cow position in an AMS and body condition scoring at the exit of an AMS. Hence, farmers with AMSs are familiar with 3D vision technology, and their acceptance of deploying 3D cameras on farms has increased mainly because of the cameras' advantages of remote sensing and distress-free to cows. Similar to dairy farmers, manufacturers in dairy automation also instill confidence in 3D vision technology. By replacing invasive sensors with 3D cameras, automation can be more animal-friendly and can lead to more sustainable farming for dairy farmers. Additionally, 3D cameras have become a common type of sensor to deploy in PLF-related scientific studies with applications for measuring and monitoring a variety of bio-responses in most livestock animals (Norton and Berckmans, 2018). Nevertheless, the extensive deployment of 3D vision technology on dairy cows could be subject to societal pressure in the future. With the growing concern among the general public with regard to animal welfare and animal rights, 3D vision systems installed on farms for continuous monitoring could be considered to violate the 'privacy' of livestock animals.

6.7 Future Work

This thesis is the first step towards fully understanding the metabolism of dairy cows by applying PLF. We focused on case studies for validating automated systems and mathematical models with a limited number of cows, breeds, and types of morphological traits. The next step in this research is to improve the robustness of the 3D vision systems and mathematical models by expanding their validation to more cows of various breeds, ages, and DIMs, and with a variety of morphological trait selections. Moreover, our integrated 3D vision systems were installed on farms equipped with AMSs. Further studies are required to explore the feasibility of implementing 3D vision systems as standalone systems on conventional farms with facilities that cows regularly visit, such as individual feeding or drinking stations. The implementation of the standalone systems will expand the morphological monitoring of dry cows and youngstock, which are in the transition periods and facing considerable disturbances (Zebeli et al., 2015). Additionally, the deployment of RCA on PLF applications using morphological traits as metabolic indicators can also be used to evaluate feed quality, feeding strategies, and the impacts of stocking rate on farms. Finally, the designs of the 3D vision systems, mathematical models, and RCA deployment have great potential to be adopted for PLF applications for different livestock animals.

Appendices

References
Summary
Training and Supervision Plan

References

Alawneh, J.I., M.A. Stevenson, N.B. Williamson, N. Lopez-Villalobos, and T. Otley. 2011. Automatic recording of daily walkover liveweight of dairy cattle at pasture in the first 100 days in milk. J. Dairy Sci. 94:4431–4440. doi:10.3168/jds.2010-4002.

Altman, D.G. 1990. Practical statistics for medical research. 1st ed. Chapman and Hall CRC, London, UK. AlZahal, O., H. AlZahal, M.A. Steele, M. Van Schaik, I. Kyriazakis, T.F. Duffield, and B.W. McBride. 2011. The use of a radiotelemetric ruminal bolus to detect body temperature changes in lactating dairy cattle. J. Dairy Sci. 94:3568–3574. doi:10.3168/jds.2010-3944.

AlZahal, O., E. Kebreab, J. France, and B.W. McBride. 2007. A mathematical approach to predicting biological values from ruminal pH measurements. J. Dairy Sci. 90:3777–3785. doi:10.3168/jds.2006-534.

Ametaj, B.N. 2010. Veterinary Science. Chapter: Metabolic disorders of dairy cattle. 1st ed. Encyclopedia of Life Support Systems, Alberta, Canada.

Azzaro, G., M. Caccamo, J.D. Ferguson, S. Battiato, G.M. Farinella, G.C. Guarnera, G. Puglisi, R. Petriglieri, and G. Licitra. 2011. Objective estimation of body condition score by modeling cow body shape from digital images. J. Dairy Sci. 94:2126–2137. doi:10.3168/jds.2010-3467.

Banos, G., and M.P. Coffey. 2012. Technical note: Prediction of liveweight from linear conformation traits in dairy cattle. J. Dairy Sci. 95:2170–2175. doi:10.3168/jds.2011-4838.

Barkema, H.W., M.A.G. Von Keyserlingk, J.P. Kastelic, T.J.G.M. Lam, C. Luby, and J.-P. Roy. 2015. Invited review: Changes in the dairy industry affecting dairy cattle health and welfare. J. Dairy Sci. 98:7426–7445. doi:10.3168/jds.2015-9377.

Barker, Z.E., J.A. Vázquez Diosdado, E.A. Codling, N.J. Bell, H.R. Hodges, D.P. Croft, and J.R. Amory. 2018. Use of novel sensors combining local positioning and acceleration to measure feeding behavior differences associated with lameness in dairy cattle. J. Dairy Sci. 101:6310–6321. doi:10.3168/jds.2016-12172.

Bava, L., A. Sandrucci, M. Zucali, M. Guerci, and A. Tamburini. 2014. How can farming intensification affect the environmental impact of milk production? J. Dairy Sci. 97:4579–4593. doi:10.3168/jds.2013-7530.

Baynes, R.E., K. Dedonder, L. Kissell, D. Mzyk, T. Marmulak, G. Smith, L. Tell, R. Gehring, J. Davis, and J.E. Riviere. 2016. Health concerns and management of select veterinary drug residues. Food Chem. Toxicol. 88:112–122. doi:10.1016/j.fct.2015.12.020.

Berckmans, D. 2008. Precision livestock farming (PLF). Comput. Electron. Agric. 62:1. doi:10.1016/j.compag.2007.09.002.

Bercovich, A., Y. Edan, V. Alchanatis, U. Moallem, Y. Parmet, H. Honig, E. Maltz, A. Antler, and I. Halachmi. 2013. Development of an automatic cow body condition scoring using body shape signature and Fourier descriptors. J. Dairy Sci. 96:8047–8059. doi:10.3168/jds.2013-6568.

Bereskin, B., and R.W. Touchberry. 1967. Some effects of pregnancy on body weight and paunch girth. J. Dairy Sci. 50:220–224. doi:10.3168/jds.S0022-0302(67)87391-0.

Bewley, J.M., A.M. Peacock, O. Lewis, R.E. Boyce, D.J. Roberts, M.P. Coffey, S.J. Kenyon, and M.M. Schutz. 2008. Potential for estimation of body condition scores in dairy cattle from digital images. J. Dairy Sci. 91:3439–3453. doi:10.3168/jds.2007-0836.

Bobe, G., J.W. Young, and D.C. Beitz. 2010. Invited review: Pathology, etiology, prevention, and treatment of fatty liver in dairy cows. J. Dairy Sci. 87:3105–3124. doi:10.3168/jds.s0022-0302(04)73446-3.

Bos, A.P., P.W.G. Groot Koerkamp, J.M.J. Gooselink, and S. Bokma. 2009. Reflexive interactive design and its application in a project on sustainable dairy husbandry systems. Outlook Agric. 38:137–145. doi:10.5367/000000009788632386.

Brandl, N., and E. Jørgensen. 1996. Determination of live weight of pigs from dimensions measured using image analysis. Comput. Electron. Agric. 15:57–72. doi:10.1016/0168-1699(96)00003-8.

Braun, U., C. Gerspach, S. Warislohner, K. Nuss, and S. Ohlerth. 2018. Ultrasonographic and radiographic findings in 503 cattle with traumatic reticuloperitonitis. Res. Vet. Sci. 119:154–161. doi:10.1016/j.rvsc.2018.05.019.

Burfeind, O., P. Sepúlveda, M.A.G. von Keyserlingk, D.M. Weary, D.M. Veira, and W. Heuwieser. 2010. Technical note: Evaluation of a scoring system for rumen fill in dairy cows. J. Dairy Sci. 93:3635–3640. doi:10.3168/jds.2009-3044.

Burmańczuk, A., P. Hola, A. Milczak, T. Piech, C. Kowalski, B. Wojciechowska, and T. Grabowski. 2018. Quercetin decrease somatic cells count in mastitis of dairy cows. Res. Vet. Sci. 117:255–259. doi:10.1016/j.rvsc.2018.01.006.

Busch, G., and A. Spiller. 2018. Consumer acceptance of livestock farming around the globe. Anim. Front. 8:1–3. doi:10.1093/af/vfx005.

Chapinal, N., A.M. de Passillé, M. Pastell, L. Hänninen, L. Munksgaard, and J. Rushen. 2011. Measurement of acceleration while walking as an automated method for gait assessment in dairy cattle. J. Dairy Sci. 94:2895–2901. doi:10.3168/jds.2010-3882.

Chebel, R.C., L.G.D. Mendonça, and P.S. Baruselli. 2018. Association between body condition score change during the dry period and postpartum health and performance. J. Dairy Sci. 101:4595–4614. doi:10.3168/jds.2017-13732.

Coffey, E.L., L. Delaby, S. Fitzgerald, N. Galvin, K.M. Pierce, and B. Horan. 2017. Effect of stocking rate and animal genotype on dry matter intake, milk production, body weight, and body condition score in spring-calving, grass-fed dairy cows. J. Dairy Sci. 100:7556–7568. doi:10.3168/jds.2017-12672.

Colak, A., B. Polat, Z. Okumus, M. Kaya, L.E. Yanmaz, and A. Hayirli. 2008. Short communication: Early detection of mastitis using infrared thermography in dairy cows. J. Dairy Sci. 91:4244–4248. doi:10.3168/jds.2008-1258.

Collard, B.L., P.J. Boettcher, J.C.M. Dekkers, D. Petitclerc, and L.R. Schaeffer. 2000. Relationships between energy balance and health traits of dairy cattle in early lactation. J. Dairy Sci. 83:2683–2690. doi:10.3168/jds.S0022-0302(00)75162-9.

CRV. 2016. Melkproductieregistratie statistiek - Rollend jaargemiddelde melkproductie landelijk. Accessed November 7, 2016. https://www.crv4all.nl/downloads/prestaties/jaarstatistieken/.

Dickinson, R.A., J.M. Morton, D.S. Beggs, G.A. Anderson, M.F. Pyman, P.D. Mansell, and C.B. Blackwood. 2013. An automated walk-over weighing system as a tool for measuring liveweight change in lactating dairy cows. J. Dairy Sci. 96:4477–4486. doi:10.3168/jds.2012-6522.

Domecq, J.J., A.L. Skidmore, J.W. Lloyd, and J.B. Kaneene. 1995. Validation of body condition scores with ultrasound measurements of subcutaneous fat of dairy cows. J. Dairy Sci. 78:2308–2313. doi:10.3168/jds.S0022-0302(95)76857-6.

Duffield, T. 2006. Minimizing subclinical metabolic diseases in dairy cows. WCDS Adv. dairy Technol. 18:43–55.

Edmonson, A.J., I.J. Lean, L.D. Weaver, T. Farver, and G. Webster. 1989. A body condition scoring chart for holstein dairy cows. J. Dairy Sci. 72:68–78. doi:10.3168/jds.S0022-0302(89)79081-0.

Enevoldsen, C., and T. Kristensen. 1997. Estimation of body weight from body size measurements and body condition scores in dairy cows. J. Dairy Sci. 80:1988–1995. doi:10.3168/jds.S0022-0302(97)76142-3.

FAO. 2009. Global agriculture towards 2050. Rome, Italy.

FAO. 2011. Global livestock production systems. Rome, Italy.

FAO. 2016. Principles for the assessment of livestock impacts on biodiversity. Rome, Italy.

FAO. 2018a. World food and agriculture - statistical pocketbook 2018. Rome, Italy.

FAO. 2018b. Dairy market review. Rome, Italy.

FAO. 2018c. Nutrient flows and associated environmental impacts in livestock supply chains. Rome, Italy.

Fischer, A., T. Luginbühl, L. Delattre, J.M. Delouard, and P. Faverdin. 2015. Rear shape in 3 dimensions summarized by principal component analysis is a good predictor of body condition score in Holstein dairy cows. J. Dairy Sci. 98:4465–76. doi:10.3168/jds.2014-8969.

Fischer, K., K. Sjöström, A. Stiernström, and U. Emanuelson. 2019. Dairy farmers' perspectives on antibiotic use: A qualitative study. J. Dairy Sci. 102:2724–2737. doi:10.3168/jds.2018-15015.

Fournel, S., A.N. Rousseau, and B. Laberge. 2017. Rethinking environment control strategy of confined animal housing systems through precision livestock farming. Biosyst. Eng. 155:96–123. doi:10.1016/j.biosystemseng.2016.12.005.

Gerosa, S., and J. Skoet. 2012. Milk availability - Trends in production and demand and mediumterm outlook. Rome, Italy.

de Graaf, S., E.J. Van Loo, J. Bijttebier, F. Vanhonacker, L. Lauwers, F.A.M. Tuyttens, and W. Verbeke. 2016. Determinants of consumer intention to purchase animal-friendly milk. J. Dairy Sci. 99:8304–8313. doi:10.3168/jds.2016-10886.

Gross, J.J., and R.M. Bruckmaier. 2015. Repeatability of metabolic responses to a nutrient deficiency in early and mid lactation and implications for robustness of dairy cows. J. Dairy Sci. 98:8634–8643. doi:10.3168/jds.2014-9246.

Gross, J.J., and R.M. Bruckmaier. 2019. Invited review: Metabolic challenges and adaptation during different functional stages of the mammary gland in dairy cows: Perspectives for sustainable milk production. J. Dairy Sci. 102:2828–2843. doi:10.3168/jds.2018-15713.

Guo, H., K. Wang, Q. Ma, W. Su, and D. Zhu. 2017. LSSA CAU : An interactive 3d point clouds analysis software for body measurement of livestock with similar forms of cows or pigs. Comput. Electron. Agric. 138:60–68. doi:10.1016/j.compag.2017.04.014.

Haile-Mariam, M., O. Gonzalez-Recio, and J.E. Pryce. 2014. Prediction of liveweight of cows from type traits and its relationship with production and fitness traits. J. Dairy Sci. 97:3173–3189. doi:10.3168/jds.2013-7516.

Halachmi, I., M. Klopčič, P. Polak, D.J. Roberts, and J.M. Bewley. 2013. Automatic assessment of dairy cattle body condition score using thermal imaging. Comput. Electron. Agric. 99:35–40. doi:10.1016/J.COMPAG.2013.08.012.

Halachmi, I., P. Polak, D.J. Roberts, and M. Klopcic. 2008. Cow body shape and automation of condition scoring. J. Dairy Sci. 91:4444–4451. doi:10.3168/jds.2007-0785.

Hansen, M.F., M.L. Smith, L.N. Smith, K. Abdul Jabbar, and D. Forbes. 2018. Automated monitoring of dairy cow body condition, mobility and weight using a single 3D video capture device. Comput. Ind. 98:14–22. doi:10.1016/j.compind.2018.02.011.

Heinrichs, A.J., H.N. Erb, G.W. Rogers, J.B. Cooper, and C.M. Jones. 2007. Variability in Holstein heifer heart-girth measurements and comparison of prediction equations for live weight. Prev. Vet. Med. 78:333–338. doi:10.1016/j.prevetmed.2006.11.002.

Heinrichs, A.J., G.W. Rogers, and J.B. Cooper. 1992. Predicting body weight and wither height in Holstein heifers using body measurements. J. Dairy Sci. 75:3576–3581. doi:10.3168/jds.S0022-0302(92)78134-X.

Guo, H., K. Wang, Q. Ma, W. Su, and D. Zhu. 2017. LSSA CAU : An interactive 3d point clouds analysis software for body measurement of livestock with similar forms of cows or pigs. Comput. Electron. Agric. 138:60–68. doi:10.1016/j.compag.2017.04.014.

Haile-Mariam, M., O. Gonzalez-Recio, and J.E. Pryce. 2014. Prediction of liveweight of cows from type traits and its relationship with production and fitness traits. J. Dairy Sci. 97:3173–3189. doi:10.3168/jds.2013-7516.

Halachmi, I., M. Klopčič, P. Polak, D.J. Roberts, and J.M. Bewley. 2013. Automatic assessment of dairy cattle body condition score using thermal imaging. Comput. Electron. Agric. 99:35–40. doi:10.1016/J.COMPAG.2013.08.012.

Halachmi, I., P. Polak, D.J. Roberts, and M. Klopcic. 2008. Cow body shape and automation of condition scoring. J. Dairy Sci. 91:4444–4451. doi:10.3168/jds.2007-0785.

Hansen, M.F., M.L. Smith, L.N. Smith, K. Abdul Jabbar, and D. Forbes. 2018. Automated monitoring of dairy cow body condition, mobility and weight using a single 3D video capture device. Comput. Ind. 98:14–22. doi:10.1016/j.compind.2018.02.011.

Heinrichs, A.J., H.N. Erb, G.W. Rogers, J.B. Cooper, and C.M. Jones. 2007. Variability in Holstein heifer heart-girth measurements and comparison of prediction equations for live weight. Prev. Vet. Med. 78:333–338. doi:10.1016/j.prevetmed.2006.11.002.

Heinrichs, A.J., G.W. Rogers, and J.B. Cooper. 1992. Predicting body weight and wither height in Holstein heifers using body measurements. J. Dairy Sci. 75:3576–3581. doi:10.3168/jds.S0022-0302(92)78134-X.

van Hertem, T., L. Rooijakkers, D. Berckmans, A. Peña Fernández, T. Norton, D. Berckmans, and E. Vranken. 2017. Appropriate data visualisation is key to Precision Livestock Farming acceptance. Comput. Electron. Agric. 138:1–10. doi:10.1016/j.compag.2017.04.003.

Kristensen, E., L. Dueholm, D. Vink, J.E. Andersen, E.B. Jakobsen, S. Illum-Nielsen, F.A. Petersen, and C. Enevoldsen. 2006. Within- and across-person uniformity of body condition scoring in danish Holstein cattle. J. Dairy Sci. 89:3721–3728. doi:10.3168/jds.S0022-0302(06)72413-4.

Hungate, R. 1966. The rumen and its microbes. 1st ed. Academic Press, New York. doi: 10.1016/C2013-0-12555-X. ISPA. 2019. ISPA forms official definition of 'Precision Agriculture.' https://www.precisionag.com/market-watch/ispa-forms-official-definition-of-precisionagriculture/.

Jackson, P., and P. Cockcroft. 2002. Clinical examination of farm animals. 1st ed. Blackwell Science, Oxford, UK. Jacobs, J.A., and J.M. Siegford. 2012. Invited review: The impact of automatic milking systems on dairy cow management, behavior, health, and welfare. J. Dairy Sci. 95:2227–2247. doi:10.3168/jds.2011-4943.

Jensen, C., S. Østergaard, J. Bertilsson, and M.R. Weisbjerg. 2015. Responses in live weight change to net energy intake in dairy cows. Livest. Sci. 181:163–170. doi:10.1016/j.livsci.2015.09.016.

Kamphuis, C., H. Mollenhorst, J.A.P. Heesterbeek, and H. Hogeveen. 2010. Detection of clinical mastitis with sensor data from automatic milking systems is improved by using decision-tree induction. J. Dairy Sci. 93:3616–3627. doi:10.3168/jds.2010-3228.

Kawasue, K., T. Ikeda, T. Tokunaga, and H. Harada. 2013. 3-dimensional shape measurement system for black cattle using KINECT sensor. Int. J. Circuits, Syst. Signal Process. 7:222–230.

Kertz, A.F., T.M. Hill, J.D. Quigley, A.J. Heinrichs, J.G. Linn, and J.K. Drackley. 2017. A 100-Year Review: Calf nutrition and management. J. Dairy Sci. 100:10151–10172. doi:10.3168/jds.2017-13062.

Kertz, A. F., L. F. Reutzel, B. A. Barton, and R. L. Ely. 1997. Body weight, body condition score, and wither height of prepartum Holstein cows and birth weight and sex of calves by parity: A database and summary. J. Dairy Sci. 80:525–529. doi:10.3168/jds.S0022-0302(97)75966-6.

Khatun, M., P.C. Thomson, K.L. Kerrisk, N.A. Lyons, C.E.F. Clark, J. Molfino, and S.C. García. 2018. Development of a new clinical mastitis detection method for automatic milking systems. J. Dairy Sci. 101:9385–9395. doi:10.3168/jds.2017-14310.

Kiruthika, T.K. 2015. Root cause analysis in health care. Int. J. Nurs. Educ. Res. 3:441. doi:10.5958/2454-2660.2015.00038.1.

Kuzuhara, Y., K. Kawamura, R. Yoshitoshi, T. Tamaki, S. Sugai, M. Ikegami, Y. Kurokawa, T. Obitsu, M. Okita, T. Sugino, and T. Yasuda. 2015. A preliminarily study for predicting body weight and milk properties in lactating Holstein cows using a 3-dimensional camera system. Comput. Electron. Agric. 111:186–193. doi:10.1016/j.compag.2014.12.020.

LeBlanc, S.J., K.D. Lissemore, D.F. Kelton, T.F. Duffield, and K.E. Leslie. 2006. Major advances in disease prevention in dairy cattle. J. Dairy Sci. 89:1267–1279. doi:10.3168/jds.s0022-0302(06)72195-6.

Leek, B.F. 1987. The control of the motility of the reticulo-rumen. Springer Netherlands, Dordrecht, The Netherlands.

Leskinen, H., L. Ventto, P. Kairenius, K.J. Shingfield, and J. Vilkki. 2019. Temporal changes in milk fatty acid composition during diet-induced milk fat depression in lactating cows. J. Dairy Sci. 102:5148–5160. doi:10.3168/jds.2018-15860.

Lowder, S.K., J. Skoet, and T. Raney. 2016. The number, size, and distribution of farms, smallholder farms, and family farms worldwide. World Dev. 87:16–29. doi:10.1016/j.worlddev.2015.10.041.

Maertens, W., J. Vangeyte, J. Baert, A. Jantuan, K.C. Mertens, S. De Campeneere, A. Pluk, G. Opsomer, S. Van Weyenberg, and A. Van Nuffel. 2011. Development of a real time cow gait tracking and analysing tool to assess lameness using a pressure sensitive walkway: The GAITWISE system. Biosyst. Eng. 110:29–39. doi:10.1016/j.biosystemseng.2011.06.003.

Maltz, E. 1997. The body weight of the dairy cow: III. Use for on-line management of individual cows. Livest. Prod. Sci. 48:187–200. doi:10.1016/S0301-6226(97)00026-2.

Mäntysaari, P., and E.A. Mäntysaari. 2015. Modeling of daily body weights and body weight changes of Nordic Red cows. J. Dairy Sci. 98:6992–7002. doi:10.3168/jds.2015-9541.

Martiskainen, P., M. Järvinen, J.P. Skön, J. Tiirikainen, M. Kolehmainen, and J. Mononen. 2009. Cow behaviour pattern recognition using a 3-dimensional accelerometer and support vector machines. Appl. Anim. Behav. Sci. 119:32–38. doi:10.1016/j.applanim.2009.03.005.

Marinello, F., A. Pezzuolo, D. Cillis, F. Gasparini, and L. Sartori. 2015. Application of Kinect-Sensor for 3-dimensional body measurements of cows. Pages 661–669 in 7th European Conference on Precision Livestock Farming, ECPLF 2015. European Conference on Precision Livestock Farming, Milan, Italy.

McCarthy, S., D.P. Berry, P. Dillon, M. Rath, and B. Horan. 2007. Influence of Holstein-Friesian strain and feed system on body weight and body condition score lactation profiles. J. Dairy Sci. 90:1859–1869. doi:10.3168/jds.2006-501.

McGuffey, R.K. 2017. A 100-Year Review: Metabolic modifiers in dairy cattle nutrition. J. Dairy Sci. 100:10113–10142. doi:10.3168/jds.2017-12987.

Meyer, N.F., and T.C. Bryant. 2017. Diagnosis and management of rumen acidosis and bloat in feedlots. Vet. Clin. North Am. Food Anim. Pract. 33:481–498. doi:10.1016/J.CVFA.2017.06.005.

Morin, P.A., Y. Chorfi, J. Dubuc, J.P. Roy, D. Santschi, and S. Dufour. 2017. Short communication: An observational study investigating inter-observer agreement for variation over time of body condition score in dairy cows. J. Dairy Sci. 100:3086–3090. doi:10.3168/jds.2016-11872.

Mostert, P.F., C.E. van Middelaar, E.A.M. Bokkers, and I.J.M. de Boer. 2018. The impact of subclinical ketosis in dairy cows on greenhouse gas emissions of milk production. J. Clean. Prod. 171:773–782. doi:10.1016/j.jclepro.2017.10.019.

Oetzel, G.R. 2017. Diagnosis and management of subacute ruminal acidosis in dairy herds. Vet. Clin. North Am. Food Anim. Pract. 33:463–480. doi:10.1016/J.CVFA.2017.06.004.

Norton, T., and D. Berckmans. 2018. Engineering advances in Precision Livestock Farming. Biosyst. Eng. 173:1–3. doi:10.1016/j.biosystemseng.2018.09.008.

Overton, T.R., J.A.A. McArt, and D.V. Nydam. 2017. A 100-year review: Metabolic health indicators and management of dairy cattle. J. Dairy Sci. 100:10398–10417. doi:10.3168/jds.2017- 13054.

Pilat, Z. 1988. Cow morphology and performance. Agris 32:481–488. Rathbun, F.M., R.S. Pralle, S.J. Bertics, L.E. Armentano, K. Cho, C. Do, K.A. Weigel, and H.M. White. 2017. Relationships between body condition score change, prior mid-lactation phenotypic residual feed intake, and hyperketonemia onset in transition dairy cows. J. Dairy Sci. 100:3685–3696. doi:10.3168/jds.2016-12085.

Roche, J.R., P.G. Dillon, C.R. Stockdale, L.H. Baumgard, and M.J. Van Baale. 2004. Relationships among international body condition scoring systems. J. Dairy Sci. 87:3076–3079. doi:10.3168/jds.S0022-0302(04)73441-4.

Roche, J.R., N.C. Friggens, J.K. Kay, M.W. Fisher, K.J. Stafford, and D.P. Berry. 2009. Invited review: Body condition score and its association with dairy cow productivity, health, and welfare. J. Dairy Sci. 92:5769–5801. doi:10.3168/JDS.2009-2431.

de Roos, A.P.W., H.J.C.M. van den Bijgaart, J. Hørlyk, and G. de Jong. 2007. Screening for subclinical ketosis in dairy cattle by fourier transform infrared spectrometry. J. Dairy Sci. 90:1761–1766. doi:10.3168/jds.2006-203.

Rosell-Polo, J.R., F.A. Cheeinx, E. Gregorio, D. Andújar, L. Puigdomènech, J. Masip, and A. Escolà. 2015. Advances in structured light sensors applications in precision agriculture and livestock farming. Adv. Agron. 133:71–112. doi:10.1016/bs.agron.2015.05.002. Ruckebusch, Y., and P. Thivend. 1980. Digestive physiology and metabolism in ruminants. 1st ed.

Springer, Dordrecht, The Netherlands. doi: 10.1007/978-94-011-8067-2. Rusu, R.B. 2009. Semantic 3D object maps for everyday manipulation in human living environments. Page 45-49. Ph.D. Thesis. Institut für Informatik, Technische Universität Müchen, Germany.

Rutten, C.J., A.G.J. Velthuis, W. Steeneveld, and H. Hogeveen. 2013. Invited review: Sensors to support health management on dairy farms. J. Dairy Sci. 96:1928–1952. doi:10.3168/jds.2012-6107.

Saborío-Montero, A., B. Vargas-Leitón, J.J. Romero-Zúñiga, and J.M. Sánchez. 2017. Risk factors associated with milk fever occurrence in grazing dairy cattle. J. Dairy Sci. 100:9715–9722. doi:10.3168/jds.2017-13065.

Salau, J., J.H. Haas, W. Junge, and G. Thaller. 2016. Extrinsic calibration of a multi-Kinect camera scanning passage for measuring functional traits in dairy cows. Biosyst. Eng. 151:409–424. doi:10.1016/j.biosystemseng.2016.10.008.

Salau, J., J.H. Haas, W. Junge, and G. Thaller. 2017. A multi-Kinect cow scanning system: Calculating linear traits from manually marked recordings of Holstein-Friesian dairy cows. Biosyst. Eng. 157:92–98. doi:10.1016/j.biosystemseng.2017.03.001.

Salfer, I.J., C.D. Dechow, and K.J. Harvatine. 2018. Annual rhythms of milk and milk fat and protein production in dairy cattle in the United States. J. Dairy Sci. 102:742–753. doi:10.3168/jds.2018-15040.

Schorr, A., and M. Lips. 2018. Influence of milk yield on profitability-A quantile regression analysis. J. Dairy Sci. 101:8350–8368. doi:10.3168/jds.2018-14434.

Schröder, U.J., and R. Staufenbiel. 2006. Invited review: Methods to determine body fat reserves in the dairy cow with special regard to ultrasonographic measurement of backfat thickness. J. Dairy Sci. 89:1–14. doi:10.3168/jds.S0022-0302(06)72064-1.

Sieber, M., A.E. Freeman, and D.H. Kelley. 1988. Relationships between body measurements, body weight, and productivity in Holstein dairy cows. J. Dairy Sci. 71:3437–3445. doi:10.3168/jds.S0022-0302(88)79949-X.

Snyder, E., and B. Credille. 2017. Diagnosis and treatment of clinical rumen acidosis. Vet. Clin. North Am. Food Anim. Pract. 33:451–461. doi:10.1016/J.CVFA.2017.06.003.

Song, X., T. Leroy, E. Vranken, W. Maertens, B. Sonck, and D. Berckmans. 2008. Automatic detection of lameness in dairy cattle-Vision-based trackway analysis in cow's locomotion. Comput. Electron. Agric. 64:39–44.

Song, X., E.A.M. Bokkers, S. van Mourik, P.W.G. Groot Koerkamp, and P.P.J. van der Tol. 2019a. Automated body condition scoring of dairy cows using 3-dimensional feature extraction from multiple body regions. J. Dairy Sci. 102 (5): 4292-4308. doi:10.3168/jds.2018-15238.

Song, X., P.P.J. van der Tol, P.W.G. Groot Koerkamp, and E.A.M. Bokkers. 2019b. Hot Topic: Automated assessment of reticulo-ruminal motility in dairy cows using 3-dimensional vision. In press by J. Dairy Sci. on July, 2019. doi:10.3168/jds.2019-16550.

Spoliansky, R., Y. Edan, Y. Parmet, and I. Halachmi. 2016. Development of automatic body condition scoring using a low-cost 3-dimensional Kinect camera. J. Dairy Sci. 99:7714–7725. doi:10.3168/jds.2015-10607.

Stajnko, D., M. Brus, and M. Hočevar. 2008. Estimation of bull live weight through thermographically measured body dimensions. Comput. Electron. Agric. 61:233–240. doi:10.1016/j.compag.2007.12.002.

Stangaferro, M.L., R. Wijma, L.S. Caixeta, M.A. Al-Abri, and J.O. Giordano. 2016. Use of rumination and activity monitoring for the identification of dairy cows with health disorders: Part I. Metabolic and digestive disorders. J. Dairy Sci. 99:7395–7410. doi:10.3168/jds.2016-10907.

Statistics Netherlands. 2016. Agriculture; crops, livestock and land use by general farm type, Region. Accessed November 7, 2016. http://statline.cbs.nl/Statweb/publication/?VW=T&DM=SLEN&PA=80783eng&D1=87,106&D2=0&D3=0&D4=a&HD=161107-1231&LA=EN&HDR=G1,G2,T&STB=G3%0A.

Sundrum, A. 2015. Metabolic disorders in the transition period indicate that the dairy cows' ability to adapt is overstressed. Animals 5:978–1020. doi:10.3390/ani5040395.

Tasch, U., and P.G. Rajkondawar. 2004. The development of a SoftSeparatorTM for a lameness diagnostic system. Comput. Electron. Agric. 44:239–245. doi:10.1016/j.compag.2004.04.001.

Tasdemir, S., A. Urkmez, and S. Inal. 2011. Determination of body measurements on the Holstein cows using digital image analysis and estimation of live weight with regression analysis. Comput. Electron. Agric. 76:189–197. doi:10.1016/j.compag.2011.02.001.

Taylor, Z., J. Nieto, and D. Johnson. 2015. Multi-modal sensor calibration using a gradient orientation measure. J. F. Robot. 32:675–695. doi:10.1002/rob.21523.

Thorup, V.M., D. Edwards, and N.C. Friggens. 2012. On-farm estimation of energy balance in dairy cows using only frequent body weight measurements and body condition score. J. Dairy Sci. 95:1784–93. doi:10.3168/jds.2011-4631.

van der Tol, P.P.J., and A. van der Kamp. 2010. Time series analysis of live weight as health indicator. Pages 230–231 in First North American Conference on Precision Dairy Management 2010, Toronto, Canada.

Tullo, E., A. Finzi, and M. Guarino. 2019. Review: Environmental impact of livestock farming and Precision Livestock Farming as a mitigation strategy. Sci. Total Environ. 650:2751–2760. doi:10.1016/j.scitotenv.2018.10.018.

UN. 2019. World population prospects 2019: Highlights (ST/ESA/SER.A/423). New York, USA. Vanrobays, M.-L., J. Vandenplas, H. Hammami, E. Froidmont, and N. Gengler. 2015. Short communication: Novel method to predict body weight of primiparous dairy cows throughout the lactation. J. Dairy Sci. 98:692–697. doi:10.3168/jds.2014-8504.

de Vries, M.J., S. van der Beek, L.M. Kaal-Lansbergen, W. Ouweltjes, and J.B. Wilmink. 1999. Modeling of energy balance in early lactation and the effect of energy deficits in early lactation on first detected estrus postpartum in dairy cows. J. Dairy Sci. 82:1927–1934. doi:10.3168/jds.S0022-0302(99)75428-7.

Wolf, C.A., G.T. Tonsor, M.G.S. McKendree, D.U. Thomson, and J.C. Swanson. 2016. Public and farmer perceptions of dairy cattle welfare in the United States. J. Dairy Sci. 99:5892–5903. doi:10.3168/jds.2015-10619.

Yan, T., C.S. Mayne, D.C. Patterson, and R.E. Agnew. 2009. Prediction of body weight and empty body composition using body size measurements in lactating dairy cows. Livest. Sci. 124:233–241. doi:10.1016/j.livsci.2009.02.003.

Zebeli, Q., K. Ghareeb, E. Humer, B.U. Metzler-Zebeli, and U. Besenfelder. 2015. Nutrition, rumen health and inflammation in the transition period and their role on overall health and fertility in dairy cows. Res. Vet. Sci. 103:126–136. doi:10.1016/j.rvsc.2015.09.020.

Summary

Feeding the growing population is a major challenge and requires increases in food production from limited natural resources. Due to globalization and the rapidly growing economies in some upper-to-middle-income countries and nearly all high-income countries throughout the world, the dairy sector has been significantly intensified and become one of the fastest-growing segments among all food production sectors. Meanwhile, intensified dairy farming remains a subject of growing concern among the general public with regard to food quality, animal health, environmental impacts, and sustainable development.

With the development of sensor technologies in recent decades, precision livestock farming (PLF) has become an innovative approach to make livestock farming more environmentally, economically, and socially sustainable. Particularly, in the dairy sector, PLF has received considerable attention with a specific focus on dairy cow health management. Currently, PLF applications have focused on detecting major health problems in dairy cows, such as mastitis, lameness, and metabolic disorders. These applications have intensively deployed different types of sensors to measure potential disease-related bio-responses and to build disease detection models. PLF aims to detect diseases and alerts farmers to treat the identified cows as early as possible. Nevertheless, PLF applications are problem-oriented and only focus on improving health management within the existing scope of farms. Additionally, these methods lack a systematic reflection of the current structures of farm management and the anticipation of reduced disease prevalence due to structural changes. Moreover, most PLF applications independently deploy single types of sensors to measure bio-responses related to specific clinical symptoms. The origin of a disease, however, is significantly associated with the chronological relations of multiple clinical symptoms. Deploying single types of sensors without considering their chronological relations to other types of sensors limits the understanding of the pathogenesis of a disease. Hence, the current PLF applications are still reactive health management methods and need to be improved to be more proactive, with a focus on identifying the causes of diseases and preventing disease reoccurrence. To improve PLF applications from reactive to proactive health management, we suggest incorporating PLF into root cause analysis (RCA), which is a method of identifying the root (main) causes of health problems in dairy cows. RCA has the potential to reveal the main causes of diseases to farmers as a systematic reflection of current farm management strategies and to improve or redesign farm management to prevent disease reoccurrence.

This thesis chose dairy cow metabolic disorders as a case study to incorporate PLF and RCA and investigate the root cause of metabolic disorders. Metabolic disorders are caused by the disturbance of 1 or more metabolic processes in a dairy cow and have a considerable impact on a cow's health, production, and reproduction. In current PLF applications, metabolic health management depends on monitoring the dairy cow metabolic indicators (e.g., milk composition, rumen pH and temperature, daily activity, and rumination time) that indicate the overall functioning of a cow's metabolism. These available metabolic indicators, however, are not specifically indicative of metabolic disorders, and the measurements of these indicators are

invasive and costly. Hence, different metabolic indicators are needed and should be automatically and noninvasively measurable on farms using low-cost sensors and have physiological or pathological meanings underlying the corresponding anomalies.

Dairy cows experience metabolic challenges throughout the year. When a cow is unable to cope with a challenge or to maintain its energy balance, this can consequently result in changes to the cow's morphological traits. These morphological traits, including body size, body condition, hair coat, and paralumbar shape, are used for the manual clinical diagnosis of metabolic disorders. Hence, morphological traits have great potential as metabolic indicators to be deployed in PLF applications. Furthermore, dairy cow morphological traits can be quantified automatically using machine vision. Among all vision cameras, 3-dimensional (3D) vision cameras have the most considerable advantages in remotely, inexpensively, and noninvasively quantifying dairy cow morphological traits. The objectives of this thesis are to design methods and models to automatically quantify dairy cow morphological traits as metabolic indicators using 3D vision and to acquire knowledge about the pathogenesis of metabolic disorders in dairy cows.

Three types of morphological traits in dairy cows were selected: body size, body condition, and body surface concavity on the left paralumbar fossa, which represents reticulo-ruminal motility and fill. In **Chapter 2**, the body-size-related morphological traits of hip height, hip width, and rump length were automatically quantified using a 3D vision camera to view the rump areas of dairy cows. The results of the automated morphological trait quantification were validated with manual body measurements as a gold standard. With these morphological traits as inputs, we achieved weight prediction performance similar to that of the manual method. Moreover, the propagation of measurement error to the prediction model was negligible, which indicated that the bottleneck in prediction was associated with insufficient prediction model inputs and not the quality of the 3D vision system. Three commonly used morphological traits of dairy cows were selected for automatic quantification, and the results demonstrated that 3D vision has great potential for automation on farms. Additionally, this chapter set guidelines for data collection, image processing, measurement error quantification, mathematical model selection, and referential assessment protocols for the follow-up chapters.

The body condition score (BCS) of a dairy cow is a metabolic indicator that is influenced by, for example, the lactation stage, feed efficiency, dietary composition, and stocking rate. The current vision-based BCS classifications use information acquired from only a limited number of cow body regions. In **Chapter 3**, body condition-related morphological traits in 8 body regions (i.e., the spinous processes, spinous to transverse processes, overhanging shelf, hook bone, pin bone, thurl area, spinous processes to hook bone, and cavity between tail head and pin bone) were quantified automatically using 3 identical 3D cameras viewing the top, rear, and right sides of a cow. A nearest-neighbor classification model was built to classify the BCS of individual cows with automatically quantified morphological traits as inputs and manual BCSs as a gold standard. The sensitivity of our 3D vision-based BCS classification was significantly higher than the sensitivities of currently available automated systems.

Dairy cow reticulo-ruminal motility is a well-established indicator of gastrointestinal health and metabolism. In **Chapter 4**, a low-cost 3D vision system was demonstrated to automatically and remotely assess dairy cow reticulo-ruminal motility. In an AMS, the body surface concavity on the left paralumbar fossa of a dairy cow was quantified automatically using a 3D camera. The concavity from all 3D images of 1 cow during 1 recording was chronologically assembled to form an undulation signal. This undulation signal consisted of cyclic oscillations that represented reticulo-ruminal contractions. The cyclic oscillation frequency was calculated using fast Fourier transformation and represented as the reticulo-ruminal motility. Our automated assessment performed similarly to the referential manual assessment. In contrast to the other available methods, this automated system is noninvasive and distress free for cows. Thus, this system is a promising tool for farmers and veterinarians to obtain information on a regular basis about the metabolic status of individual cows and can aid in farm management and clinical diagnoses.

Chapter 5 describes an on-farm longitudinal study that integrated all the 3D vision systems and mathematical models designed in Chapters 2, 3, and 4 to regularly monitor all 3 types of morphological traits over 66 days. All anomalies in the morphological traits at both the herd and individual levels were identified and chronologically assembled to investigate the root causes of metabolic disorders. Among all the morphological traits, the herd level rumen fill can serve as a metabolic indicator that responds rapidly to feeding practice changes. As a case study, a cow with metabolic disorders was analyzed by applying RCA to all the available metabolic indicators of the cow over 66 days. The root cause of this case was that the farmer lacked information about the cow's metabolism when he adjusted the feeding practices several times. This chapter developed a promising method of applying RCA to farms to assist dairy farmers in managing dairy cow metabolic health.

This thesis demonstrated the application of 3D vision technology for automating dairy cow morphology quantification on farms. The design of the vision systems and mathematical models were validated on farms, demonstrating the great potential of these tools for farmers to deploy in daily farm management. The automatically quantified morphological traits were shown to be significantly correlated with the metabolism of cows. The root cause of a metabolic indicator was revealed by chronologically combining all metabolic indicators and applying RCA. This thesis developed and validated a method to incorporate PLF and RCA to assist farmers in dairy cow metabolic health management, providing the first step towards fully understanding the pathogenesis of metabolic disorders in dairy cows. The next step of research should be to improve the robustness of the 3D vision systems and mathematical models by expanding the validations to more cows of various breeds, ages, and lactation stages, and with a variety of morphological trait selections. Moreover, further studies are required to explore the feasibility of implementing 3D vision systems as stand-alone systems for managing dry cows and youngstock, which are in transition periods and face considerable disturbances. Finally, the deployment of RCA in PLF applications using morphological traits as metabolic indicators can assist farmers in evaluating feed quality and feeding strategies to prevent metabolic disorder reoccurrences.

Training and Supervision Plan (TSP)

Graduate School WIAS

GENERAL INFORMATION AND LEARNING GOALS	
Name PhD candidate	Xiangyu Song
Project title	The skin-deep beauty of dairy cows --- Investigation of metabolic disorders by using morphological traits quantified with 3-dimensional vision
Group	Farm Technology, Animal Production Systems
Daily supervisor(s)	Rik van der Tol, Eddie Bokkers
Supervisor(s)	Peter Groot Koerkamp
PhD study advisor	Richard Crooijmans
Project term	1st OCT 2014 1st OCT 2019
Submitted	1st APR 2015/1st SEPT 2016/1st JUL 2019 first plan / midterm / certificate

EDUCATION AND TRAINING (minimum 30 credits)				
A. The Basic Package			year	credits
WIAS introduction day **(mandatory)**			2015	
WIAS course on essential skills **(recommended)**			2015	
Research integrity & ethics in animal sciences **(mandatory)**			2017	
Subtotal Basic Package				**3.0**
B. Disciplinary Competences (minimum 2 courses)			year	credits
Research proposal			2014	
Adaptative animals and livestock farming systems in a globally changes			2014	
Statistics for the life sciences			2015	
Subtotal Disciplinary Competences				**9.5**
C. Professional Competences (minimum 2 courses)			year	credits
Scientific writing			2014	
WAPS member			2015-2017	
Chairman of WIAS Science Day committee			2016	
Interpersonal communication for PhD students			2016	
Project and time management			2017	
Subtotal Professional Competences				**9.9**
D. Presentation Skills (maximum 4 credits)			year	credits
Body measurements of dairy calf using a 3-D camera in an automatic feeding system,			2014	
Dairy cow body condition scoring in automatic milking systems by 3D vision, CIGR 2014,			2014	
Automated identification of anatomical landmarks of dairy cow in three-dimensional vision,			2018	
Automatic body condition scoring of dairy cows using multiple 3D cameras, AGENG 2018,			2018	
Subtotal presentations				**4.0**
E. Teaching competences (max 6 credits)		Student	year	credits
Error analysis of Quantifying dairy cow body size	FTE Master Thesis	Roel Vernooij	2014	
Validation of using 3D-image variables to predict	APS Master Thesis	Elles Leijdekkers	2017	
Monitoring subcutaneous fat changes in dairy	FTE Master Thesis	Jeoren de Bruin	2019	
Subtotal Teaching competences				**6.0**
Education and Training Total (minimum 30 credits)				**32.4**

The research described in this thesis was financially supported by Lely Industries N.V.. Financial support from Wageningen University and Lely Industries N.V. for printing this thesis is gratefully acknowledged.

Cover design by Dennis Hendriks / ProefschriftMaken.nl
Printed by ProefschriftMaken / Gigaprint on FSC-certified paper